



# Tracking orbital and suborbital climate variability in the westernmost Mediterranean over the past 13,000 years: New insights from paleoperspectives on marine productivity responses

Ricardo D. Monedero-Contreras<sup>a,\*</sup>, Francisca Martínez-Ruiz<sup>a</sup>, Francisco J. Rodríguez-Tovar<sup>b</sup>, José M. Mesa-Fernández<sup>b</sup>, Francesca Sangiorgi<sup>c</sup>

<sup>a</sup> Instituto Andaluz de Ciencias de la Tierra (CSIC), Armilla, Spain

<sup>b</sup> Departamento de Estratigrafía y Paleontología, Universidad de Granada, Granada, Spain

<sup>c</sup> Dept. Earth Sciences, Utrecht University, the Netherlands

## ARTICLE INFO

Handling editor: A. Voelker

### Keywords:

Paleoproductivity  
Dinoflagellates  
Mediterranean sea  
Barite  
Marine geochemistry

## ABSTRACT

This study presents a comprehensive analysis of a sediment record from the Western Alboran Basin (core GP04PC), utilizing palynological and geochemical tools to investigate marine productivity responses to orbital and suborbital climate variability over the past 13,000 years. High productivity during the Younger Dryas humid phase (~12.4–11.7 ka) and the Holocene humidity optimum (~10.5–8.5 ka) was driven by increased local river discharges resulting from rapid mountain glaciers melting and enhanced regional precipitation. During the late Holocene, frequent flood events linked to negative North Atlantic Oscillation (NAO) incursions potentially led to multicentennial-scale productivity increases. The findings indicate that periods characterized by wet regional conditions and increased river run-off, influenced by orbital (e.g., insolation cycles) and suborbital factors (e.g., NAO and Atlantic Meridional Overturning Circulation changes), consistently enhanced marine productivity in the Western Alboran Basin. The study also reveals that the current high productivity and carbon export in the Western Alboran Basin are maintained by active upwelling and downwelling systems driven by a persistent positive NAO phase following the southward migration of the Intertropical Convergence Zone (ITCZ) that occurred around 6.5 ka. Furthermore, geochemical proxies support a strong detrital influence on trace metal concentrations, including barium (Ba), in deep Western Alboran sediments during the Holocene. This limits the use of Ba/Al ratios for accurately reconstructing productivity changes and highlights the importance of dinocyst analysis as a complementary tool for robust marine productivity reconstructions in this region. These observations provide valuable paleoperspectives on marine ecosystem responses to climate variability, contributing to the development of robust long-term productivity models essential for adapting to ongoing environmental changes in the region, and demonstrating the strong influence of North Atlantic climate and ocean dynamics on centennial-scale productivity oscillations in this region.

## 1. Introduction

Climate change and anthropogenic activities bear an impact on oceanographic processes such as vertical mixing and thermohaline circulation, and intensify ocean stressors that include acidification, warming, and deoxygenation (Schmidtke et al., 2017; Breitburg et al., 2018). These changes alter the biogeochemical cycles of macronutrients and oligoelements (e.g., C, N, P, Si, and trace metals), subsequently impacting nutrient availability and marine productivity (Gruber, 2011;

Gruber et al., 2021). Analyses of primary production derived from satellite data over the past two decades, presented in the Intergovernmental Panel on Climate Change (IPCC) report, revealed a decrease in marine productivity (up to -3.0 %) at low and mid latitudes (IPCC, 2023). Biogeochemical models also outlined in this report support a global decline in primary production of 2.1 % per decade attributed to the shoaling of the mixed layer and decreasing nitrate concentrations, based on data obtained from 1998 to 2015. These potential changes in marine productivity pose a global-scale threat to marine ecosystems and

\* Corresponding author.

E-mail address: [ricardo.monedero@csic.es](mailto:ricardo.monedero@csic.es) (R.D. Monedero-Contreras).

<https://doi.org/10.1016/j.quascirev.2024.109001>

Received 31 July 2024; Received in revised form 9 October 2024; Accepted 9 October 2024

Available online 14 October 2024

0277-3791/© 2024 The Authors. Published by Elsevier Ltd. This is an open access article under the CC BY-NC license (<http://creativecommons.org/licenses/by-nc/4.0/>).

seafood supplies (Polovina et al., 2008; Lozier et al., 2011; Capotondi et al., 2012; Mena et al., 2019).

Robust long-term projections (spanning decades to centuries) of productivity responses to current climate change are therefore essential. However, fully understanding the potential feedback mechanisms and climatic factors that influence these long-term variations in marine productivity remains a complex task, requiring oceanographic data from timescales exceeding those provided by instrumental records. In this context, marine paleoarchives have proven to be indispensable tools; it has been demonstrated that marine responses to past climate changes, as obtained through paleoceanographic reconstructions, can be effectively incorporated into future projections (Kiessling et al., 2023). This integration helps to more accurately constrain the centennial-scale productivity changes that may occur in various marine settings due to ongoing climate change (Oschlies et al., 2018; Mancini et al., 2023a, 2023b).

Among various global regions, the Mediterranean Sea is notably affected by climate change due to its unique features: its semi-enclosed nature, location, relatively short water-mass residence time, and intricate seafloor morphology (Lionello et al., 2006; Lionello and Scarascia, 2018; Malanotte-Rizzoli et al., 2014). Within the Mediterranean Sea, the Alboran Sea—located in the westernmost Mediterranean region—is currently one of the most productive (marine primary productivity) (Morán and Estrada, 2001; Bárcena et al., 2004; Macias et al., 2015; Yebra et al., 2018; Mena et al., 2019). However, biogeochemical models predict that reduced vertical mixing in the western Mediterranean Basin, driven by lower surface water density (i.e., salinity), will lead to increased oligotrophy due to a diminished nutrient supply from deeper waters (Macias et al., 2015). In this regard, integrating contemporary observations with paleoperspectives is crucial for accurately constraining the long-term changes in primary productivity in the region.

The high sedimentation rates in the Alboran Sea provide an exceptional high-resolution archive of past climatic and oceanographic changes in the westernmost Mediterranean region (Rodrigo-Gámiz et al., 2014a, 2014b, 2015; Pérez-Asensio et al., 2020; Morcillo-Montalbá et al., 2021). Consequently, marine sediment records from this region have enabled high-resolution productivity reconstructions through various climatic events over the last millennia (Ausín et al., 2015a, 2015b; Penaud et al., 2016). Additionally, the westernmost Mediterranean region is strongly influenced by recent short-term variations (spanning from centuries to decades) in the atmospheric patterns of the North Atlantic (Fletcher et al., 2013; Fletcher and Zielhofer, 2013). Therefore, the deep sediment record of the Alboran Sea not only facilitates the reconstruction of productivity changes at a high temporal resolution in the westernmost Mediterranean, but also serves as a witness to atmospheric and ocean circulation patterns in the North Atlantic region, which significantly influence global circulation and climate (Cacho et al., 2000; Rogerson et al., 2012; Bartolomé et al., 2015).

To gain key paleoperspectives on the environmental triggers of productivity changes and on the long-term productivity responses to climate variability in the westernmost Mediterranean, as well as insights into past changes in North Atlantic atmospheric and ocean circulation patterns, this study presents a multiproxy reconstruction of oceanographic and environmental conditions in the westernmost Mediterranean region over the last 13,000 years. This period encompasses the Younger Dryas (YD: 13–11.7 ka) and the three Holocene intervals: early Holocene (11.7–8.2 ka), middle Holocene (8.2–4.2 ka), and late Holocene (4.2 ka – present), as defined by Walker et al. (2012). We focused on reconstructing changes in primary productivity and nutrient availability at multicentennial resolution. This was achieved using a combination of palynological and geochemical tools (section 3), applied to a sediment record recovered from the Western Alboran Basin at a water depth of 1306.5 m, previously dated by Morcillo-Montalbá et al. (2021). The information derived from the palynological and geochemical results of the present study is integrated with data from other marine sediment

and terrestrial Holocene records from the southern Iberian Peninsula, obtained in previous studies (section 6). This integration allows for a discussion of the core data to support regional-scale interpretations and assess potential land-sea influences on primary productivity dynamics.

## 2. Oceanographic and climatic setting

The analyzed sediment record (GP04PC) is from the Western Alboran Basin, which undergoes pronounced seasonal productivity increases and represents one of the most productive areas in the Mediterranean (D'Ortenzio and Ribera d'Alcalà, 2009; Siokou-Frangou et al., 2010; Christaki et al., 2011; Basterretxea et al., 2018). The climate of the Alboran Sea region—located between southern Iberia and North Africa in the westernmost part of the Mediterranean Sea (see Fig. 1)—is influenced by the interaction of African subtropical, North Atlantic, and Mediterranean climate systems (Rodó et al., 1997; Dünkloh and Jacobeit, 2003). The current regional climate is characterized by hot and arid summers and comparatively wetter winters, controlled by an atmospheric high-pressure situated in the North Atlantic Ocean, above the Azores archipelago (Sumner et al., 2001). The Alboran Sea experiences an annual mean sea surface temperature (SST) of  $19.5 \pm 0.3$  °C, with a strong seasonal contrast, ranging from 15 °C in February to 25 °C in August (Macias et al., 2016). Furthermore, it receives intermittent torrential riverine discharges from Morocco and Spain, as well as eolian dust inputs from the African margin, particularly the Sahara Desert, resulting in deep-sea sediments enriched in the lithogenic fraction (around 70 %) (Liquete et al., 2005; Palanques et al., 2005; Zúñiga et al., 2008).

The modern oceanographic setting of the Alboran Sea features three distinct water-masses with varying physiochemical parameters, i.e. temperature, salinity, and density. The upper part of the Alboran Sea water-column is occupied by the Modified Atlantic Water (MAW) between 0 and 200 m below sea level (mbsl), which flows eastward from the Gibraltar Strait and exhibits low salinity and density (Millot, 1999, 2009; Millot and Taupier-Letage, 2005). The MAW leads to the formation of two anticyclonic gyres: the quasi-permanent Western Alboran Gyre (WAG) and the seasonal (unstable) Eastern Alboran Gyre (EAG) (Millot, 1999; Fabres et al., 2002). Upwelling systems, characterized by cold waters and high productivity, occur at the northern edge of WAG due to the offshore pushing of MAW by north-westerlies and WAG currents (Tintoré et al., 1988; Sarhan et al., 2000; Sanchez-Vidal et al., 2005). An intense front, known as the Malaga Front, often develops at the northern edge of the WAG, where MAW meets upwelled Mediterranean water (Sarhan et al., 2000). The intensity of the WAG varies throughout the year, with weaker intensity in winter compared to summer and early autumn, possibly due to interannual variability in SST (García-Lafuente et al., 2017). WAG surface currents transport the upwelled nutrients—and associated biologically-mediated carbon—from the Iberian margin to the center of the Western Alboran Basin, where the vertical flux related to the WAG downwelling favors its export to the deep ocean (Fabres et al., 2002; Yebra et al., 2018).

Found underlying the MAW, at intermediate depths (between 200 and 600 mbsl) in the Alboran Sea, is the Levantine Intermediate Water (LIW) produced in the Levantine Basin (Eastern Mediterranean) and characterized by high salinity. The deeper water-column part, below the LIW (i.e., below 600 mbsl), is occupied by the Western Mediterranean Deep Water (WMDW), which is formed in the Gulf of Lion due to evaporation and cooling of the sea surface mostly during cold and windy winters (Fig. 1) (Millot, 1999). Deep-water formation in the Gulf of Lion is influenced by variability in wind stress and the discharge of fluvial water on the shelf, which preconditions buoyancy (Frigola et al., 2007; Cisneros et al., 2019). At the end of the general Mediterranean cyclonic pattern, the dense LIW and WMDW leave the Mediterranean Basin as mixture through the Strait of Gibraltar, forming the Mediterranean Outflow Water (MOW). This outflow is primarily driven by the Bernoulli aspiration effect caused by the narrowing and shallowing of the

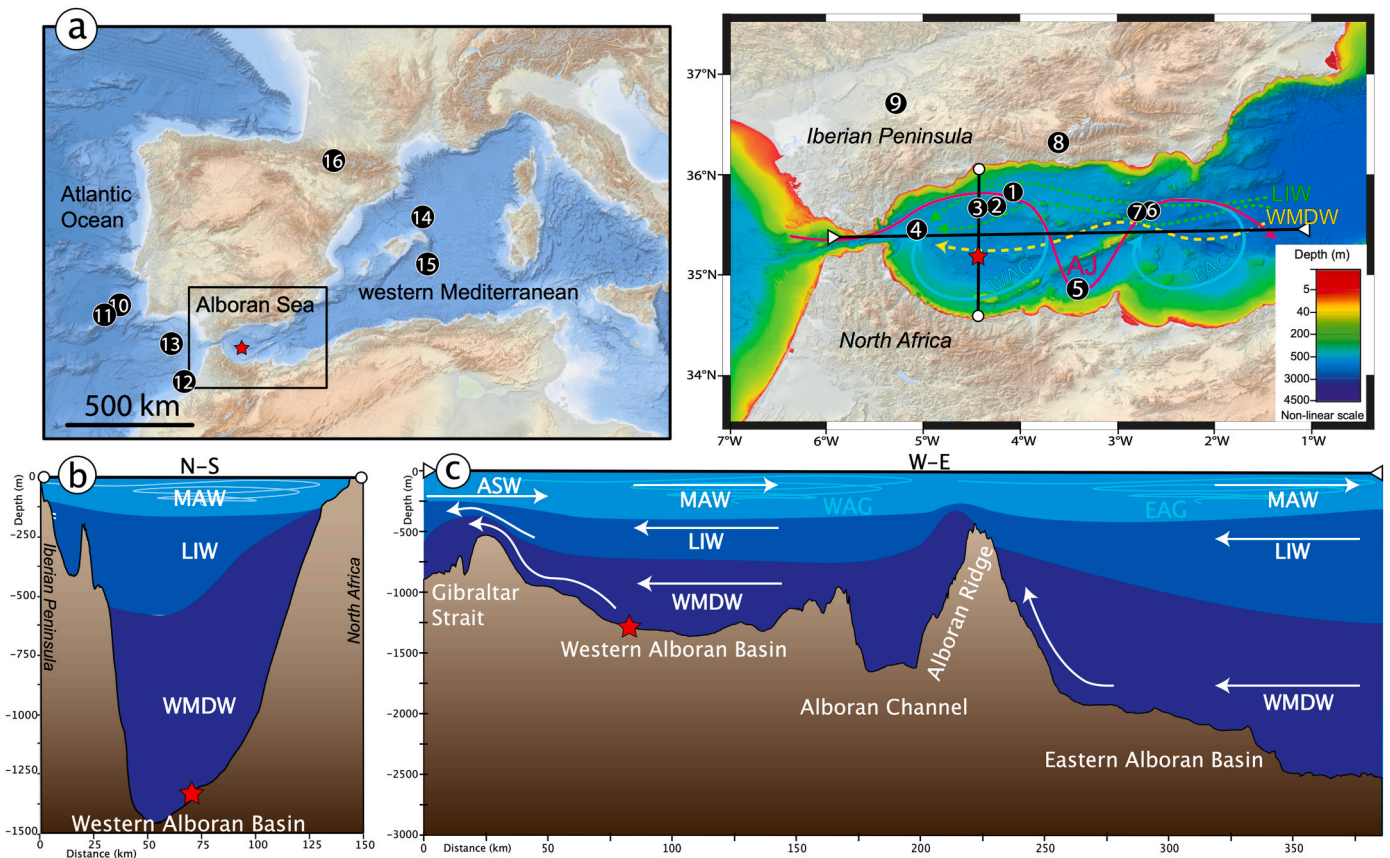


**Fig. 1.** Oceanographic setting. **Fig. 1a.** Bathymetric map of Alboran Sea. Black lines represent the bathymetric transects of **Fig. 1b** (N-S) and **1c** (W-E). The location of core GP04PC (Lat. 35.7871° N, Long. 4.5343° W; water depth 1306.5 mbsl) is indicated by a red star. The location of diverse marine and continental from previous studies used for comparison in this study are indicated by numbered black circles on the maps: (1) HER-GC-T1 (659 mbsl; Ausín et al., 2015b); (2) TTR17-434G (1108 mbsl; Mesa-Fernández et al., 2022); (3) ODP 976 (1108 mbsl; Combourieu-Nebout et al., 1999, 2009; Dormoy et al., 2009); (4) CEUTA10PC08 (914 mbsl; Ausín et al., 2015a); (5) GeoB18131-1 (457 mbsl; Wang et al., 2019); (6) MD95-2043 (1841 mbsl; Cacho et al., 2000, 2002; Fletcher et al., 2010, 2013; Penaud et al., 2011, 2016); (7) TTR12-293G (1840 mbsl; Rodrigo-Gámiz et al., 2011); (8) PADUL-15-05 (Padul wetland, Grant et al., 2016); (9) LB-15-01 (La Ballestera lake, Sevilla; García-Alix et al., 2022); (10) MD95-2042 (3146 mbsl; Penaud et al., 2011; Chabaud et al., 2014); (11) Shackleton Site U1385 (2578 mbsl; Datema et al., 2017) and SHK06-5K (2646 mbsl; Ausín et al., 2020); (12) MD04-2805CQ (859 mbsl; Penaud et al., 2010); (13) MD99-2339 (1170 mbsl; Penaud et al., 2016); (14) MD99-2343 (2391 mbsl; Frigola et al., 2007); (15) ODP Site 975 (2415 mbsl; Jiménez-Espejo et al., 2008); (16) stalagmite record (Seso Cave; Bartolomé et al., 2015). **Fig. 1b.** North to South (N-S) bathymetric transect of Western Alboran Basin. **Fig. 1c.** West to East (W-E) bathymetric transect of Western and Eastern Alboran basins. The different water-masses are illustrated with different colors. WAG: Western Alboran Gyre, EAG: Eastern Alboran Gyre, MAW: Modified Atlantic Water, AJ: Atlantic Jet, LIW: Levantine Intermediate Water and WMDW: Western Mediterranean Deep Water). The directions of the currents are indicated with arrows.

Gibraltar Strait (Millot, 1999). The MOW plays a crucial role in the broader oceanographic dynamics, including the distribution of salinity and temperature anomalies in the North Atlantic (García-Lafuente et al., 2021).

Previous studies by Cacho et al. (2000) and Rogerson et al. (2012) highlighted how deep marine sediments in the westernmost Mediterranean capture detailed oceanographic and climatic variability on millennial-scales, mainly controlled by insolation changes driven by orbital forcing, such as the precession cycle. This region also experiences centennial-scale changes primarily influenced by atmospheric and oceanographic variations in the North Atlantic, including changes in the Atlantic Meridional Overturning Circulation (AMOC), fluctuations in the latitudinal shifts/contractions of the Intertropical Convergence Zone (ITCZ), and changes in the North Atlantic Oscillation (NAO) patterns (López-Moreno et al., 2011; Frigola et al., 2008; Rodrigo-Gámiz et al., 2011; Fletcher et al., 2013; Bartolomé et al., 2015; Di Rita et al., 2018; Toney et al., 2020; García-Alix et al., 2021). The NAO is a decadal-scale atmospheric pattern driven by fluctuations in sea-level pressure between the Icelandic low and the Azores high-pressure centers; it exerts significant control on the present-day climate variability in the region (Hurrell, 1995; Rodó et al., 1997; Trigo et al., 2002). A positive NAO phase, characterized by a major pressure difference, results in stronger

north-westerlies and dry, cold winters in southern Europe, the Mediterranean, and northern Africa. Conversely, a negative NAO phase, marked by a lower pressure difference, leads to weaker north-westerly winds and increased precipitation in these regions (Wanner et al., 2001; Ilvonen et al., 2022; Benito et al., 2023).

### 3. Paleoceanographic and paleoenvironmental proxies

This study integrates various palynological and geochemical tools to comprehensively understand oceanographic and environmental conditions over the last 13,000 years in the Western Alboran Basin. It particularly focuses on reconstructing productivity responses to rapid climate variability and assessing potential links between changes in North Atlantic atmospheric patterns and the climatic and oceanographic conditions in the westernmost Mediterranean region. These proxies provide insights into environmental factors influencing marine productivity, such as nutrient availability, redox conditions, temperature variations, water-column structure, current dynamics, and changes in fluvial and aeolian input, while mitigating potential biases associated with each proxy.

### 3.1. Marine palynology: Dinocyst analysis for paleoproductivity

Dinoflagellates are (predominantly) marine single-cell protists and an important component of the eukaryotic plankton community. During their life cycle they may produce organic-walled hypnozygotic cysts, called dinocysts (Taylor, 1987). Dinoflagellate communities are very responsive to changes in nutrient availability in surface waters (Taylor et al., 2008), hence changes in dinocyst abundance and assemblages in marine sediment records have been used to reconstruct changes in primary productivity (Combourieu-Nebout et al., 1999; Radi and de Vernal, 2008; Penaud et al., 2010, 2011, 2016; Hardy et al., 2018). In marine sediment records, dinocyst analysis has become a key tool in paleoenvironmental studies for understanding eukaryotic productivity responses to oceanographic changes (e.g., nutrient availability, SST, surface current patterns, upwelling systems and water-mass mixing) linked to past climate variability (Sluijs et al., 2006; de Vernal and Marret, 2007; Sangiorgi et al., 2021).

Dinocysts can be classified mainly into two groups according to their feeding strategies: Peridinioid cysts (P-cysts) and Gonyaulacoid cysts (G-cysts) (Versteegh, 1994). P-cysts are almost exclusively formed by heterotrophic dinoflagellates that thrive on phytoplankton like diatoms and organic matter (OM) (Jacobson and Anderson, 1986). They usually dominate areas with high annual productivity associated with high nutrient availability (Sangiorgi and Donders, 2004; de Vernal and Marret, 2007; Pospelova et al., 2008; Zonneveld et al., 2013). G-cysts consist exclusively of autotrophic or mixotrophic dinoflagellates (Powell et al., 1992; Sangiorgi et al., 2006). Increased stratification and enhanced nutrient loads from rivers favor autotrophic dinoflagellates (G-cysts) relative to other non-flagellated groups such as diatoms. Dinocyst assemblages dominated by P-cysts (heterotroph dominance) have been previously identified as the primary cyst signal for upwelling (Dale et al., 2002; Dale, 2009; Bringué et al., 2014). However, it is important to note that P-cysts are more prone to degradation and oxidation in the water column and within the sediments than G-cysts (e.g., Versteegh and Zonneveld, 2002; Zonneveld et al., 2007).

Accumulation rates of total dinocysts, P-cysts, and G-cysts are expressed as the number of cysts per cm<sup>2</sup> of sediment per year ( $n$  cysts/cm<sup>2</sup> × yr) (Table 1). Dinocyst accumulation rates were obtained using the mass accumulation rate data for core GP04PC from Morcillo-Montalbá et al. (2021) and vertically plotted. Additionally, the accumulation rate of specific G-cyst and P-cysts species were individually plotted, as well as the relative percentages of each group and species to gather further paleoceanographic and environmental information according to their present hydrogeographic distribution and environmental affinities (Zonneveld et al., 2009). These species include *Brigantedinium* spp., *Selenopemphix* spp., *Trinovantedinium applanatum*, *Nematosphaeropsis labyrinthus*, *Operculodinium centrocarpum*, *Lingulodinium machaerophorum*, *Spiniferites* spp. and *Impagidinium* spp. It has been demonstrated that these species are abundant in Alboran Sea sediments and mark important paleoceanographic changes in the westernmost Mediterranean (Penaud et al., 2011, 2016).

*Brigantedinium* spp. cysts are generally the most abundant in high productivity, high nutrient environments (Dale and Fjellså, 1994; Zonneveld et al., 2001, 2013; de Vernal and Marret, 2007). This heightened cyst production, as a response to increased nutrient availability, can be tied to factors such as upwelling, frontal activity, or the input of river and/or meltwaters (Montesor et al., 1998; de Vernal and Hillaire-Marcel, 2000; Zonneveld and Brummer, 2000; Fujii and Matsumoto, 2006; Pospelova et al., 2010). It is important to take into account the fact that high occurrences of *Brigantedinium* spp. can also be linked to better preservation under hypoxic or anoxic bottom conditions (Combourieu-Nebout et al., 1998; Zonneveld et al., 2001; Penaud et al., 2010, 2011). *Selenopemphix* spp. and *T. applanatum* cysts are abundant in sediments deposited in mesotrophic/eutrophic coastal environments (Marret and Zonneveld, 2003).

High *L. machaerophorum* cyst concentrations are observed in

**Table 1**

Proxies used for the paleoceanographic reconstruction and interpretation synthesis.

Marine productivity	
Dinocyst accumulation rate ( $n$ cysts/cm <sup>2</sup> yr)	High when marine productivity is high.
Heterotrophic dinocyst accumulation rate ( $n$ cysts/cm <sup>2</sup> yr)	High when prey availability (e.g., diatoms and OM) and marine productivity is high.
Autotrophic dinocyst accumulation rate ( $n$ cysts/cm <sup>2</sup> yr)	High when marine productivity is high.
C <sub>org</sub> %	High when marine export productivity is high and during enhanced OM preservation. Susceptible to postdepositional oxidation.
δ <sup>13</sup> C <sub>carb</sub>	High when surface water productivity is high. Also influenced by vertical mixing and OM source.
Ba/Al	Reflects pelagic barite content. High when marine export productivity is high. Signal can be masked by high detrital input.
Redox conditions	
Mo/Al	High during porewater euxinia. It can be enriched during under suboxic conditions in association with Mn-oxyhydroxides during reventilation.
U/Al	High during porewater anoxia. Can suffer postdepositional remobilization. Tends to associate with OM under anoxic conditions.
V/Al	High during porewater anoxia/euxinia. Tends to associate with OM under anoxic conditions or iron sulfides during euxinia.
Others Al-normalized RSTMs (Cu, Co, Zn, Ni, Cr and Pb)	Tend to associate with Fe-sulfides during euxinic porewater or with Mn-oxyhydroxides during suboxic bottom-waters.
Mn/Al	High during suboxic bottom-water. Mn peaks tend to develop at the top of organic-rich sediments during rapid bottom-water reventilation. Also, at the current oxidation front as Mn-oxyhydroxides.
Bottom-current intensity	
Ti/Ca	High when bottom-current intensity is high.
Detritic input	
Rb/Al and Mg/Al	High when fluvial input is high. Higher during wet regional conditions.
Zr/Al and Ti/Al	High when aeolian input is high. Higher during arid regional conditions.
Mg/Ti	Synthesizes the relative proportion of aeolian input versus fluvial input, which depends on regional climate conditions. Higher values indicate more humid conditions, while lower values suggest more arid conditions.
Organic matter source	
C <sub>org</sub> /N <sub>total</sub> vs. δ <sup>13</sup> C <sub>org</sub> cross-plot	Indicates main source of OM (marine vs terrestrial).

sediments below (seasonal) upwelling cells (Sangiorgi and Donders, 2004; Zonneveld et al., 2013), in seasonally stratified sectors affected by river plumes as occurred during sapropel deposition in Eastern Mediterranean (van Helmond et al., 2015; Zwiép et al., 2018), and in nutrient-rich brackish environments such as the Black Sea (Marret and Zonneveld, 2003). *O. centrocarpum* is considered one of the most cosmopolitan species. However, in Alboran and Atlantic Iberian Margin sediments, the increases in *O. centrocarpum* cysts are considered potential signs of the influence of river plumes and of increased Atlantic surface water inflow into the Gulf of Cadiz (Penaud et al., 2016). *N. labyrinthus* is a cosmopolitan species that may be present in high relative abundances in sediments deposited in cool/eutrophic marine environments and in ocean frontal systems (Marret and Zonneveld, 2003). Regarding certain *Impagidinium* species (i.e., *I. aculeatum* and

*I. sphaericum*), Penaud et al. (2010, 2016) suggest that they are enriched in westernmost Mediterranean and North Atlantic sediments during periods characterized by warmer surface waters (i.e., Bölling-Allerød and Holocene).

*Spiniferites* spp. is a group that encompasses species with different ecological affinities and geographical distributions, ranging from temperate to equatorial coastal regions (Zonneveld et al., 2013; Penaud et al., 2010, 2011, 2016; Datema et al., 2017). Consequently, the accumulation rate of *Spiniferites* spp. cysts cannot be used to reconstruct Western Alboran SST. Still, the accumulation rate of *Spiniferites* spp. may offer qualitative insights into surface water primary productivity and complement the information provided by other dinocyst groups and species. Although the identification of *Spiniferites* species was not conducted in this study, Penaud et al. (2016) provide detailed data on the accumulation rates of these species throughout the study interval in core MD99-2339 (located in the Gulf of Cadiz, with a 300-year resolution) to elucidate changes in SST.

### 3.2. Geochemical proxies for productivity

Barium (Ba) content in marine sediments has been broadly used as a proxy to reconstruct past oceanic export productivity (e.g., Francois et al., 1995; McManus et al., 1998; Gingele et al., 1999; Paytan and Griffith, 2007; Carter et al., 2020). Ba increases in westernmost Mediterranean sediments have been related to increases in pelagic barite ( $\text{BaSO}_4$ ) and thus linked to periods of increased primary productivity and OM degradation in the mesopelagic zone (Table 1) (e.g., Jiménez-Espejo et al., 2007; Jiménez-Espejo et al., 2008; Martínez-Ruiz et al., 2015). While the high detrital input in Alboran Sea basin normally dilutes the pelagic barite content (with detrital Ba input expected to be higher than in other Mediterranean basins), the pelagic barite is generally well preserved in this basin. Barite only dissolves in sediments with sulfate-depleted porewaters and may reprecipitate upon encountering oxidized conditions (e.g., oxidation fronts) resulting in marked Ba/Al ratio peaks above or below the organic-rich sediments (e.g., Henkel et al., 2012; Grema et al., 2022). When pelagic barite dissolution and Ba remobilization are not observed, the Ba/Al ratio can be successfully applied as a qualitative paleoproductivity proxy (e.g., Martínez-Ruiz et al., 2000; Carter et al., 2020; Light et al., 2023).

The OM content in marine sediments is normally expressed as  $C_{\text{org}}\%$  or TOC% (Total Organic Carbon dry weight %).  $C_{\text{org}}$  in marine sediments represents just a fraction of the total biological productivity in surface waters, since only a small OM fraction “escapes” the efficient C-cycling and oxidation in the water-column and reaches the seafloor; this fraction is known as “export productivity” (Table 1) (Canfield, 1994; Tribouillard et al., 2006). During sinking and deposition OM suffers degradation, so that  $C_{\text{org}}\%$  does not directly reflect surface water productivity, but rather the interplay between surface water productivity, water-column redox conditions, accumulation rate and degree of preservation within the sediments, since after deposition OM may still suffer oxidation. Notwithstanding, changes in  $C_{\text{org}}\%$  in marine sediments tend to reflect correlative changes in surface water productivity.

The main control on the  $\delta^{13}\text{C}_{\text{org}}$  signature variation is the vegetation type (marine vs continental plants) from which the OM derive: marine algae are isotopically heavier than land plants (Meyers, 1994 and references therein). Consequently, variations in  $\delta^{13}\text{C}_{\text{org}}$  help to recognize the main source of OM in export productivity in deep-marine basins (Table 1). In this sense, the  $C_{\text{org}}/N_{\text{total}}$  ratio is also used to identify variations in OM input and relative composition of land- and marine-derived components of sedimentary OM (Meyers, 1994). Algae typically have atomic  $C_{\text{org}}/N_{\text{total}}$  ratios between 4 and 10, whereas vascular land plants have  $C_{\text{org}}/N_{\text{total}}$  ratios of  $\geq 20$ . Selective degradation of OM components during early diagenesis might influence the original organic geochemical signals. But despite extensive early diagenetic losses of OM and of some of its important biomarker compounds,  $C_{\text{org}}/N_{\text{total}}$  ratio and  $\delta^{13}\text{C}_{\text{org}}$  appear to undergo little change (Meyers,

1994; Tyson, 1995). Consequently, the  $\delta^{13}\text{C}_{\text{org}}$  vs  $C_{\text{org}}/N_{\text{total}}$  cross-plot is a robust tool that allows one to assess the main source of OM that reaches deep-marine basins.

Meanwhile, variations in  $\delta^{13}\text{C}$  in the shell of the planktonic foraminifera *Globigerina bulloides* can indicate variations in marine productivity in the photic zone (Table 1). The carbon isotopic composition of planktonic foraminifera shells (i.e.,  $\delta^{13}\text{C}_{\text{carb}}$ ) tend to reflect the carbon isotopic composition of the dissolved inorganic carbon in ambient water. *G. bulloides* is a nonsymbiotic species; hence, photosynthesis would not influence the fractionation of carbon isotopes (Naidu and Niituma, 2004). *G. bulloides* take carbon for shell growth in the  $^{12}\text{C}/^{13}\text{C}$  ratio present in the upper water-column. The isotopic carbon composition in the upper water-column can vary as a function of biological processes and productivity intensity in the photosynthetic zone. During kinetic fractionation, photosynthetic organisms preferentially take the lighter over the heavier isotope. Therefore,  $\delta^{13}\text{C}_{\text{carb}}$  variations in *G. bulloides* serve to identify changes in marine productivity, where less negative  $\delta^{13}\text{C}_{\text{carb}}$  values indicate more intense marine productivity.

Changes in the source of OM, as well as the proportion of C3 and C4 plants, can significantly affect the  $\delta^{13}\text{C}$  signals in *G. bulloides* shells. Variations in these factors can lead to differing  $\delta^{13}\text{C}$  values, complicating the interpretation of paleoceanographic and paleoclimatic records. For instance, a higher proportion of C4 plants, which utilize a different photosynthetic pathway than C3 plants, can result in more enriched  $\delta^{13}\text{C}$  values (Fogel and Cifuentes, 1993). Similarly, shifts in OM sources—such as from terrestrial to marine or from different types of vegetation—can alter the isotopic composition (Meyers, 1994; Katz et al., 1999; Schouten et al., 2000).

### 3.3. Geochemical proxies for redox conditions

Under oxygen-deficient conditions in marine systems, authigenic minerals (e.g., sulfides and oxyhydroxides) enriched in trace metals (TMs) precipitate, leading to an enrichment of redox-sensitive trace metals, herein RSTMs (e.g., Mo, U, V, Re, Cu, Co, Ni, Cr, Zn and Pb) in the sediments. In marine sediments Mo, Ni, Co, Cu, Cr, Zn and Pb can be authigenically fixed (i) in association with Mn and Fe oxyhydroxides under suboxic conditions, or (ii) in association with iron sulfides under euxinic conditions, whereas U tends to be enriched in association with OM under anoxic to euxinic conditions (Algeo and Maynard, 2004; Tribouillard et al., 2006, 2012; Monedero-Contreras et al., 2023b). To assess the variability of TMs, their concentrations are normalized to aluminum (Al). This normalization approach is preferred because Al is considered a conservative element and accounts for the influence of detrital input variability, which can significantly affect TM concentrations (Tribouillard et al., 2006; Algeo and Li, 2020; Algeo and Liu, 2020; Paul et al., 2023).

Once Al-normalized, these trace metals can serve as redox proxies to discern different redox conditions in modern and ancient marine environments (Berner, 1981; Tyson and Pearson, 1991; Calvert and Pedersen, 1993, 2007; Crusius et al., 1996; Warning and Brumsack, 2000; Algeo and Maynard, 2004; Tribouillard et al., 2006; Little et al., 2015; Paul et al., 2023). Consequently, Al-normalized metals (e.g., Fe/Al, Mn/Al, U/Al, V/Al, Mo/Al, Ni/Al, Cu/Al, Cr/Al, Co/Al, Zn/Al and Pb/Al) are employed to identify paleoredox changes in the westernmost Mediterranean deep-waters over the last 13,000 years and recognize potential geochemical processes during early diagenesis (e.g., post-depositional oxidation) (Table 1) (Moreno et al., 2004; Jiménez-Espejo et al., 2007; Rodrigo-Gámiz et al., 2011; Nieto-Moreno et al., 2011, 2013; Mesa-Fernández et al., 2022; Monedero-Contreras et al., 2023a, 2023b).

### 3.4. Geochemical detrital proxies

Aluminum-normalized detrital elements have been widely used to illustrate terrigenous fluctuations in the Mediterranean region

(Martínez-Ruiz et al., 2015; Calvert and Pedersen, 2007; Frigola et al., 2007, 2008; Jiménez-Espejo et al., 2007; Jiménez-Espejo et al., 2008; Rodrigo-Gámiz et al., 2011). Zr/Al and Ti/Al ratios were used to assess variations in aeolian input, as enrichments in Zr and Ti in Mediterranean sediments are primarily associated with increased content of zircon and rutile minerals, respectively, which are predominantly supplied by Sahara dust during arid periods (Table 1) (Jiménez-Espejo et al., 2014). In turn, Rb/Al and Mg/Al ratios are used to assess fluvial input variability. These elemental ratios were successfully employed to track fluvial input variability over the last 20 ka in the Eastern Alboran Basin by Rodrigo-Gámiz et al. (2011), as Rb and Mg tend to be enriched in association with clay minerals delivered to the western Mediterranean by rivers (Table 1). Additionally, the Ti/Ca ratio has been used as a proxy to assess Alboran Sea bottom-water dynamics throughout the Holocene (Table 1) (Mesa-Fernández et al., 2022).

## 4. Material and methods

### 4.1. Core description, chronology and sampling

The studied marine sediment record is a piston core, GP04PC, 872.25 cm in length, recovered from the West Alboran Sea Basin at 1306.5 mbsl during the oceanographic cruise Gasalb onboard the R/V Pelagia in November 2011 (Fig. 1). The core site (35.7871° N, 4.5343° W) is located below the quasi-permanent anticyclonic gyre WAG. Core sediment lithology is very homogeneous and dominated by dark-greenish hemipelagic mud-clays with some foraminifera and shell fragments, with intervals of increased OM content (Morcillo-Montalbá et al., 2021). The GP04PC age model based on  $^{14}\text{C}$  dates was determined by Morcillo-Montalbá et al. (2021). Ten samples were selected for extracting 10 mg of planktonic foraminifer *G. bulloides* (size fraction >125  $\mu\text{m}$ ). The GP04PC chronology was generated using the R-code package rbacon 3.6.2 software (Blaauw and Christen, 2011) and the Marine20 calibration curve (Heaton et al., 2020). According to the GP04PC age model, the 872.25 cm long core covers the last 35,000 years (Fig. 2). For detailed age model information, refer to Morcillo-Montalbá et al. (2021). This study focuses on the YD and the Holocene (past ~13 ka), represented by the top ~250 cm of the GP04PC core, with a mean sedimentation rate of 20 cm/kyr (Fig. 2). The age model for the studied interval (last 13 ka) is based on three  $^{14}\text{C}$  data points: 116.75 cm, 217.75 cm, and 320.75 cm (Morcillo-Montalbá et al., 2021, Fig. 2). However, the age model for the entire length of GP04PC sediment core considers ten  $^{14}\text{C}$  data points (Fig. 2). The studied section was sampled at 1.5 cm intervals for geochemical analysis (XRF and ICP-MS), with a total of 85 samples and a temporal resolution of ~145 years. Out of the 85 samples, 45 samples were selected for palynological and organic geochemical analyses, providing a resolution of ~250–300 years for dinocyst analysis covering the last 13 ka.

### 4.2. Dinoflagellate cysts

Sediment samples for dinocyst analysis were prepared at the Utrecht University GeoLab using a standard palynological preparation technique. Each sample, consisting of ~2–4 g of dry-weight sediment, was oven-dried at 60 °C and exactly weighed. One *Lycopodium clavatum* tablet (19,855,  $\pm 829$  spores) was added to each sample to ensure quantitative control (Wood, 1996; Mertens et al., 2012). Carbonates were removed by gradually adding hydrochloric acid (HCl, 30 %), the samples settled overnight, and were then rinsed with demineralized water to obtain a neutral pH. To remove silicates, the samples were processed with cold hydrofluoric acid (HF, 38 %) and placed for 2 h on a shaker. Samples were decanted and any precipitated fluorosilicates were removed with HCl 30 %. The remaining residues were sieved over a 10  $\mu\text{m}$  nylon mesh screen. The sieved residues were diluted with deionized water in 1.5 ml safe-tubes and carefully poured over a cover slip using a Pasteur-pipette. Subsequently, a microscopic slide was mounted over

Core depth (cm)	$^{14}\text{C}$ AMS age (yrs BP)	Calibrated age (cal. yrs BP)
116.75	6210 $\pm$ 35	6441 $\pm$ 232
217.75	10,290 $\pm$ 60	11,431 $\pm$ 340
320.75	12,510 $\pm$ 80	13,987 $\pm$ 192
422.75	15,160 $\pm$ 90	17,659 $\pm$ 386
565.25	18,600 $\pm$ 140	22,230 $\pm$ 491
572.75	19,710 $\pm$ 110	22,571 $\pm$ 437
667.25	21,890 $\pm$ 180	27,171 $\pm$ 456
716.75	24,960 $\pm$ 170	29,119 $\pm$ 591
809.25	28,040 $\pm$ 230	32,547 $\pm$ 630
872.25	31,700 $\pm$ 500	35,241 $\pm$ 976

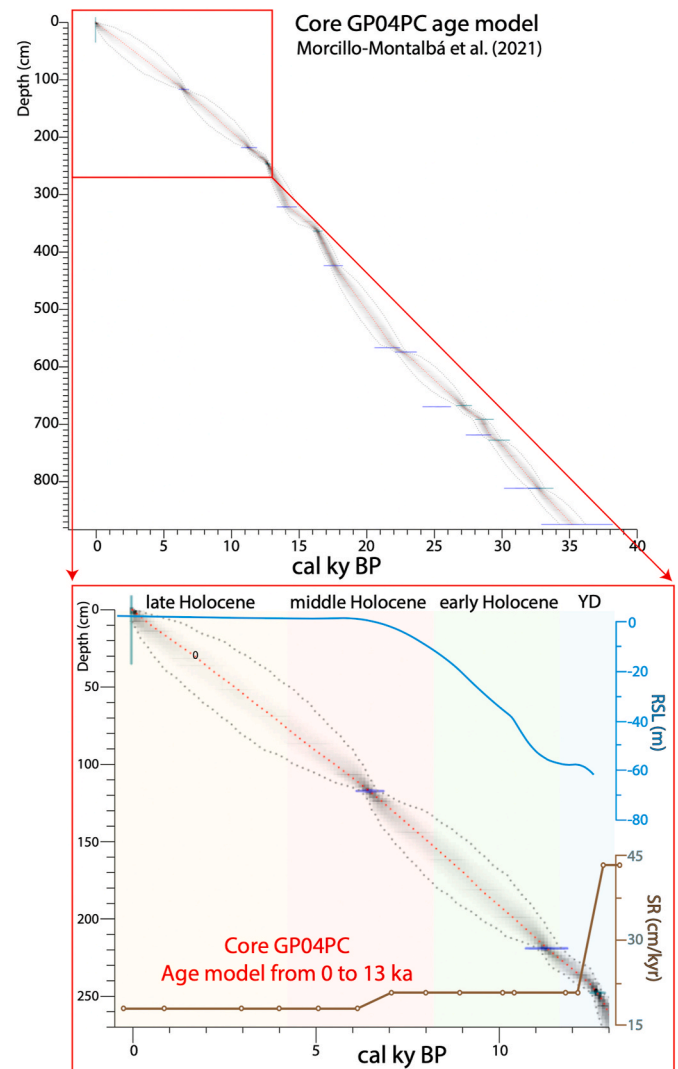


Fig. 2. GP04PC age model from Morcillo-Montalbá et al. (2021) based on Accelerator mass spectrometry (AMS)  $^{14}\text{C}$  dates. The studied time interval has been magnified and Relative Sea Level (RSL) from Lambeck et al. (2014) and sedimentation rate (SR) of core GP04PC (Morcillo-Montalbá et al., 2021) for the last 13 ka are plotted for context. Refer to Morcillo-Montalbá et al. (2021) for age model details.

the cover slip using transparent glue. A systematic count of a minimum of 280 dinoflagellate cysts (dinocysts) was conducted on each slide using an Olympus BX41 microscope at 40X magnification. Dinocyst taxonomy followed Williams et al. (2017), and dinocyst identification was performed following Zonneveld and Pospelova (2015).

### 4.3. Major and trace element analyses

Major elements in discrete bulk sediment samples were analyzed in fused beads by means of XRF. Analyses were carried out at Instituto Andaluz de Ciencias de la Tierra (IACT, CSIC-UGR, Spain), with a S4 Pioneer from BRUKER, equipped with a 4 kW wavelength dispersive X-ray fluorescence spectrometer (WDXRF) and a Rh anode X-ray tube (60 kV, 150 mA). XRF precision was better than  $\pm 0.3\%$  for major elements. Trace elements in discrete sediment samples were measured at the Scientific Instrumentation Center (CIC, University of Granada, Spain) with an ICP-MS NexION 300d (PerkinElmer) spectrometer using Rh as internal standard. For trace elements, ICP-MS precision was better than  $\pm 5\%$  for analyte concentrations of 10 ppm (Bea et al., 1996). For ICP-MS analyses, samples were oven-dried at  $60\text{ }^\circ\text{C}$  and then powdered in an agata mortar. Samples were processed in batches of 25–30 samples and an analytical blank was added to each batch. Solutions for ICP-MS analyses were prepared using 0.1 g of powdered sample in Teflon vessels, where successive acidifications with  $\text{HNO}_3$  (ultra-pure, a 69 % concentration) and HF (48 % concentration) were performed at  $130\text{ }^\circ\text{C}$  until evaporation. A final acid digestion with  $\text{HNO}_3$  and water at  $80\text{ }^\circ\text{C}$  for 1h was performed to achieve a total acid dissolution/digestion of the samples. Subsequently, dissolved samples were diluted with Milli-Q water in volumetric flasks of 100 ml (Bea et al., 1996).

### 4.4. Organic carbon analyses

The total organic carbon content ( $C_{\text{org}}\%$ ), total nitrogen content ( $N_{\text{total}}\%$ ), and stable carbon isotopic composition of the OM ( $\delta^{13}C_{\text{org}}$ ) were obtained in GP04PC core samples at the Geolab of Utrecht University (The Netherlands). Dried samples were powdered with an agata mortar and 1g of sample was weighed in a 50 ml Greiner centrifuge tube. To remove carbonates, dried sediments were acidified with 25 ml of 1M HCl, followed by 4 h of shaking, centrifugation and decanting. This procedure was repeated but with 12 h of shaking. Then, samples were washed twice with demineralized water to remove acids, and oven-dried for 72 h at  $60\text{ }^\circ\text{C}$ . The decalcified and dried sediments were weighed (about 15–20 mg) in silver foil cups.

The  $C_{\text{org}}\%$  and  $N_{\text{total}}\%$  were obtained using an Elemental Analyzer (EA) IsoLink CN IRMS System from Thermo Scientific. This system includes the Flash IRMS Elemental Analyzer, a Delta V Advantage IRMS, and a ConFlo IV Universal Interface that allowed carbon isotope measurements of the sedimentary OM (i.e.,  $\delta^{13}C_{\text{org}}$ ). The  $C_{\text{org}}\%$  and  $N_{\text{total}}\%$  are expressed as weight percentage (wt %) of the dried sediment. Based on the standard deviation of replicate runs of laboratory standards (atropine, acetanilide and IVA), analyzed before and after the series, and after each 12 measurements, the analytical error (standard deviation) was on average  $< 0.2\text{ wt } \%$  for  $C_{\text{org}}\%$  and  $N_{\text{total}}\%$ . The  $\delta^{13}C_{\text{org}}$  values are reported relative to the Vienna Pee Dee Belemnite (V-PDB) standard and corrected for blank contribution. NBS-19 was used as the standard and the analytical reproducibility of  $\delta^{13}C_{\text{org}}$  was usually better than  $0.1\text{ } \%$ .

$\delta^{13}C$  was also measured in the carbonate present in the shell of planktonic foraminifera ( $\delta^{13}C_{\text{carb}}$ ) and calculated using the same equation.  $\delta^{13}C_{\text{carb}}$  analysis was performed on ca. 10 specimens of *G. bulloides* (size fraction  $>125\text{ }\mu\text{m}$ ) picked from intervals of the 3 cm sediment samples. Selecting *G. bulloides* having a size fraction greater than  $125\text{ }\mu\text{m}$  ensures isotopic consistency and ecological representativeness, as larger specimens are more likely to have reached isotopic equilibrium with ambient seawater, minimizing vital effects. The carbon isotopic composition of foraminiferal samples was analyzed with an automated Finnigan-MAT Kiel Device Type I, coupled to a Finnigan-MAT 251 mass spectrometer at the Leibniz Laboratory for Radiometric Dating and Stable Isotope Research from the Christian Albrechts University of Kiel (Germany). Results were also calibrated to the V-PDB by means of the NBS-19 carbonate isotope standard and by calibrated lab standards. The analytical reproducibility of the instrument was  $\pm 0.07\text{ } \%$  for  $\delta^{18}\text{O}$  and  $\pm 0.04\text{ } \%$  for  $\delta^{13}C$  (Morcillo-Motalbá et al., 2021). Both  $\delta^{13}C$  values (i.e.,

$\delta^{13}C_{\text{org}}$  and  $\delta^{13}C_{\text{carb}}$ ) were obtained by means of the following equation:  $\delta^{13}C = (([^{12}C]/[^{13}C])_{\text{sample}}/([^{12}C]/[^{13}C])_{\text{standard}} - 1) \times 1000\text{ } \%$ .

## 5. Results

### 5.1. Dinocyst analysis

The GP04PC record contains abundant and well-preserved dinocysts, with accumulation rates ranging from  $\sim 1500$  to over 30,000 cysts per kyr. Interestingly, some dinocysts have diagenetic pyrite crystals infilling their cavities, particularly in samples corresponding to the YD and Organic-Rich Layer-1a (ORL-1a). Only species and groups exceeding 5 % in one or more samples were individually plotted and considered in a relative percentage plot, following the methodology of Datema et al. (2017) (Fig. 3). Among the Protoperidinium heterotrophic cysts (P-cysts), *Brigantedinium* spp. and *S. quanta* are the most abundant. *Brigantedinium* cysts are the most abundant cysts of all, at times representing more than 75 % of the total counted cysts. *Impagidinium* spp., *O. centrocarpum* and *L. machaerophorum* are present throughout the entire GP04PC core. During the YD there is a higher accumulation rate of P-cysts (around 18,000 cysts per kyr) and G-cysts (around 15,000 cysts per kyr), but it decreases rapidly during the onset of the early Holocene ( $\sim 11.7\text{ ka}$ ). From  $\sim 12.4$  to  $11.7\text{ ka}$  *O. centrocarpum*, *Spiniferites* spp. and *L. machaerophorum* cysts exhibit their highest accumulation rates. Moreover, the *Nematosphaeropsis* spp. cyst accumulation rate is high during this period (over 4000 cysts per kyr) (Fig. 4).

From  $\sim 10$  to  $8.5\text{ ka}$  there is an increase in cyst accumulation rate (around 5000 cysts per kyr), in both P-cysts (e.g., mainly *Brigantedinium* cysts; around 4500 cysts per kyr) and G-cysts (e.g., mainly *Spiniferites* spp. and *Impagidinium* spp. cysts; around 1000 and 250 cysts per kyr; respectively). Right after this increase, total cyst flux decreased, reaching close to 1500 cysts per kyr around  $7.6\text{ ka}$ . From  $\sim 7.6\text{ ka}$  to the present, the cyst accumulation rate is low. However, around  $4.5\text{ ka}$  and throughout the late Holocene, an increase in *L. machaerophorum*, *Spiniferites* spp. and *S. quanta* cyst accumulation rates is seen (Fig. 4). Consult Supplementary Material for detailed results.

### 5.2. Geochemical data

#### 5.2.1. Aluminum-normalized trace metal contents

The enrichment patterns of various trace metals in the studied record (Fig. 5a) display distinctive trends over the last 13 ka (Figs. 6 and 7). From 13 to  $12.3\text{ ka}$ , most trace metals, including Ba, Mo, Fe, U, Cu, and Zn, exhibit lower concentrations compared to the significant increase observed around  $12.3\text{ ka}$ . Notably, these elements show a sharp rise in concentration at  $\sim 12.3\text{ ka}$ , followed by an abrupt decline around  $11.7\text{ ka}$  (Figs. 6 and 7). Between  $\sim 11.7$  and  $6.8\text{ ka}$ , trace metals such as Ba, U, V, Cu, Co, Cr, Zn, and Pb maintain consistent enrichment levels (Figs. 6 and 7). During this period, only Mo and Fe show minor increases in concentration, particularly between  $\sim 10$  and  $8.5\text{ ka}$  (Fig. 6), and this enrichment is accompanied by an increase in  $C_{\text{org}}$  content (Figs. 6 and 7). After  $6.8\text{ ka}$ , concentrations of most trace metals decrease; however, Cu and V display significant variability from  $\sim 5$  to  $2\text{ ka}$ , while U remains moderately enriched from  $\sim 4.5$  to  $1\text{ ka}$  (Fig. 6). Within the uppermost interval of core GP04PC ( $\sim 0.5\text{ ka}$ ), Mn, Fe, Mo, Cu, Zn, and Pb exhibit a peak. It is noteworthy that this is the only interval where Mn showed a marked enrichment (Fig. 6). The Ba record does not have evident peaks that might be linked to diagenetic remobilization (Fig. 7).

#### 5.2.2. Aluminum-normalized detrital elements

Ti/Al values remain high throughout the entire YD period, while Rb/Al values are consistently low (Fig. 7). The Zr/Al ratio increases from  $\sim 12.4$  to  $11.7\text{ ka}$ , accompanied by an increase in Mg/Al ratios. However, at  $\sim 11.7\text{ ka}$ , Zr/Al values show a marked decrease, which remains steady until  $\sim 0.5\text{ ka}$ , when Zr/Al values increase again (Fig. 7). Between  $\sim 11.7$  and  $6.8\text{ ka}$ , Ti/Al ratios gradually decrease, while Rb/Al ratios

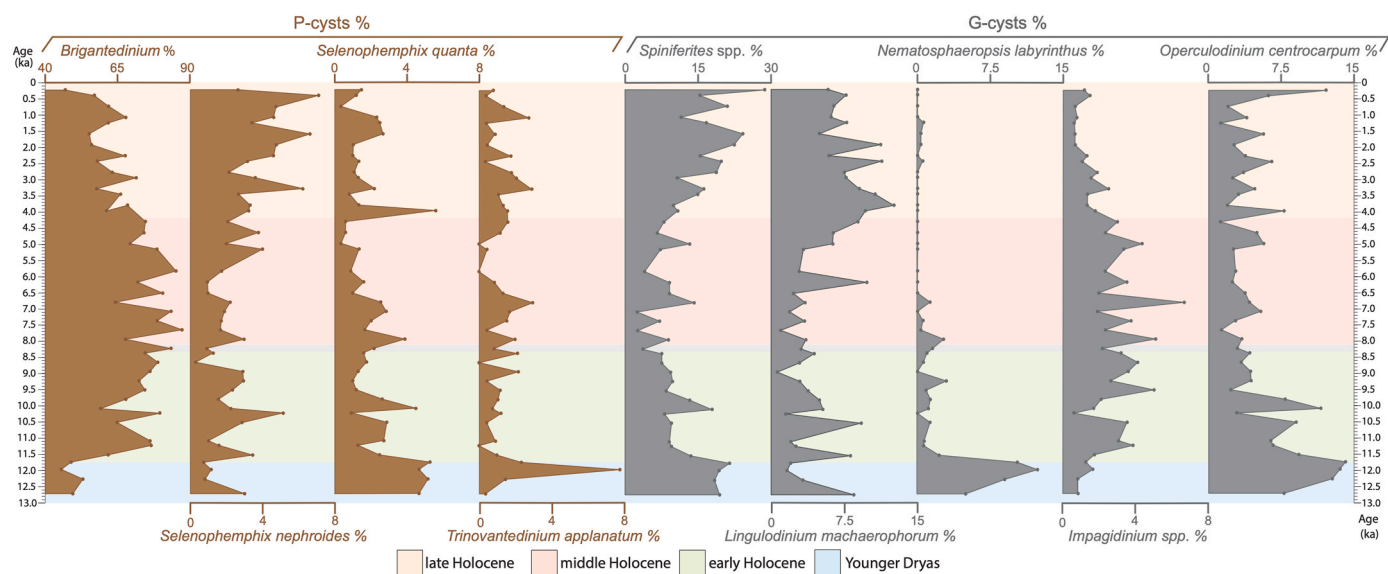


**Fig. 3.** Relative abundances of dinocyst taxa that exceed 5 % in one or more samples at Western Alboran Basin (core GP04PC) over the last 13 kyr. These species include *Brigantidium* spp., *Selenopemphix quanta*, *Selenopemphix nephroides*, *Trinovantedinium applanatum*, *Nematosphaeropsis labyrinthus*, *Operculodinium centrocarpum*, *Lingulodinium machaerophorum*, *Spiniferites* spp. and *Impagidinium* spp. P-cysts: Protoperidinium cysts, G-cysts: Gonyaulacoid cysts.

gradually increase. Around 6.8 ka, Mg/Al and Rb/Al ratios show a significant decrease, while Ti/Al values exhibit a marked increase that persists until the present (Fig. 7). Additionally, from ~6.8 ka to the present, Rb/Al and Ti/Al ratios strongly fluctuate. From ~3.5 to 1.5 ka, Mg/Al values show a minor increase, but after ~1.5 ka, they steadily decrease (Fig. 7).

During the YD, Ti/Ca values decrease, reaching their lowest levels of the entire studied interval (last 13 ka) at the end of the YD period, around 11.7 ka (Fig. 7). At the onset of the early Holocene, Ti/Ca values rise sharply. From ~11.7 to 7 ka, Ti/Ca values gradually decrease, reaching their lowest values within the Holocene around 7 ka (Fig. 7). Between ~7 and 4.2 ka, Ti/Ca ratios increase, followed by a decrease around 4.2 ka until 3 ka. After this, Ti/Ca values progressively increase, reaching peak values in the present (Fig. 7).

#### 5.2.3. Organic carbon content and organic matter source

Over the past 13,000 years, sediment composition reveals varying OM content. During the YD, OM content is relatively high ( $C_{org} > 0.8\%$  at ~12 ka), but it decreases to 0.6 % between ~11.7 and 10.0 ka. From ~10.0 to 8.5 ka sediments are notably enriched in OM, with  $C_{org}$  content reaching its maximum value (0.86 %) over the last 13.0 ka. From ~8.5 to 7.5 ka,  $C_{org}$  content progressively decreases, reaching its lowest level (~0.5 %) within the study interval (Fig. 7). From 6.8 ka to the present,  $C_{org}$  content progressively increases, exceeding 0.8 % at the top of the core. Regarding the  $C_{org}/N_{total}$  ratio, most samples show values around 5, while  $\delta^{13}C_{org}$  values in most samples are close to  $-22\%$  (Figs. 5 and 7). These results suggest that, over the last 13 ka, OM in all GP04PC sediment samples primarily originates from a marine source (Meyers, 1994). Moreover, the OM in deep sediments of the Western Alboran Basin is predominantly a mixture of bacteria and marine particulate organic carbon (POC), with negligible terrestrial OM (Meyers, 1994, Fig. 5).

#### 5.2.4. $\delta^{13}C_{carb}$ values

$\delta^{13}C_{carb}$  values vary from  $-2$  to  $0\%$  (Fig. 5); its vertical (i.e., chronological) trend can be divided in three phases. In the first phase, spanning from 13 to 11.7 (i.e., YD period), most values range from  $-0.5$  to  $0\%$ . In the second phase, from 11.7 to 6.8 ka,  $\delta^{13}C_{carb}$  exhibits more negative values and relatively low variability, with most values ranging between  $-2$  and  $-1.5\%$ . The third phase, from 6.8 ka to present, is characterized by a progressive increase in  $\delta^{13}C_{carb}$  values, from ~ $-1.5$

to  $0.5\%$ . However, during the late Holocene (from ~4.2 ka to present) the  $\delta^{13}C_{carb}$  values exhibit abrupt variability, with a seesaw-like trend (Fig. 7).

## 6. Discussion

### 6.1. Marine productivity responses to climate variability in westernmost Mediterranean over the last 13 ka

The studied sediment record has provided relevant paleoperspectives to better constrain the climatic and oceanographic factors controlling the long-term (from several decades to centuries) marine productivity responses in the Mediterranean. The applied multiproxy approach made it possible to identify two distinct oceanographic periods of greater marine productivity and nutrient availability over the past 13,000 years: (i) during the YD humid/warmer phase (~12.4–11.7 ka), with exceptionally high productivity conditions; and (ii) during the Holocene humidity optimum (~10.5–8.5 ka). Furthermore, throughout the late Holocene (approximately 4.2 ka to the present), the Western Alboran Basin underwent suborbital productivity oscillations and maintained higher productivity conditions as compared to most other basins in the Mediterranean, despite regional aridification. Each scenario of enhanced marine productivity is demonstrated to be governed by the interplay of diverse regional and local oceanographic and climatic conditions, and to operate at different time scales, as explained below.

#### 6.1.1. Younger Dryas humid phase (~12.4–11.7 ka)

In the westernmost Mediterranean, the YD can be divided into two phases with contrasting climatic conditions: a dry/cold phase (~13–12.4 ka) and a humid/warmer phase (~12.4–11.7 ka) (Combourieu-Nebout et al., 1999, 2009; Dormoy et al., 2009; Rodrigo-Gámiz et al., 2011, 2014b; Bartolomé et al., 2015). From ~13 to 12.4 ka, the Alboran Sea was characterized by cold SST (below ~ $15\text{ }^{\circ}\text{C}$ ; Cacho et al., 2001, 2002; Rodrigo-Gámiz et al., 2014a; Català et al., 2019; Morcillo-Montalbà et al., 2021) and sea-level around 40 m below the present (Fig. 2; Lambeck et al., 2014). During this arid phase, cold conditions promoted a re-advance of the glaciers that had persisted during the Bølling-Allerød, and even the formation of new glaciers in the Alps and Pyrenees mountains (García-Ruiz et al., 2016 and references therein). Marine productivity during this period in the westernmost Mediterranean was moderate, according to dinocyst accumulation rates,

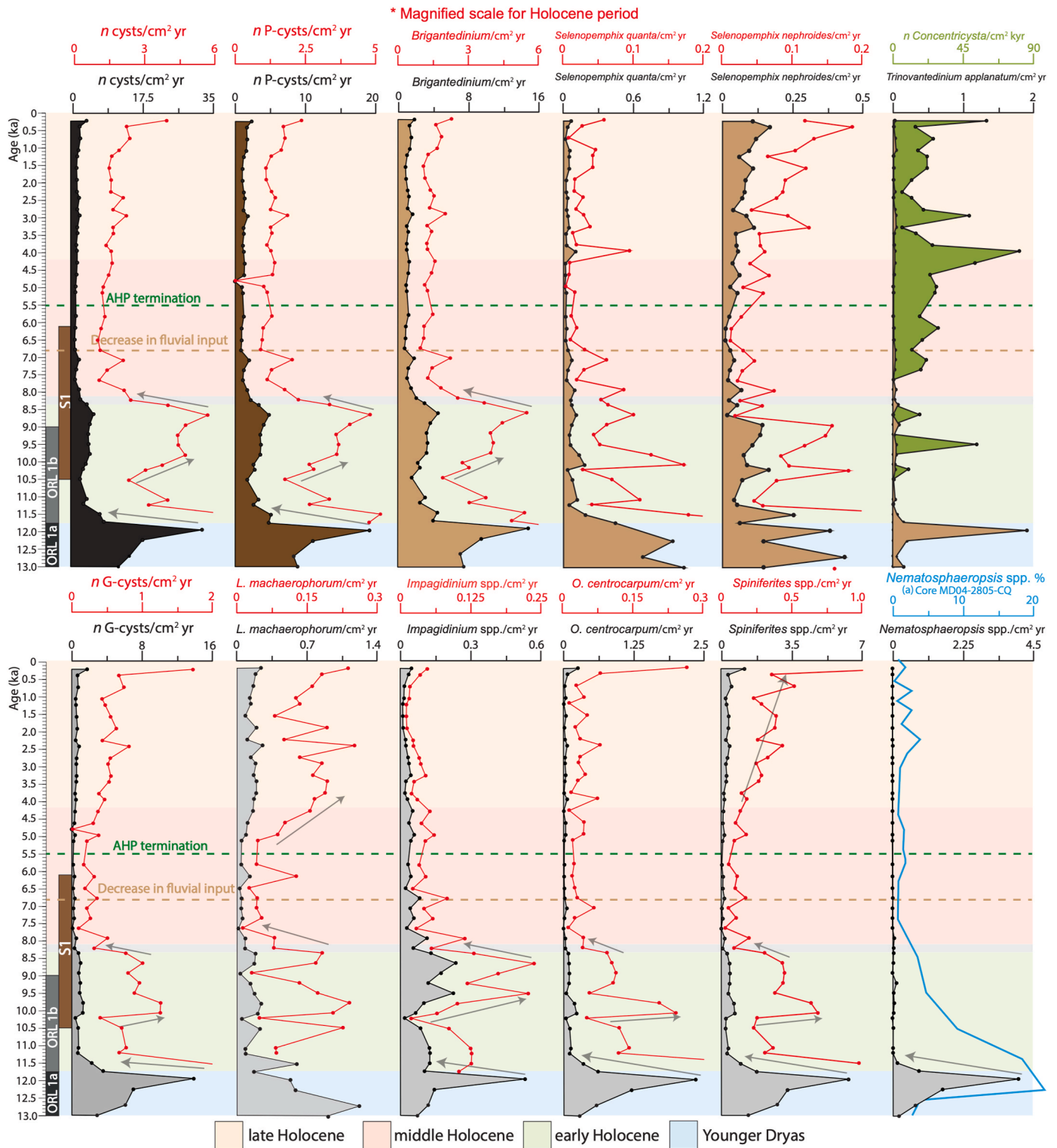
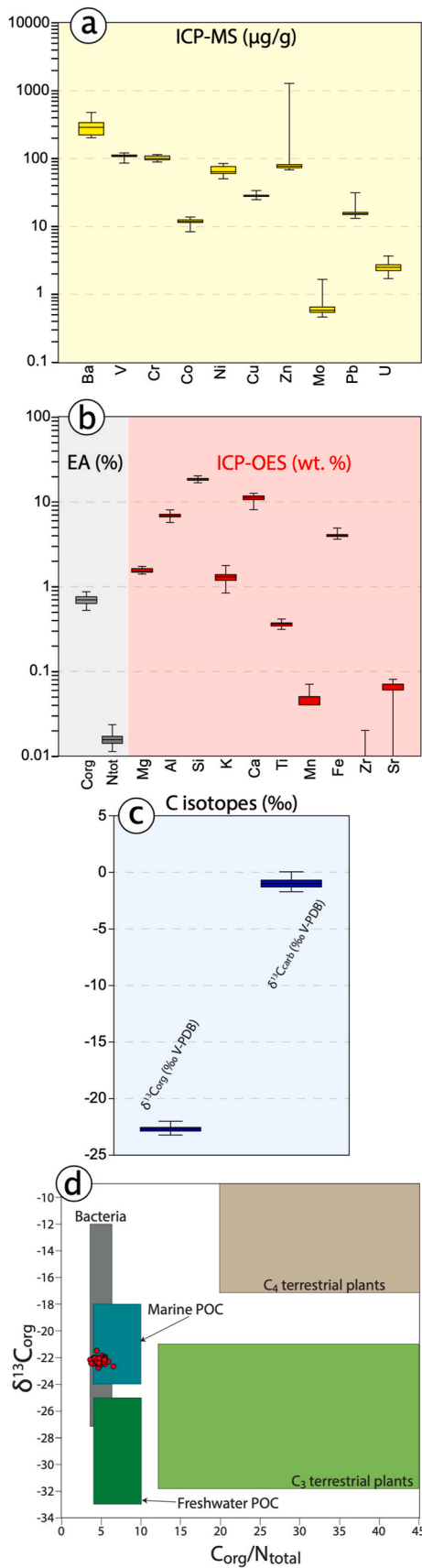


**Fig. 4.** Vertical-plots of cyst accumulation rates (expressed as  $n$  cysts/cm<sup>2</sup> yr) over the last 12.5 ka (yr = year). This includes the accumulation rates of total cysts, P-cysts, G-cysts and specific dinocysts species. All taxa that exceed 5 % in one or more samples are included. *Concentricystes* (euglenoid cysts) accumulation rate is plotted in green. (a) *Nematosphaeropsis labyrinthus* vertical plot in core MD04-2805-CQ (859 mbsl) located at West Morocco Margin (Penaud et al., 2010). Arrows indicate the main trends. Vertical plots with magnified scales are illustrated in red to highlight the changes throughout the Holocene period that are masked by the high dinocyst accumulation rates during the YD humid phase. ORL: Organic-Rich Layer, S1: Sapropel 1, AHP: African Humid Period.

pelagic barite and OM content (Figs. 4 and 7). In addition, there was very active LIW circulation and intense MOW, about twice that of the present day (Trias-Navarro et al., 2023).

During the YD humid phase (also known in westernmost

Mediterranean as interval YD-b; Ausín et al., 2015b), Alboran Sea SST experienced a marked temperature increase of ~5 °C (from ~13 °C to 18 °C) (Cacho et al., 2001, 2002; Rodrigo-Gámiz et al., 2014a; Català et al., 2019; Morcillo-Montalbá et al., 2021). LIW and MOW circulation



(caption on next column)

**Fig. 5.** Geochemical data as box-whisker plots. The box represents the inter-quartile range, the line in the box represents the median and the whiskers represent the 5th and 95th percentiles. (a) Trace metal concentrations expressed in µg/g log<sub>10</sub> scale. (b) Major concentrations, C<sub>org</sub> and N<sub>tot</sub> expressed in wt.% log<sub>10</sub> scale. EA: Elemental Analyzer. (c) δ<sup>13</sup>C<sub>org</sub> and δ<sup>13</sup>C<sub>carb</sub> values expressed as ‰. (d) Modified cross-plot from Meyers (1994) showing distinctive source combinations of atomic C/N ratios and organic δ<sup>13</sup>C<sub>org</sub> values of marine algae, lacustrine algae, C<sub>3</sub> land plants and C<sub>4</sub> land plants. POC: particulate organic carbon. GP04PC data is shown as red dots.

weakened significantly during this period (Trias-Navarro et al., 2023). The shift towards more humid conditions in the westernmost Mediterranean Sea began to register around 12.4 ka in Western Alboran sediments, according to the rise in fluvial input signaled by the increased Mg/Al ratio in the studied core (GP04PC) (Fig. 7). This climatic shift around 12.4 ka is also documented at the southwest Iberian Margin (core SHK06-5K; Ausín et al., 2020), in the Algero-Balearic Basin (ODP Site 975; Jiménez-Espejo et al., 2008), and in the Eastern Alboran Basin (core TTR12-293G; Rodrigo-Gámiz et al., 2011). Please refer to Fig. 1 for location of these cores. The exceptionally high dinocyst accumulation rates and the geochemical productivity proxies (Ba/Al ratio and C<sub>org</sub>%) suggest that this shift towards more humid conditions is accompanied by an abrupt increase in marine productivity (Fig. 7). The high abundance of P-cysts (*Brigantedinium*, *Selenopnephix* spp., *T. applanatum* cysts) and *N. labyrinthus* cysts (Fig. 4) further supports cool/eutrophic surface waters during a YD humid phase in the Western Alboran Basin. This aligns with Penaud et al. (2016) observations of high accumulation rates of *N. labyrinthus*, *Spiniferites elongatus* and *Spiniferites lazus* cysts in the Gulf of Cadiz in conjunction with cool/eutrophic conditions in the Northeast Atlantic region. Furthermore, the high abundance of *L. machaerophorum* and *O. centrocarpum* cysts (Fig. 4) suggests seasonally stratified waters and enhanced fluvial run-off in the Western Alboran Basin, as well as increased Atlantic surface water inflow during the YD humid phase, as noted by Penaud et al. (2016) at the Gulf of Cadiz.

Interestingly, neither core GeoB18131-1, located at an intermediate water depth (457 mbsl) in the North African margin of the Western Alboran Basin, nor core CEUTA10PC08 (914 mbsl), closer to the Iberian margin, registered enhanced planktonic foraminifera or coccolithophore productivity during the YD humid phase (Fig. 8) (Wang et al., 2019; Ausín et al., 2015a). This suggests strong spatial productivity variability within the Western Alboran Basin during the YD humid phase and may also be linked to increased stratification and enhanced nutrient loads from rivers, which favored autotrophic dinoflagellate (G-cysts) productivity over other non-flagellated groups. However, the simultaneous increase in dinocyst accumulation rate around 12.4 ka seen for Shackleton Site U1385, in the southern West Iberian Margin (Atlantic Ocean; Fig. 1) (Datema et al., 2017), suggests strong similarities in productivity dynamics between the Northeast Atlantic Ocean and the Western Alboran Basin.

During the YD humid phase, the Iberian Peninsula witnessed frequent extreme flood events, and Iberian Mountain glaciers underwent intense melting (García-Ruiz et al., 2016; Benito et al., 2023; Hernández et al., 2023). Bartolomé et al. (2015) studied an exceptionally high-resolution stalagmite record in the Seso Cave System (Central Pyrenees, Spain; Fig. 1) and suggested that humid conditions in southwestern Europe around 12.4 ka (also known as mid-Greenland Stadial 1 in the Northern Hemisphere) can be traced to a reactivation of the AMOC, which transported moisture and heat from lower latitudes (McGee et al., 2014). In this context, the Western Alboran deep sediment record represents one of the southernmost locations where the mid-Greenland Stadial 1 transition is observed. Therefore, the increase in local river run-off during the YD humid phase—originating from intense continental glacier melting and increased regional precipitation—coupled with enhanced inflow of nutrient-enriched Atlantic water, would have supplied sufficient nutrients to sustain remarkably

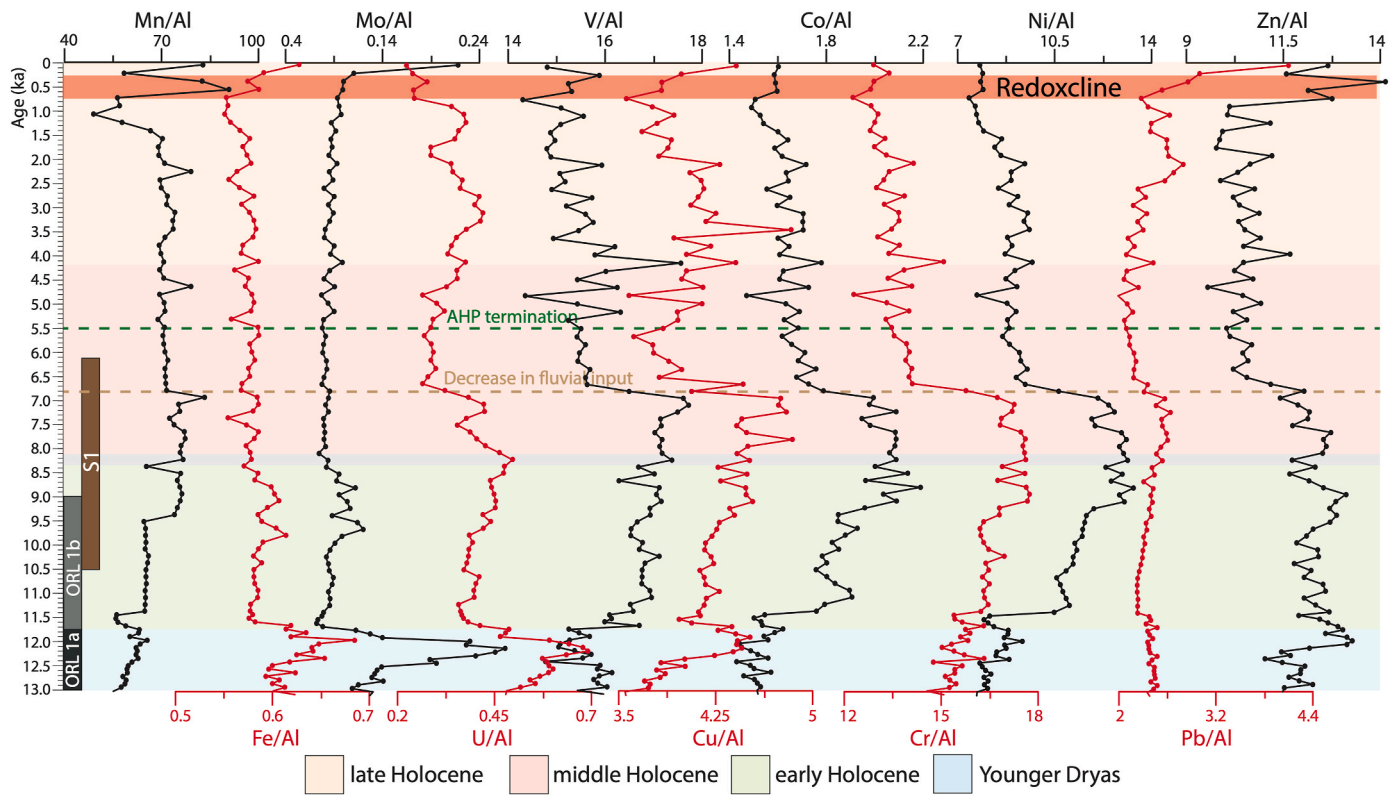


**Fig. 6.** Vertical-plots (also known as chemostratigraphic profiles) of Al-normalized RSTMs concentrations ( $[\text{RSTMs}]/[\text{Al}]$ ; ppm/%) over the last 13 ka in core GP04PC. S1 interval from Grant et al. (2016). Values expressed as  $10^{-4}$ . ORL: Organic-Rich Layer, S1: Sapropel 1, AHP: African Humid Period.

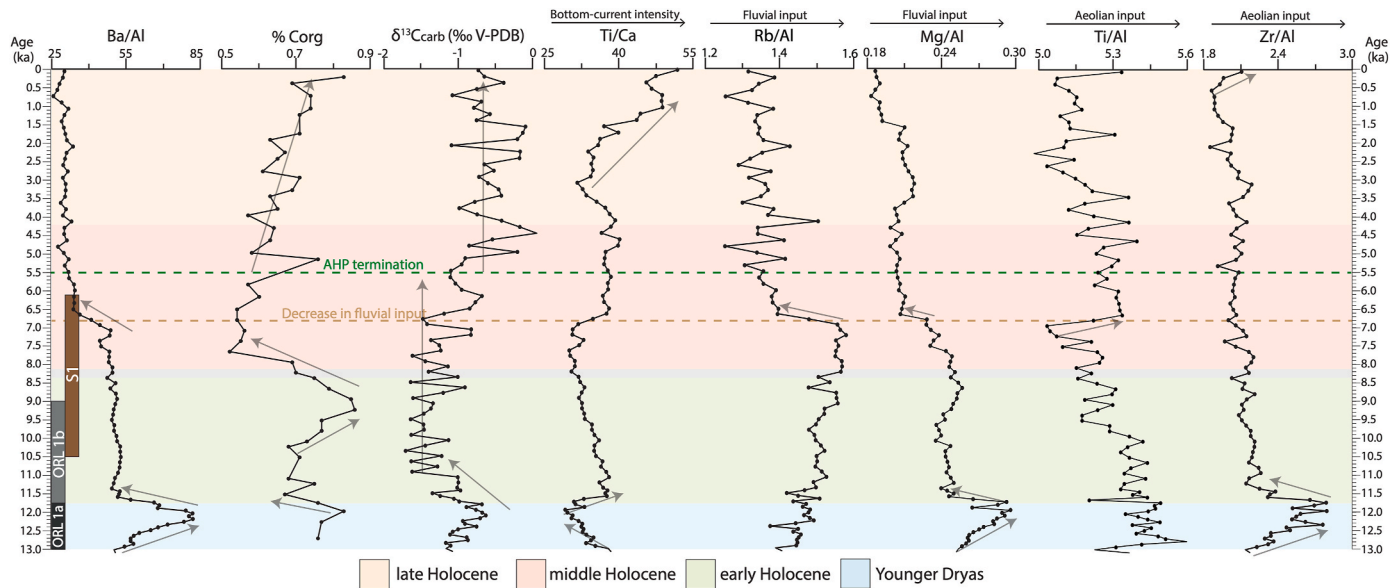


**Fig. 7.** Vertical-plots of different geochemical proxies for productivity (Ba/Al, %C<sub>org</sub> and  $\delta^{13}\text{C}_{\text{carb}}$ ), (ii) bottom currents intensity (Ti/Ca), (iii) fluvial input (Mg/Al and Rb/Al), and (iv) aeolian input (Zr/Al and Ti/Al) over the last 13 ka in core GP04PC. Arrows indicate the main trends. Ba/Al values expressed as  $10^{-4}$  (ppm/%), while Ti/Ca, Rb/Al, Ti/Al and Zr/Al values are expressed as  $10^{-3}$  (%/%). ORL: Organic-Rich Layer, S1: Sapropel 1, AHP: African Humid Period.

high productivity within the Western Alboran (Fig. 9), as supported by previous studies (Bárcena et al., 2001; Jiménez-Espejo et al., 2008; Ausín et al., 2015b). The high Zr/Al ratio values in the Western Alboran Basin during the YD humid phase could also derive from enhanced Zr input of fluvial origin. A similar situation is recognized during the humid sapropel event S5 in the eastern Mediterranean (Monedero-Contreras et al., 2023b). Increasing river run-off is further supported by

geochemical fluvial proxies such as Mg/Al and Rb/Al ratios.

Enhanced freshwater input also caused the Western Alboran Basin to undergo a reduction in surface water salinity, resulting in greater surface water buoyancy and a stratified water-column. A scenario of nutrients from deeper water layers transported to surface waters by upwelling systems or vertical mixing can therefore be discarded as responsible for the high marine productivity. As mentioned above, during this time

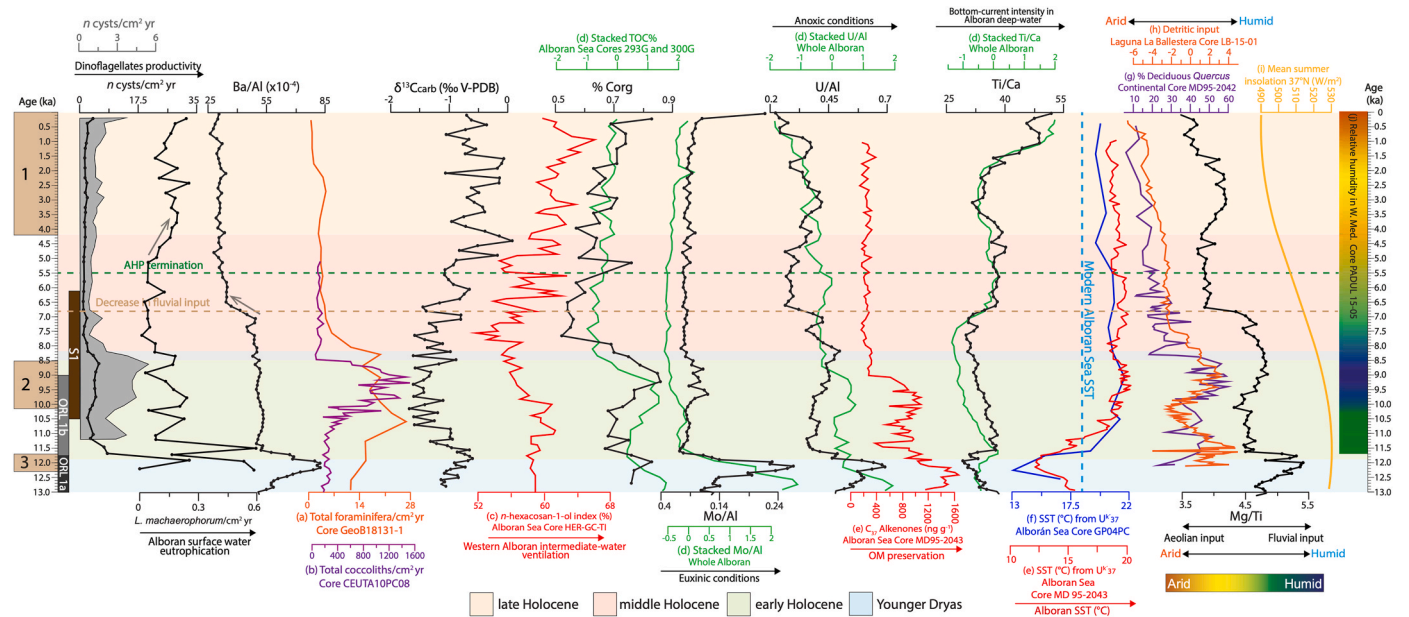


**Fig. 8.** Comparison with vertical-plots of diverse environmental and oceanographic proxies obtained by previous studies. These studies include marine and continental Holocene records from the westernmost Mediterranean region covering the last 13 ka. Black plots are from this study. In solid gray we present dinocyst accumulation rate ( $n$  cysts/cm<sup>2</sup> yr) with a magnified scale to highlight Holocene variability. Additionally, we propose the ratio Mg/Ti (%/%) to encapsulate changes in fluvial input vs aeolian input, thereby reflecting changes in the regional climatic conditions (Table 1). Plots from previous studies are presented in different colors: (a) Wang et al. (2019) in orange, (b) Ausín et al. (2015a) in purple, (c) Ausín et al. (2015b) in red, (d) Mesa-Fernández et al. (2022) in green, (e) Cacho et al. (2002) in red, (f) Morcillo-Montalbá et al. (2021) in blue, (g) Chabaud et al. (2014) in purple, (h) García-Alix et al. (2022) in orange, (i) Berner (1981) in yellow, and (j) Ramos-Román et al. (2018a) as a color bar. Location of cores are presented in Fig. 1. Brown rectangles indicate the different productivity scenarios illustrated in Figs. 9–11. (1) Late Holocene (last 4.2 kyr); (2) Holocene humidity optimum (from ~10.5 to 8.5 ka); (3) YD humid phase (from ~12.3 to 11.7 ka). Refer to Fig. 1 for location of cores. ORL: Organic-Rich Layer, S1: Sapropel 1, AHP: African Humid Period.

AMOC was reactivated (Lane et al., 2013; Bartolomé et al., 2015 and references therein), most likely enhancing the inflow of sub-polar low-salinity Atlantic Water into the Alboran Basin. The low-salinity Atlantic influx, combined with the increased freshwater input into the Gulf of Lion (mainly derived from a rapid melting of glaciers in the Alps and Pyrenees after the YD cold phase), hindered vertical mixing and WMDW formation, which promoted strong deep-water stagnation in the Western Alboran deep-waters (Bárcena et al., 2001). A similar process occurred during Heinrich Events, wherein surface water freshening—primarily driven by an enhanced influx of low-salinity polar waters into the westernmost Mediterranean—slowed down or even collapsed the deep-water overturning system of the Gulf of Lion and reinforced the water-column stratification in the western Mediterranean basins (Sierro et al., 2005).

RSTM trends indicate strong oxygen-depletion in Alboran deep-waters. It would have enhanced organic carbon preservation and supported water-column stratification and deep-water restriction in the Western Alboran Basin during this period (Figs. 6 and 8). Weakened bottom-current intensity in Western Alboran deep-waters (revealed by the low Ti/Ca values) also supports deep-water stagnation during the YD humid phase and agrees with results from Mesa-Fernández et al. (2022); see Fig. 8. Porewater anoxia/euxinia, produced by stable deep-water stagnation, promoted the authigenic precipitation of iron-sulfides in association with trace metals (e.g., Mo, Cu and Zn) and the authigenic enrichment of U in association with OM (Fig. 6) (Tribouillard et al., 2006, 2012, 2021). Furthermore, the coexistence of pelagic barite with iron sulfides in the sediments representing the YD humid phase (~12.4–11.7 ka) would suggest that sulfate depletion in the sediments was limited, as barite crystals did not dissolve (Passier et al., 1997; Sangiorgi et al., 2006; Monedero-Contreras et al., 2023a).

During the YD – early Holocene transition (from ~11.8 to 11.5 ka), dinoflagellate productivity decreased abruptly, affecting both autotrophic and heterotrophic dinoflagellates (Fig. 4). Attesting to this are more

negative  $\delta^{13}\text{C}_{\text{carb}}$  values and an abrupt decrease in pelagic barite content (Fig. 7). Between ~11.5 and 10.5 ka, the western Mediterranean witnessed a shift towards more arid/cold conditions (Fletcher et al., 2010; Rodrigo-Gámiz et al., 2011), corroborated by a decrease in fluvial input marked by lower Mg/Al values. Weakened local river discharges owing to more arid regional conditions reduced nutrient availability in Western Alboran surface water, thereby terminating an exceptionally high productivity phase. Additionally, around 11.7 ka, enhanced Alboran deep-water ventilation and circulation are evidenced by the abrupt decrease in RSTM concentrations and increased Ti/Ca values. The abrupt decrease in the dinocyst accumulation rate (especially in *N. labyrinthus* and *T. applanatum* cysts; Fig. 4) in the Western Alboran Basin is synchronously observed in the Gulf of Cadiz (core MD99-2339; Penaud et al., 2016), at the West Iberian Margin (Site U1385; Datema et al., 2017), and at the West Morocco Margin (core MD04-2805 CQ; Penaud et al., 2010) (Fig. 8), which represent the Southeastern region of the North Atlantic Ocean. This corroborates the idea that Western Alboran Basin productivity is highly influenced by North Atlantic climatic and ocean dynamics.

### 6.1.2. Holocene humidity optimum (~10.5–8.5 ka)

The Western Alboran Basin experienced a noteworthy increase in marine productivity from ~10.5 to 8.5 ka, after an arid period of reduced marine productivity and intense deep-water currents from around 11.5 to 10.5 ka, indicated by the rise in dinocyst accumulation rates (both autotrophic and heterotrophic dinoflagellates) and OM content (Figs. 4 and 7). Yet this period of increased marine productivity is not well reflected in barite content, as the high detrital input probably masks the marine barite content signal (Fig. 7). This time interval (~10.5–8.5 ka) coincides with the Holocene humidity optimum, a period in southern Europe often referred to as the Holocene climatic optimum; it is attributed to a summer insolation maximum in the Northern Hemisphere during a precession minimum that gave rise to a

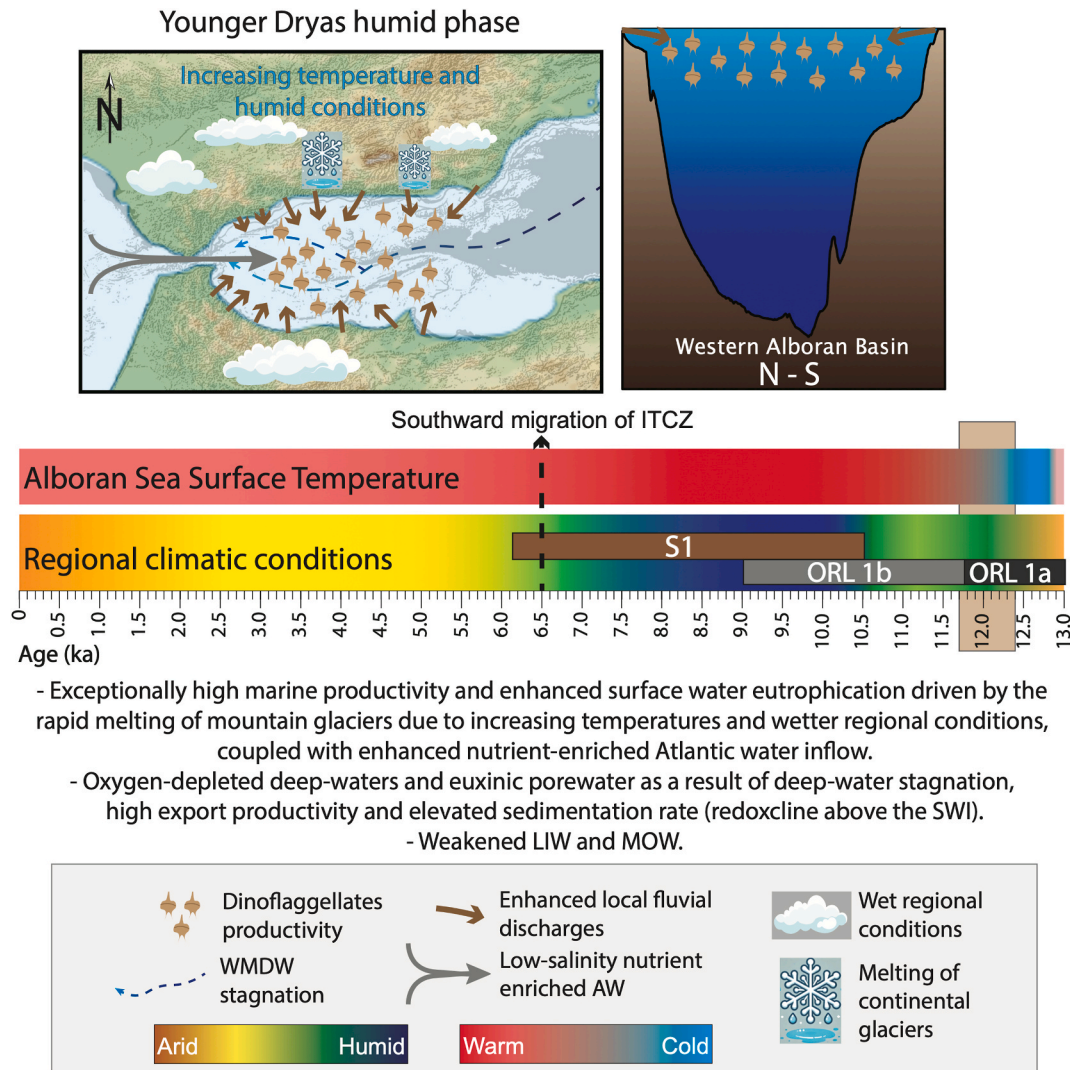


**Fig. 9.** Oceanographic setting in Western Alboran Basin during the YD humid phase (from ~12.3 to 11.7 ka). The main factors controlling marine productivity are emphasized. WAG: Western Alboran Gyre, WMDW: Western Mediterranean Deep Water, LIW: Levantine Intermediate Water, NAO: North Atlantic Oscillation, YD: Younger Dryas, SWI: Sediment-water interface, ORL: Organic-Rich Layer, S1: Sapropel 1.

northward migration of the ITCZ (Rossignol-Strick, 1999; Haug et al., 2001; Schneider et al., 2014). In the westernmost Mediterranean region this period is governed by warm and humid conditions, evidenced by pollen and geochemical records in lake sediments from the Padul wetland (Granada, Spain) and La Ballestera lake (Sevilla, Spain) (Figs. 8 and 10) (Ramos-Román et al., 2018a; García-Alix et al., 2022).

Particularly, the observed increases in accumulation rates of *Brigatodinium*, *Selenopemphix* species (*S. quanta* and *S. nephroides*) and *L. machaerophorum* cysts point to seasonal eutrophic surface waters. The higher abundance of *Impagidinium* spp. cysts (mainly represented by *I. aculeatum* cysts; Supplementary Material) moreover suggests warmer Alboran Sea surface waters during this period (Fig. 4), likewise surmised by Penaud et al. (2016) at the Gulf of Cadiz (core MD99-2339). Records from cores CEUTA 10PC08 (914 mbsl, Fig. 1; Ausín et al., 2015a) and GeoB18131-1 (457 mbsl, Fig. 1; Wang et al., 2019) point out an enhanced marine productivity in the Western Alboran Basin during this period, as evidenced by coccolith and planktonic foraminifera accumulation rates, respectively (Fig. 8). An increase in OM content from ~10.5 to 9 ka also occurs in marine core TTR17-434G, close to the studied core (Figs. 1 and 7) (Mesa-Fernández et al., 2022). Accordingly, enhanced marine productivity would have prevailed in the entire Western Alboran Basin, including the North African margin area.

However,  $\delta^{13}\text{C}_{\text{carb}}$  trend does not evidence greater marine productivity during this period (Fig. 7) suggests that  $\delta^{13}\text{C}_{\text{carb}}$  values may be influenced by other factors, e.g. increased input of terrigenous material (characterized by low C isotopes) due to a rise in continental run-off (Fig. 10).

Low Ti/Ca values occurred during the Holocene humidity optimum, indicating a concomitant Western Alboran Basin weakening of deep-water currents (Fig. 7). The higher abundance of *L. machaerophorum* cysts also supports a (seasonally) stratified water-column in the Western Alboran Basin from ~10.5 to 8.5 ka, and possibly reduced surface water salinity due to enhanced river run-off and seasonal thermal stratification (see Fig. 4). The increase in local fluvial discharges can be attributed to the climatic shift towards more humid conditions in the southern Iberian region around 10.5 ka (Dormoy et al., 2009; Mesa-Fernández et al., 2018; Camuera et al., 2021, 2022; García-Alix et al., 2021). Enhanced riverine discharge in the Western Alboran Basin throughout the Holocene humidity optimum is supported by the increase in Rb/Al and Mg/Al values, the decrease in Ti/Al values, and the higher concentration of trace metals, strongly influenced by the detritic fraction (e.g., Co, Ni, Cu and Tribovillard, 2021, Figs. 6 and 7).

During this warmer period, vast freshwater volumes were released into the Atlantic Ocean due to melting of North Atlantic icebergs.

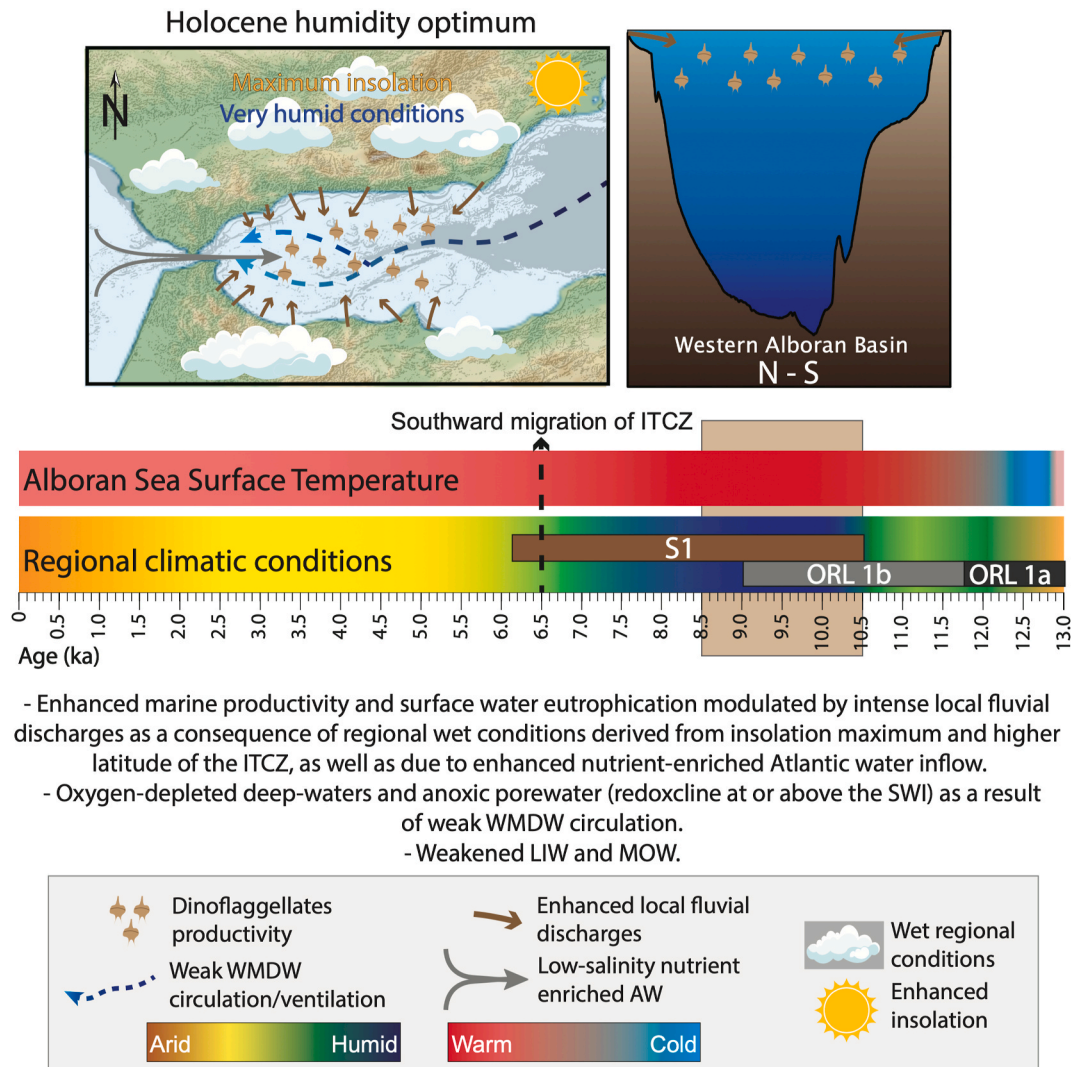


**Fig. 10.** Oceanographic setting in Western Alboran Basin during the Holocene humidity optimum (from ~10.5 to 8.5 ka). The main factors controlling marine productivity are emphasized. WAG: Western Alboran Gyre, WMDW: Western Mediterranean Deep Water, LIW: Levantine Intermediate Water, NAO: North Atlantic Oscillation, YD: Younger Dryas, SWI: Sediment-water interface, ORL: Organic-Rich Layer, S1: Sapropel 1.

Consequently, the low-salinity Atlantic inflow into the westernmost Mediterranean reinforced Alboran Sea surface water freshening, as occurred at the end of the Heinrich events (Sierro et al., 2005; Jiménez-Espejo et al., 2008; Grant et al., 2016). Glaciers in the Alps also experienced intense melting during the Holocene humidity optimum, shrinking to sizes smaller than those observed in the late 20th century (Ivy-Ochs et al., 2009). The result was a significant release of freshwater into the Gulf of Lion, weakening WMDW formation and promoting deoxygenation of western Mediterranean deep settings (Frigola et al., 2007; Jiménez-Espejo et al., 2008; Mesa-Fernández et al., 2022). Subsequently, from ~10 to 8.5 ka, sluggish WMDW circulation and weak water-column vertical-mixing caused oxygen depletion in Western Alboran deep-water (Fig. 10). Mo enrichment in association with iron sulfides within the sediments further suggests intermittent porewater euxinia (Tribovillard et al., 2006; Scott and Lyons, 2012). The oxygen-depleted conditions in Alboran deep-water from ~10 to 8.5 ka led to enhanced OM preservation, as indicated by the obtained  $C_{org}$  trend and supported by the  $C_{37}$  Alkenone trend of core MD95-4043 (Cacho et al., 2002), and by the TOC% trend in core TTR17-434G (Mesa-Fernández et al., 2022) (Figs. 7 and 8). It is remarkable that during the Holocene, trace metals, including U—a conservative RSTM not typically influenced by detrital fraction variability—follow a trend

similar to those of Rb/Al and Mg/Al ratios, which are fluvial proxies (Fig. 7). This observation suggests that trace metals trends are strongly influenced by the detrital fraction in the Western Alboran Basin.

The humid and warm interval of western Mediterranean (from ~10.5 to 8.5 ka) that led to increased dinoflagellate productivity and deep-water deoxygenation in the Western Alboran Basin overlaps in time with the deposition of sapropel S1 in the Eastern Mediterranean (Fig. 4), and more specifically with section S1a, deposited before S1 interruption linked to the 8.2 ka cold event (de Lange et al., 2008; Jiménez-Espejo et al., 2015; Grant et al., 2016; Filippidi and de Lange, 2019). Consequently, LIW circulation in the Mediterranean was weaker at this time, meaning lower oxygen content in the western Mediterranean mid-depths (Ausín et al., 2015b; Fink et al., 2015; Wang et al., 2019; Zirks et al., 2019). Weak LIW circulation promoted a strong reduction of Mediterranean Outflow Water flow during this period (Voelker et al., 2006). Hence, from ~10.5 to 8.5 ka, the weak circulation of oxygen-depleted LIW reinforced OM preservation in the Western Alboran Basin. As a consequence, enhanced OM accumulation/preservation and RSTM fixation during the Holocene humidity optimum in the Western Alboran deep sediments can be linked to the conjunction of different factors: (i) high marine productivity due to surface water fertilization by local rivers and enhanced flux of

nutrient-rich Atlantic surface water, (ii) weak circulation of oxygen-depleted LIW due to Eastern Mediterranean deoxygenation during S1a deposition, favoring OM preservation during its transit through the Western Alboran water-column, and (iii) decreased Alboran deep-water ventilation because of a weakened formation of WMDW at the Gulf of Lion (Fig. 10).

#### 6.1.3. 8.2 ka cold event in Western Alboran Basin

Intermittent porewater euxinia and deep-water deoxygenation, which began ~10 ka, ceased before the 8.2 ka cold event (also known as Bond event 5; Bond et al., 1997), characterized in the westernmost Mediterranean region by arid and cold conditions (Rodrigo-Gámiz et al., 2011). The cold/arid regional conditions reduced local river discharges and promoted active WMDW formation and ventilation of the western Mediterranean deep settings (Frigola et al., 2007), including the deep Alboran Basin (Jiménez-Espejo et al., 2008; Rogerson et al., 2008; Rodrigo-Gámiz et al., 2011; Pérez-Asensio et al., 2020). As a result, the 8.2 ka cold event decreased marine productivity in the Western Alboran Basin—including dinoflagellate, planktonic foraminifera and coccolithophore productivity, while hindering OM preservation, marking the demise of Organic-Rich Layer-1b (ORL-1b) in the Western Alboran Basin (Figs. 4–8). However, the end of ORL-1b occurred earlier in the Eastern Alboran Basin (8.9 ka; Mesa-Fernández et al., 2022) than in the Western Alboran Basin (8.2 ka), signaling that the latter remained restricted for a longer period.

Conversely, in the Eastern Mediterranean basins (e.g., Levantine and Adriatic basins), high productivity and weak deep-water ventilation resumed after the 8.2 ka cold event, leading to the deposition of sapropel interval S1b from ~8 to ~6.1 ka (Fink et al., 2015; van Helmond et al., 2015; Zwiep et al., 2018). This highlights the decoupling of productivity dynamics between eastern and western Mediterranean basins. Furthermore, there is no Mn enrichment or signs of OM oxidation linked to a rapid reventilation of Western Alboran deep-water during the 8.2 ka cold event (Fig. 6), as occurred during some sapropel reventilation events related to abrupt Eastern Mediterranean deep-water renewal, where Mn-oxyhydroxides precipitated intensely owing to penetration of the oxidation front in the sediments (Thomson et al., 1993; Reitz et al., 2006; Filippidi and de Lange, 2019; Monedero-Contreras et al., 2023a, 2023b).

#### 6.1.4. Mid-Holocene climatic shift in westernmost Mediterranean

In the Western Alboran Basin, humid conditions ceased between 7 and 6.5 ka, as evidenced by the decrease in fluvial input and increase in aeolian input shown by geochemical proxies. The marked decrease in fluvial input affected the background concentration of trace elements, including Ba and U, highlighting the strong detrital influence on trace metal concentration trends in deep Western Alboran sediments. It is interesting to note that, in the wake of this regional climatic shift and up to the present, marked suborbital (multidecadal) variations in geochemical proxies linked to climate oscillations are observed in the westernmost Mediterranean. This climatic transition gave rise to an intensification of Western Alboran deep currents, evidenced by the increase in Ti/Ca values (Fig. 7), and enhanced Alboran intermediate-water ventilation and upwelling activity, as revealed by the Holocene hexacosan-1-ol index and the nannofossil accumulation rate trends from Ausín et al. (2015b) (Fig. 8). An abrupt intensification of WMDW formation is also observed around 7 ka in the Minorca slope, attributed by Frigola et al. (2007) to stronger north-westerlies. Consequently, the arid modern conditions in the south of the Iberian Peninsula (i.e., the westernmost Mediterranean) emerged around 6.5 ka—roughly 1000 years earlier than in Northern Africa and the Sahara region, where humid conditions persisted until the end of the African Humid Period around 5.5–5 ka (Tierney et al., 2011). This observation is consistent with findings by de Menocal (2015), in that the end of the African Humid Period progressed from north to south, with monsoon rains diminishing first in the north and gradually receding further south, in line with the

expected southward migration of the ITCZ due to orbital forcing and recorded vegetation changes in southern Europe (Wanner et al., 2008; Bout-Roumzeilles et al., 2013; Fletcher et al., 2013; Chabaud et al., 2014; Schneider et al., 2014). Furthermore, this observation is supported by South Iberian continental records that registered the regional climatic shift towards more arid conditions around 7–6.5 ka on the basis of geochemical proxies and pollen records (Fig. 8) (Mesa-Fernández et al., 2018; Ramos-Román et al., 2018a, 2018b; García-Alix et al., 2022; Jiménez-Moreno et al., 2022, 2023).

#### 6.1.5. Late Holocene (4.2 ka – present)

The higher accumulation rates of *L. machaerophorum* and *S. nephroides* cysts support a moderate increase in nutrient availability and productivity in Western Alboran surface water during the late Holocene (Fig. 4), given that these dinocyst species can be considered eutrophication proxies in the westernmost Mediterranean (Penaud et al., 2016). The higher  $\delta^{13}\text{C}_{\text{carb}}$  and  $\text{C}_{\text{org}}$  values also support an increase in marine productivity during this period (Fig. 7). However, this marine productivity increase is relatively low in comparison with the rise registered during the YD humid phase or Holocene humidity optimum. More abundant *L. machaerophorum* cysts during the late Holocene are also observed at the (southern) West Iberian Margin (Shackleton Site U1385; Datema et al., 2017) and at the Gulf of Cadiz (core MD99-2339; Penaud et al., 2016). Meanwhile, a lower accumulation rates of *Brigantidium* spp. cysts during this period (Fig. 4) is likewise observed at the Gulf of Cadiz (core MD99-2339; Penaud et al., 2016), suggesting a strong North Atlantic signature in westernmost Mediterranean dinocyst assemblages.

The low Mg/Al values and the increase in Ti/Al values support arid regional conditions during the late Holocene (Fig. 7). This is corroborated by the low Mg/Ti values during this period (Table 1 and Fig. 8). This aligns with regional continental and pollen records (Fletcher et al., 2013; Chabaud et al., 2014; Ramos-Román et al., 2018a, 2018b; García-Alix et al., 2022). The arid conditions and strong north-westerlies during the late Holocene facilitated active Ekman transport along the Iberian Peninsula coastline, promoting anticyclonic Alboran gyres (i.e., WAG and EAG; Fig. 1) and upwelling cells at the northern edge of the WAG (Sarhan et al., 2000; Ruiz et al., 2001; Pérez-Folgado et al., 2003; Ausín et al., 2015a, 2015b; Garcia-Jove et al., 2022), as well as active WMDW formation (Frigola et al., 2007; Mesa-Fernández et al., 2022). Thus, the increase in nutrient availability and marine productivity during the late Holocene in the Western Alboran Basin seems to have been driven by the establishment of seasonal upwelling systems, influenced by atmospheric and climatic conditions in the westernmost Mediterranean and the North Atlantic region, resulting from the southward migration of the ITCZ around 6.5 ka.

One of the intriguing features of the GP04PC sediment core record is the multicentennial-scale climate variability (seesaw trend) during the late Holocene indicated by some geochemical proxies (e.g., Rb/Al, Ti/Al,  $\text{C}_{\text{org}}\%$  and  $\delta^{13}\text{C}_{\text{carb}}$ ; Fig. 7). This seesaw trend is also reflected in RSTMs highly influenced by the detrital fraction (e.g., Cu, Zn, V, Co; Fig. 6). This variability occurs despite the absence of insolation changes, polar ice-sheet collapse, or meltwater pulses that influenced global thermohaline circulation and climate variability during the YD and early Holocene. Changes in NAO patterns have been suggested as a key driver for the suborbital climatic oscillations in the western Mediterranean during the late Holocene (Jalut et al., 1997, 2000; Frigola et al., 2007; Bout-Roumzeilles et al., 2013; Fletcher and Zielhofer, 2013; Fletcher et al., 2013; Cisneros et al., 2019; Ilvonen et al., 2022), inducing centennial and even multicentennial changes in productivity in the westernmost Mediterranean (Ausín et al., 2015b). In this context, the Iberian Peninsula would have seen frequent periods of extreme flood events linked to negative NAO incursions throughout the late Holocene (Fig. 11) (Degeai et al., 2015; Benito et al., 2023). Consequently, the marked increases in the irregular Rb/Al ratio,  $\delta^{13}\text{C}_{\text{org}}$  and C/N trends throughout the late Holocene can be linked to punctual fluvial input

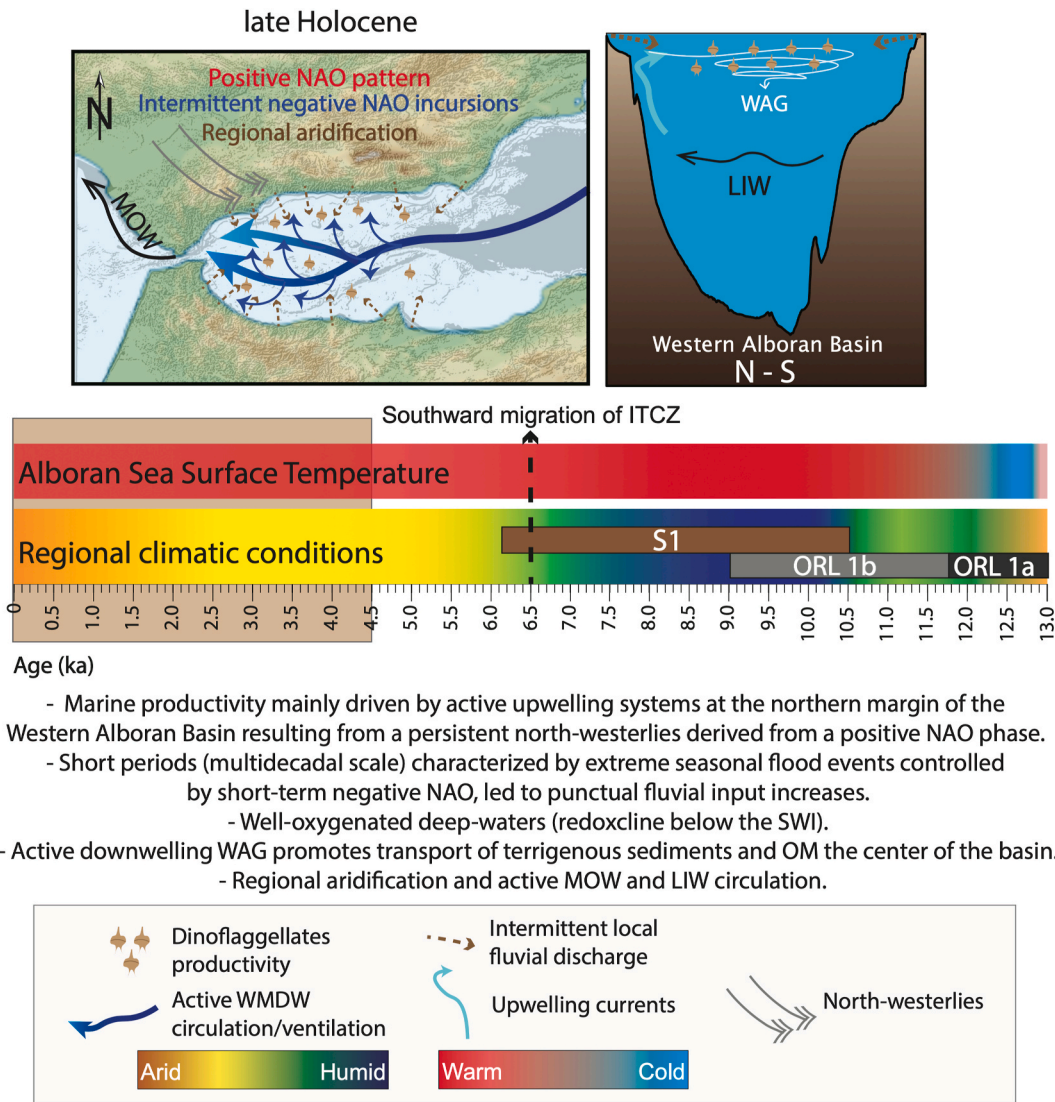


**Fig. 11.** Oceanographic setting in Western Alboran Basin during the late Holocene (last 4.2 kyr). The main factors controlling marine productivity are emphasized. WAG: Western Alboran Gyre, WMDW: Western Mediterranean Deep Water, LIW: Levantine Intermediate Water, NAO: North Atlantic Oscillation, YD: Younger Dryas, SWI: Sediment-water interface, ORL: Organic-Rich Layer, S1: Sapropel 1.

increases (see Fig. 7 for Rb/Al ratio and  $\delta^{13}\text{C}_{\text{org}}$  trends and Supplementary Material for C/N trend), possibly linked to centennial-scale humid periods with more frequent regional flood events, as also noted by Martín-Puertas et al. (2010). Even so, the possibility that the abrupt variations in the Rb/Al trend are linked to changes in bottom-current intensity —associated with oscillations in WMDW formation due to changes in North Atlantic atmospheric patterns during the late Holocene, as described by Frigola et al. (2007)— cannot be dismissed. These potential variations in bottom-current intensity are not registered in the Ti/Ca ratio trend, however (Fig. 7).

*Concentricystes* sp., which are euglenoid cysts having a unique fingerprint shape linked to eutrophic freshwater environments, found in marine sediments after events of enhanced river run-off (Yang et al., 2022; van de Schootbrugge et al., 2024), have been documented in core GP04PC primarily since ~ 7 ka, but more consistently throughout the late Holocene (Fig. 4). The *Concentricystes* sp. trend therefore suggests pulses of increased fluvial input in the Western Alboran Basin over the last ~7 ka, intensified in the late Holocene. This observation also implies effective transport of biomass from the northern continental margin of the Alboran Sea to the center of the basin, facilitated by active WAG and AJ currents developed after the southward migration of the ITCZ

(Fig. 11). This scenario is compatible with modern indications of the torrential nature of relatively small rivers in catchment basins around the Alboran Sea, playing a significant role as contributors of freshwater and nutrients in the form of large sediment plumes during seasonal flood events (Fabres et al., 2002; Masqué et al., 2003; Liqueste et al., 2005; Lobo et al., 2006). Yet in a regional aridification context governed by a persistent positive NAO pattern and arid conditions (Trouet et al., 2009; Martín-Puertas et al., 2010; Olsen et al., 2012; Toney et al., 2020), upwelling induced by strong north-westerlies appears to be the constant source of nutrients during the late Holocene and at present, since local rivers act as fertilizers of the Alboran Sea surface waters only during extreme flood events (Fig. 11). Consequently, centennial-scale changes in marine productivity dynamics and nutrient availability throughout the late Holocene can be attributed to changes in the governing NAO-like pattern (Ausín et al., 2015b; Cisneros et al., 2019).

Regarding the dynamics of Western Alboran deep currents, the deep sediments in this region do not straightforwardly register the multi-decadal fluctuations of WMDW intensity during the late Holocene —unlike those at the Minorca slope (Frigola et al., 2007; Cisneros et al., 2019). This observation suggests that deep-water current intensity during the late Holocene in the Western Alboran Basin is influenced by

factors beyond WMDW formation, e.g. changes in LIW intensity (Cisneros et al., 2019) and the strength of the Bernoulli aspiration effect produced by the Gibraltar Strait (Mesa-Fernández et al., 2022). The only synchronous change observed at both locations would be the reduction of bottom-current intensity around 4 ka, attributed to more stable atmospheric conditions in southern Europe (Frigola et al., 2007). However, while weakened bottom-current intensity is maintained throughout the late Holocene at the Minorca Slope, in the Western Alboran Basin, bottom-current intensity increases again around 2 ka (Fig. 7). The increase in Ti/Ca values around 2 ka suggests a strengthening of the Bernoulli aspiration effect, which promoted effective Western Alboran deep-water renewal/ventilation and active MOW during the late Holocene, as previously interpreted by Mesa-Fernández et al. (2022) in the Eastern Alboran Basin (Fig. 8). The low concentration of RSTMs also supports enhanced Western Alboran deep-water ventilation/oxygenation during the late Holocene (Fig. 11). This observation highlights the importance of the Gibraltar aspiration strength of WMDW on the MOW intensity during the late Holocene and on the Alboran deep-water redox conditions at present.

## 6.2. North Atlantic influence in westernmost Mediterranean climatic and oceanographic conditions

The westernmost Mediterranean, particularly the Western Alboran Basin, has experienced significant climatic and oceanographic influences from the North Atlantic throughout the last 13 ka. These influences have profoundly impacted local productivity dynamics, dinocyst assemblages and the detrital composition of deep sediments (Figs. 3 and 4). During the YD and early Holocene (13–6.5 ka), millennial- and multicentennial-scale productivity changes in the Western Alboran Basin were primarily influenced by regional climate conditions controlled by orbital insolation changes and fluctuations in the AMOC, driven by meltwater pulses and ice-sheet disintegration events in the North Atlantic (Fig. 12) (Frigola et al., 2007; Bartolomé et al., 2015). The geochemical results demonstrate that these North Atlantic changes also influenced the deep-water redox conditions, water-column stability, and bottom-current intensity in the Western Alboran Basin.

An intriguing aspect of the YD phases is the decoupling and offset timing of enhanced productivity and redox conditions between the Eastern and Western Alboran basins (Fig. 8). In the Eastern Alboran Basterretxea et al. (2018) documented enhanced marine productivity and oxygen-depleted deep waters during the first YD phase (arid and cool phase; from 13 to 12.4 ka) (Fig. 8). In contrast, our study suggests that the Western Alboran Basin underwent such conditions during the second YD phase (warmer and humid phase), mirroring more North-eastern Atlantic records. Moreover, productivity dynamics and dinocyst assemblages in the Western Alboran Basin over the last 13 ka correlate better with those registered in southeastern North Atlantic records (Gulf of Cadiz, Penaud et al., 2016; West Iberian Margin, Datema et al., 2017; West Morocco Margin, Penaud et al., 2010) than with those in other Mediterranean areas (e.g., Adriatic Sea and Levantine Basin; Fink et al., 2015; van Helmond et al., 2015; Zwiep et al., 2018). This observation, together with the discrepancy between these two neighboring Alboran basins, underscores the influence of changes in the North Atlantic on productivity dynamics in the Western Alboran Basin and highlights the capacity of Western Alboran deep-sediment records to act as a witness of potential changes in Atlantic atmospheric and ocean circulation patterns on millennial to centennial scales owing to its elevated sedimentation rate (Nieto-Moreno et al., 2011).

From around 6.5 ka onwards, following the southward migration of the ITCZ driven by orbital forcing, climatic variability in the Western Alboran Basin became increasingly dominated by multidecadal- and centennial-scale atmospheric changes in the North Atlantic. These shifts played a crucial role in short-term freshwater input and productivity oscillations in the western Mediterranean basins (Fig. 12) (Fletcher et al., 2013; Degeai et al., 2015; Ausín et al., 2015b; Cisneros et al.,

2019). This can be related with the establishment of the present climate system in the western Mediterranean region: from being mostly controlled by external solar forcing, to being dominated by North Atlantic atmospheric-oceanic dynamics (Jiménez-Moreno et al., 2020). During the last ~6.5 ka, both positive and negative NAO modes took place in the westernmost Mediterranean, as indicated by the winter-NAO index reconstruction by Olsen et al. (2012) (Fig. 12). These shifts impacted freshwater (fluvial) input and water-column stability in the Alboran Sea (Nieto-Moreno et al., 2011, 2013; Català et al., 2019) (Fig. 12). Consequently, suborbital (i.e., centennial-scale) productivity oscillations in the Western Alboran Basin during the late Holocene were influenced by changes in the NAO patterns (Ausín et al., 2015a, 2015b). Notably, from ~3 to 2 ka, the subtle increase in Mg/Ti indicates relatively more humid conditions, while Ti/Ca indicates weakened bottom current intensity in the Western Alboran Basin (Fig. 8). These changes could be linked to NAO pattern, as this period is dominated by a negative NAO phase (Olsen et al., 2012) (Fig. 12). This observation aligns with the precipitation reconstruction for the westernmost Mediterranean by Martín-Puertas et al. (2010), which indicates increased precipitation during this period, based on the Rb/Al ratio from Zoñar Lake (Cordoba, Spain) sediments and the Mg/Al ratio from Alboran Sea sediments.

## 6.3. Anthropogenic signals in Western Alboran deep sediments

An increase in aeolian input is observed in the uppermost sediments of core GP04PC, as indicated by a rise in Ti/Al values (Fig. 7), suggesting enhanced regional aridification around ~0.2 ka. This trend may be associated with deforestation and degradation due to anthropic activities, i.e. agriculture in the southern Iberian Peninsula (Martín-Puertas et al., 2009; Mulitza et al., 2010; Gázquez-Sánchez et al., 2023). The significant decrease in water discharge and sediment supply of Western Alboran rivers since the first half of the 20th century, attributed to anthropogenic aridification and the damming of local rivers, including the Guadalfeo River and the Adra River—two main rivers draining Sierra Nevada (Liquete et al., 2005; Bergillos and Ortega-Sánchez, 2017)—raises concerns about potential impacts on water-column dynamics and marine productivity in the Mediterranean (Ludwig et al., 2009). In this regard, achieving centennial resolution of dinocyst data for the last two centuries in the Western Alboran Basin would help to assess whether the anthropogenic reduction in freshwater and sediment supply has affected marine productivity, and to discriminate between the pre- and post-industrial state of Western Alboran Sea, as in the Adriatic Sea (Sangiorgi and Donders, 2004).

Interestingly, Fe and Mn peaks are recognized at 10 cm depth in the core, marking the present position of the oxidation front (i.e., the redoxcline) (Fig. 6). In this interval, both precipitated as Mn-Fe oxyhydroxides (Tribouillard et al., 2006), as seen in some modern Eastern Mediterranean settings, e.g. the Eratosthenes Seamount (Monedero-Contreras et al., 2023b) and the Otranto Strait sill (South Adriatic Sea) (Filippidi and de Lange, 2019). RSTMs such as Zn, Pb, and Mo also precipitated in association with Mn and Fe oxyhydroxides (Fig. 6), as seen in the “marker bed” during sapropel termination/ventilation (Monedero-Contreras et al., 2023a). Therefore, the enrichment in Pb, Cu and Zn, above the Mn-peak, might be attributed to mining of heavy metal sulfides in the South of Spain, a historically significant industry in the region over roughly the last three centuries (Leblanc et al., 2000; Olfas and Nieto, 2015; Romero-Baena et al., 2018). The significant enrichment in Pb (a highly toxic metal) at the top of the core might also be linked to anthropogenic atmospheric pollution over the last century (Álvarez-Iglesias et al., 2012). At any rate, the sediment record of the Western Alboran Basin stands as a valuable tool for envisaging the impacts of anthropogenic activities in the Iberian Peninsula over the past centuries at centennial or even multidecadal resolution (Nieto-Moreno et al., 2011).

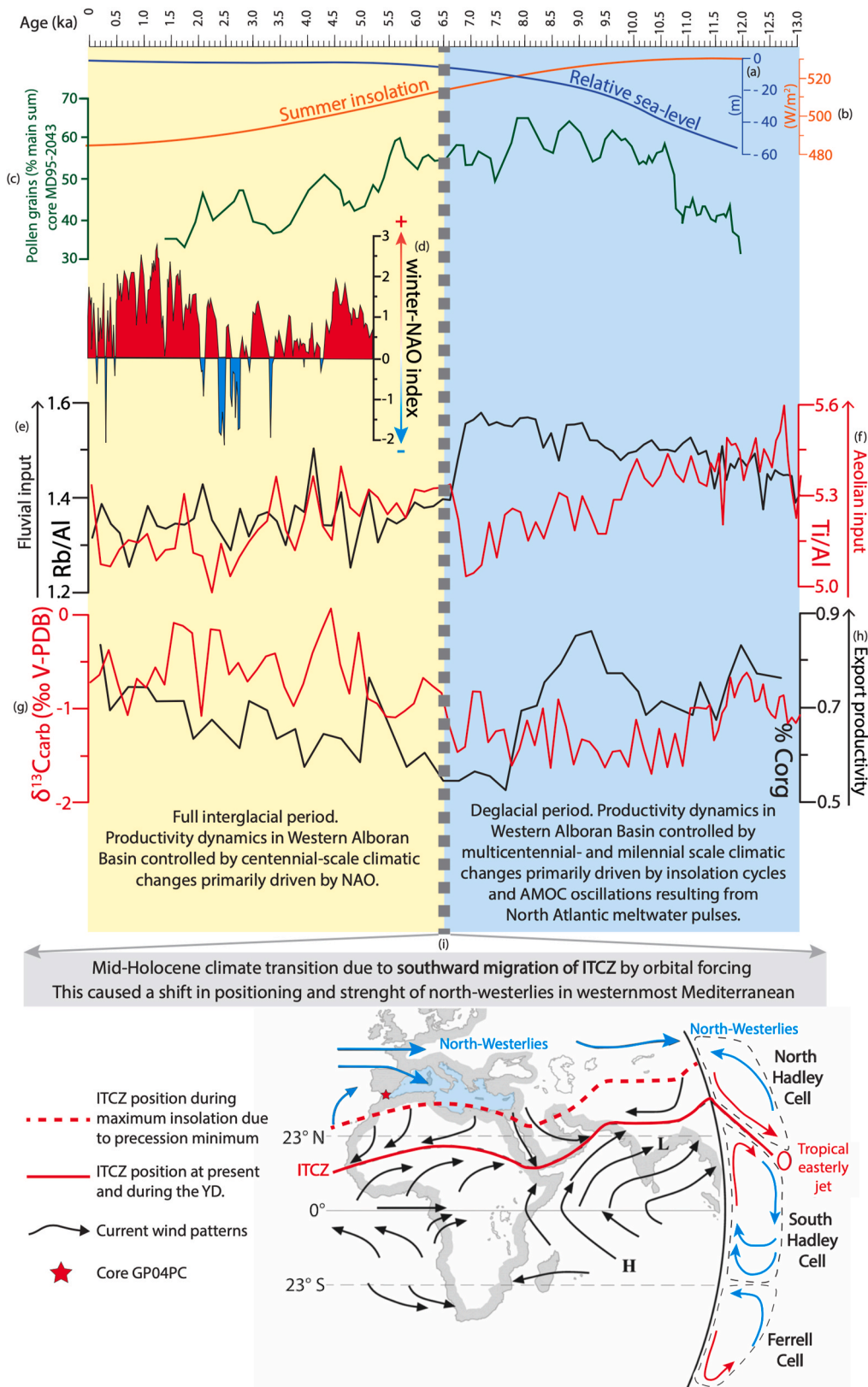


**Fig. 12.** Main climatic systems and oceanic factors controlling productivity dynamics in the Western Alboran Basin at different time scales, before and after the southward migration of the ITCZ around 6.5 ka. Modified from Fletcher et al. (2013). Modified from Fletcher et al. (2013). (a) Summer insolation curve (June, 65°N) (Bergillos and Ortega-Sánchez, 2017); (b) Relative Sea level (Lambeck et al., 2014); (c) Temperate and Mediterranean forest record in Eastern Alboran Basin (core MD95-2043; 1841 mbsl); (d) Winter-NAO index (Olsen et al., 2012); (e) Rb/Al ratio as fluvial input proxy in core GP04PC; (f) Rb/Al (as 10<sup>-3</sup>, %/%) ratio as fluvial input proxy in core GP04PC; (g)  $\delta^{13}C_{carb}$  in core GP04PC; (h)  $C_{org}$  % as export productivity proxy in core GP04PC; (i) Scheme of southward migration of ITCZ around 6.5 ka. Modified from Rohling et al. (2009).

## 7. Conclusions

Beyond unraveling the climatic and oceanographic evolution of the Alboran Sea over the past 13,000 years, the obtained results provide paleoperspectives on marine productivity responses to orbital and sub-orbital climate variability. These insights reveal complex interactions of environmental and oceanographic factors influencing productivity dynamics under a changing climate. Such knowledge is crucial for developing more robust long-term (centennial to multicentennial) productivity projections for the region.

During the Younger Dryas humid phase (~12.4–11.7 ka), characterized by water-column stratification in the Western Alboran Basin, remarkably high marine productivity resulted from: (i) enhanced nutrient-enriched Atlantic water inflow, and (ii) increased local river discharges due to increased regional precipitation, attributed to the reactivation of the AMOC, plus rapid glacier melting from rising temperatures. Similarly, during the Holocene humidity optimum (~10.5–8.5 ka), marine productivity increased primarily due to elevated local river discharges driven by astronomically forced maximum insolation. Additionally, periods of intermittent flood events linked to negative NAO incursions during the late Holocene potentially produced punctual marine productivity increases. Altogether, these observations reveal that over the past 13,000 years, periods of wet regional conditions and enhanced river run-off in the westernmost Mediterranean—controlled by orbital (e.g., insolation cycles) and suborbital factors (e.g., NAO and AMOC changes)—have enhanced marine productivity in the Western Alboran Basin. Our findings moreover attest to the strong influence of North Atlantic climate and ocean dynamics on centennial-scale productivity oscillation in the westernmost Mediterranean.

All along the Holocene, the Ba/Al trend, as well as most Al-normalized RSTM trends, mirrors the fluvial input trend, pointing to a strong detrital influence on trace metal concentration in Western Alboran deep sediments. Thus, fluctuations in the Ba/Al ratio may not accurately reflect changes in marine pelagic barite content, since the high detrital input characterizing the Alboran Sea Basin could have masked the productivity signals derived from increases in marine barite. In this westernmost Mediterranean context, dinocyst analysis emerges as an excellent complementary tool for reconstructing marine productivity.

Throughout the late Holocene, and as compared to most Mediterranean basins, the Western Alboran Basin witnessed enhanced marine productivity and carbon export despite reduced river discharges due to regional aridification. This is due to active upwelling and downwelling systems driven by strong north-westerlies resulting from a persistent positive NAO pattern, which started to develop after the southward migration of the ITCZ around 6.5 ka. Yet in the event that upwelling activity ceases, local rivers would be insufficient to sustain high productivity, thereby reducing biologically-mediated carbon export in the region. Hence, water-column mixing currently has a more significant impact on marine productivity than decreased fluvial inputs produced by regional aridification.

### CRedit authorship contribution statement

**Ricardo D. Monedero-Contreras:** Conceptualization, Investigation, Methodology, sample preparation, interpretation, Writing – original draft. **Francisca Martínez-Ruiz:** Funding acquisition, Supervision, interpretation, Writing – review & editing. **Francisco J. Rodríguez-Tovar:** Supervision, Writing – review & editing. **José M. Mesa-Fernández:** Writing – review & editing. **Francesca Sangiorgi:** interpretation, Writing – review & editing.

### Declaration of competing interest

The authors declare that they have no known competing financial interests or personal relationships that could have appeared to influence the work reported in this paper.

## Acknowledgment

This study has been funded by Grants PID2019-104624RB-I00, PID2019-104625RB-I00, and TED2021-131697B-C22 funded by MCIN/AEI/10.13039/501100011033, Grants FEDER/Junta de Andalucía P18-RT-3804 and P18-RT-4074, and by Research Groups RNM-179 and RNM-178 funded by the Junta de Andalucía. We thank the GeoLab staff from Utrecht University, more precisely the Organic Geochemistry Lab, Stable Isotope Lab and Palynology Lab, for their valuable contributions to organic matter analyses and their assistance in preparing palynomorph slides. We are also grateful to the Center for Scientific Instrumentation (CIC, University of Granada) and the XRF Unit of the Instituto Andaluz de Ciencias de la Tierra (CSIC) for ICP and XRF analyses, respectively. Lastly, we thank editor Dr. Antje Voelker and the two anonymous reviewers for their insightful feedback, which has significantly improved the quality of this study.

## Appendix A. Supplementary data

Supplementary data to this article can be found online at <https://doi.org/10.1016/j.quascirev.2024.109001>.

## Data availability

I have attached the link to my data at the Attach File step

## References

- Algeo, T.J., Li, C., 2020. Redox classification and calibration of redox thresholds in sedimentary systems. *Geochem. Cosmochim. Acta* 287, 8–26. <https://doi.org/10.1016/j.gca.2020.01.055>.
- Algeo, T.J., Liu, J., 2020. A re-assessment of elemental proxies for paleoredox analysis. *Chem. Geol.* 540, 119549. <https://doi.org/10.1016/j.chemgeo.2020.119549>.
- Algeo, T.J., Maynard, J.B., 2004. Trace-element behavior and redox facies in core shales of Upper Pennsylvanian Kansas-type cyclothem. *Chem. Geol.* 206, 289–318. <https://doi.org/10.1016/j.chemgeo.2003.12.009>.
- Álvarez-Iglesias, P., Rubio, B., Millos, J., 2012. Isotopic identification of natural vs. anthropogenic lead sources in marine sediments from the inner Ría de Vigo (NW Spain). *Sci. Total Environ.* 437, 22–35. <https://doi.org/10.1016/j.scitotenv.2012.07.063>.
- Ausín, B., Flores, J.A., Sierro, F.J., Bárcena, M.-A., Hernández-Almeida, I., Francés, G., Gutiérrez-Arnillas, E., Martrat, B., Grimalt, J.O., Cacho, I., 2015a. Coccolithophore productivity and surface water dynamics in the Alboran Sea during the last 25kyr. *Palaeogeogr. Palaeoclimatol. Palaeoecol.* 418, 126–140. <https://doi.org/10.1016/j.palaeo.2014.11.011>.
- Ausín, B., Flores, J.A., Sierro, F.J., Cacho, I., Hernández-Almeida, I., Martrat, B., Grimalt, J.O., 2015b. Atmospheric patterns driving Holocene productivity in the Alboran Sea (western mediterranean): a multiproxy approach. *Holocene* 25, 583–595. <https://doi.org/10.1177/0959683614565952>.
- Ausín, B., Hodell, D.A., Cutmore, A., Eglinton, T.I., 2020. The impact of abrupt deglacial climate variability on productivity and upwelling on the southwestern Iberian margin. *Quat. Sci. Rev.* 230, 106139. <https://doi.org/10.1016/j.quascirev.2019.106139>.
- Bárcena, M.A., Cacho, I., Abrantes, F., Sierro, F.J., Grimalt, J.O., Flores, J.A., 2001. Paleoproductivity variations related to climatic conditions in the Alboran Sea (western Mediterranean) during the last glacial-interglacial transition: the diatom record. *Palaeogeogr. Palaeoclimatol. Palaeoecol.* 167, 337–357. [https://doi.org/10.1016/S0031-0182\(00\)00246-7](https://doi.org/10.1016/S0031-0182(00)00246-7).
- Bárcena, M.A., Flores, J.A., Sierro, F.J., Pérez-Folgado, M., Fabres, J., Calafat, A., Canals, M., 2004. Planktonic response to main oceanographic changes in the Alboran Sea (Western Mediterranean) as documented in sediment traps and surface sediments. *Mar. Micropaleontol.* 53, 423–445. <https://doi.org/10.1016/j.marmicro.2004.09.009>.
- Bartolomé, M., Moreno, A., Sancho, C., Stoll, H.M., Cacho, I., Spötl, C., Belmonte, Á., Edwards, R.L., Cheng, H., Hellstrom, J.C., 2015. Hydrological change in southern Europe responding to increasing North Atlantic overturning during Greenland Stadial 1. *Proc. Natl. Acad. Sci. USA* 112, 6568–6572. <https://doi.org/10.1073/pnas.1503990112>.
- Basterretxea, G., Font-Muñoz, J.S., Salgado-Hernanz, P.M., Arrieta, J., Hernández-Carrasco, I., 2018. Patterns of chlorophyll interannual variability in Mediterranean biogeographical regions. *Remote Sens. Environ.* 215, 7–17. <https://doi.org/10.1016/j.rse.2018.05.027>.
- Bea, F., Montero, P., Stroth, A., Baasner, J., 1996. Microanalysis of minerals by an Excimer UV-LA-ICP-MS system. *Chem. Geol.* 133, 145–156. [https://doi.org/10.1016/S0009-2541\(96\)00073-3](https://doi.org/10.1016/S0009-2541(96)00073-3).
- Benito, G., Greenbaum, N., Medialdea, A., Calle, M., Sanchez-Moya, Y., Machado, M., Ballesteros-Cánovas, J.A., Corella, J.P., 2023. Late Pleistocene-Holocene multi-

- decadal patterns of extreme floods in NW Iberia: the Duero River palaeoflood record. *Quat. Sci. Rev.* 321, 108356. <https://doi.org/10.1016/j.quascirev.2023.108356>.
- Bergillos, R.J., Ortega-Sánchez, M., 2017. Assessing and mitigating the landscape effects of river damming on the Guadalfeo River delta, southern Spain. *Landsc. Urban Plann.* 165, 117–129. <https://doi.org/10.1016/j.landurbplan.2017.05.002>.
- Berner, R.A., 1981. A new geochemical classification of sedimentary environments. *J. Sediment. Res.* 51, 359–365. <https://doi.org/10.1306/212F7C7F-2B24-11D7-8648000102C1865D>.
- Blaauw, M., Christen, J.A., 2011. Flexible paleoclimate age-depth models using an autoregressive gamma process. *Bayesian Analysis* 6, 457–474. <https://doi.org/10.1214/1339616472>.
- Bond, G., Showers, W., Cheseby, M., Lotti, R., Almasi, P., de Menocal, P., Priore, P., Cullen, H., Hajdas, I., Bonani, G., 1997. A pervasive millennial-scale cycle in North Atlantic Holocene and Glacial climates. *Science* 278, 1257–1266. <https://doi.org/10.1126/science.278.5341.1257>.
- Bout-Roumazeilles, V., Combourieu-Nebout, N., Desprat, S., Siani, G., Turon, J.L., Essallami, L., 2013. Tracking atmospheric and riverine terrigenous supplies variability during the last glacial and the Holocene in central Mediterranean. *Clim. Past* 9, 1065–1087. <https://doi.org/10.5194/cp-9-1065-2013>, 2013.
- Breitbart, D., Levin, L.A., Oshlies, A., Grégoire, M., Chavez, F.P., Conley, D.J., Garçon, V., Gilbert, D., Gutiérrez, D., Isensee, K., Jacinto, G.S., Limburg, K.E., Montes, I., Naqvi, S.W.A., Pitcher, G.C., Rabalais, N.N., Roman, M.R., Rose, K.A., Seibel, B.A., Telszewski, M., Yasuhara, M., Zhang, J., 2018. Declining oxygen in the global ocean and coastal waters. *Science* 359, eaam7240. <https://doi.org/10.1126/science.aam7240>.
- Bringué, M., Pospelova, V., Field, D.B., 2014. High resolution sedimentary record of dinoflagellate cysts reflects decadal variability and 20th century warming in the Santa Barbara Basin. *Quat. Sci. Rev.* 105, 86–101. <https://doi.org/10.1016/j.quascirev.2014.09.022>.
- Cacho, I., Grimalt, J.O., Sierro, F.J., Shackleton, N., Canals, M., 2000. Evidence for enhanced Mediterranean thermohaline circulation during rapid climatic coolings. *Earth Planet Sci. Lett.* 183, 417–429. [https://doi.org/10.1016/S0012-821X\(00\)00296-X](https://doi.org/10.1016/S0012-821X(00)00296-X).
- Cacho, I., Grimalt, J., Canals, M., Saffi, N., Schönfeld, R., 2001. Variability of the western Mediterranean Sea surface temperature during the last 25,000 years and its connection with the Northern Hemisphere climate changes. *Paleoceanography* 16, 40–52. <https://doi.org/10.1029/2000pa000502>.
- Cacho, I., Grimalt, J.O., Canals, M., 2002. Response of the Western Mediterranean Sea to rapid climatic variability during the last 50,000 years: a molecular biomarker approach. *J. Mar. Syst.* 33, 253–272. [https://doi.org/10.1016/S0924-7963\(02\)00061-1](https://doi.org/10.1016/S0924-7963(02)00061-1).
- Calvert, S.E., Pedersen, T.F., 1993. Geochemistry of recent oxic and anoxic sediments: implications for the geological record. *Mar. Geol.* 113, 67–88. [https://doi.org/10.1016/0025-3227\(93\)90150-T](https://doi.org/10.1016/0025-3227(93)90150-T).
- Calvert, S.E., Pedersen, T.F., 2007. Chapter fourteen elemental proxies for palaeoclimatic and palaeoceanographic variability in marine sediments: interpretation and application dev. *Mar. Geol.* 567–644. [https://doi.org/10.1016/S1572-5480\(07\)01019-6](https://doi.org/10.1016/S1572-5480(07)01019-6).
- Camuera, J., Jiménez-Moreno, G., Ramos-Román, M.J., García-Alix, A., Jiménez-Espejo, F.J., Toney, J.L., Anderson, R.S., 2021. Chronological control and centennial-scale climatic subdivisions of the Last Glacial Termination in the western Mediterranean region. *Quat. Sci. Rev.* 255, 106814. <https://doi.org/10.1016/j.quascirev.2021.106814>.
- Camuera, J., Ramos-Román, M.J., Jiménez-Moreno, G., García-Alix, A., Ilvonen, L., Ruha, L., Gil-Romera, G., González-Sampériz, P., Seppä, H., 2022. Past 200 kyr hydroclimate variability in the western mediterranean and its connection to the african humid periods. *Sci. Rep.* 12, 9050. <https://doi.org/10.1038/s41598-022-12047-1>.
- Canfield, D.E., 1994. Factors influencing organic carbon preservation in marine sediments. *Chem. Geol.* 114, 315–329. [https://doi.org/10.1016/0009-2541\(94\)90061-2](https://doi.org/10.1016/0009-2541(94)90061-2).
- Capotondi, A., Alexander, M.A., Bond, N.A., Curchitser, E.N., Scott, J.D., 2012. Enhanced upper ocean stratification with climate change in the CMIP3 models. *J. Geophys. Res. Oceans* 117, 1–23. <https://doi.org/10.1029/2011JC007409>.
- Carter, S.C., Paytan, A., Griffith, E.M., 2020. Toward an improved understanding of the marine barium cycle and the application of marine barite as a paleoproductivity proxy. *Minerals* 10, 421. <https://doi.org/10.3390/min10050421>.
- Català, A., Cacho, I., Frigola, J., Pena, L.D., Lirer, F., 2019. Holocene hydrography evolution in the Alboran Sea: a multi-record and multiproxy comparison. *Clim. Past* 15, 927–942. <https://doi.org/10.5194/cp-15-927-2019>.
- Chabaud, L., Sánchez Goñi, M.F., Desprat, S., Rossignol, L., 2014. Land-sea climatic variability in the eastern North Atlantic subtropical region over the last 14,200 years: atmospheric and oceanic processes at different timescales. *Holocene* 24, 787–797. <https://doi.org/10.1177/0959683614530439>.
- Christaki, U., vanWambeke, F., Lefevre, D., Lagaria, A., Prieur, L., Pujó-Pay, M., Grattapanche, J.-D., Colombet, J., Psarra, S., Dolan, J.R., Sime-Ngando, T., Conan, P., Weinbauer, M.G., Moutin, T., 2011. Microbial food webs and metabolic state across oligotrophic waters of the Mediterranean Sea during summer. *Biogeosciences* 8, 1839–1852. <https://doi.org/10.5194/bg-8-1839-2011>.
- Cisneros, M., Cacho, I., Frigola, J., Sanchez-Vidal, A., Calafat, A., Pedrosa-Pàmies, R., Rumin-Caparrós, A., Canals, M., 2019. Deep-water formation variability in the north-western Mediterranean Sea during the last 2500 yr: a proxy validation with present-day data. *Global Planet. Change* 177, 56–68. <https://doi.org/10.1016/j.gloplacha.2019.03.012>.
- Combourieu-Nebout, N., Paterne, M., Turon, J.L., Siani, G., 1998. A high-resolution record of the last deglaciation in the central Mediterranean Sea: palaeovegetation and palaeohydrological evolution. *Quat. Sci. Rev.* 17, 303–317. [https://doi.org/10.1016/S0277-3791\(97\)00039-5](https://doi.org/10.1016/S0277-3791(97)00039-5).
- Combourieu-Nebout, N., Londeix, L., Baudin, F., Turon, J.L., Von Grafenstein, R., Zahn, R., 1999. Quaternary marine and continental paleoenvironments in the western Mediterranean (Site 976, Alboran Sea): palynological evidence. In: *Proceedings of the Ocean Drilling Program*, vol. 161. Scientific Results, pp. 457–468.
- Combourieu-Nebout, N., Peyron, O., Dormoy, I., Desprat, S., Beaudouin, C., Kotthoff, U., Marret, F., 2009. Rapid climatic variability in the west Mediterranean during the last 25 000 years from high resolution pollen data. *Clim. Past* 5, 503–521. <https://doi.org/10.5194/cp-5-503-2009>.
- Crusius, J., Calvert, S., Pedersen, T., Sage, D., 1996. Rhenium and molybdenum enrichments in sediments as indicators of oxic, suboxic, and sulfidic conditions of deposition. *Earth Planet Sci. Lett.* 145, 65–78. [https://doi.org/10.1016/S0012-821X\(96\)00204-X](https://doi.org/10.1016/S0012-821X(96)00204-X).
- Dale, B., 2009. Eutrophication signals in the sedimentary record of dinoflagellate cysts in coastal waters. *J. Sea Res.* 61, 103–113. <https://doi.org/10.1016/j.seares.2008.06.007>.
- Dale, B., Fjellså, A., 1994. Dinoflagellate cysts as paleoproductivity indicators: state of the art, potential, and limits. In: Zahn, R., Pedersen, T.F., Kaminski, M.A., Labeyrie, L. (Eds.), *Carbon Cycling in the Glacial Ocean: Constraints on the Ocean's Role in Global Change*, vol. 17. NATO ASI Series, pp. 521–537. [https://doi.org/10.1007/978-3-642-78737-9\\_22](https://doi.org/10.1007/978-3-642-78737-9_22).
- Dale, B., Dale, A.L., Jansen, J.F., 2002. Dinoflagellate cysts as environmental indicators in surface sediments from the Congo deep-sea fan and adjacent regions. *Paleoceanogr. Palaeoclimatol. Palaeoecol.* 185, 309–338. [https://doi.org/10.1016/S0031-0182\(02\)00380-2](https://doi.org/10.1016/S0031-0182(02)00380-2).
- Datema, M., Sangiorgi, F., De Vernal, A., Reichert, G.J., Lourens, L.J., Slujs, A., 2017. Comparison of qualitative and quantitative dinoflagellate cyst approaches in reconstructing glacial-interglacial climate variability at West Iberian Margin IODP 'Shackleton' Site U1385. *Mar. Micropaleontol.* 136, 14–29. <https://doi.org/10.1016/j.marmicro.2017.08.003>.
- de Lange, G.J., Thomson, J., Reitz, A., Slomp, C.P., Speranza Principato, M., Erba, E., Corsetti, C., 2008. Synchronous basin-wide formation and redox-controlled preservation of a Mediterranean sapropel. *Nat. Geosci.* 1, 606–610. <https://doi.org/10.1038/ngeo283>.
- De Menocal, P.B., 2015. End of the African Humid Period. *Nat. Geosci.* 8, 86–87. <https://doi.org/10.1038/ngeo2355>.
- de Vernal, A., Hillaire-Marcel, C., 2000. Sea-ice cover, sea-surface salinity and halo-/thermocline structure of the northwest North Atlantic: modern versus full glacial conditions. *Quat. Sci. Rev.* 19, 65–85. [https://doi.org/10.1016/S0277-3791\(99\)00055-4](https://doi.org/10.1016/S0277-3791(99)00055-4).
- de Vernal, A., Marret, F., 2007. Chapter nine organic-walled dinoflagellate cysts: tracers of sea-surface conditions. *Developments in marine geology 1*, 371–408. [https://doi.org/10.1016/S1572-5480\(07\)01014-7](https://doi.org/10.1016/S1572-5480(07)01014-7).
- Degeai, J.P., Devillers, B., Dezileau, L., Oueslati, H., Bony, G., 2015. Major storm periods and climate forcing in the western Mediterranean during the late Holocene. *Quat. Sci. Rev.* 129, 37–56. <https://doi.org/10.1016/j.quascirev.2015.10.009>.
- Di Rita, F., Fletcher, W.J., Aranbarri, J., Margaritelli, G., Lirer, F., Magri, D., 2018. Holocene forest dynamics in central and western Mediterranean: periodicity, spatio-temporal patterns and climate influence. *Sci. Rep.* 8, 8929. <https://doi.org/10.1038/s41598-018-27056-2>.
- Dormoy, I., Peyron, O., Combourieu Nebout, N., Goring, S., Kotthoff, U., Magny, M., Pross, J., 2009. Terrestrial climate variability and seasonality changes in the Mediterranean region between 15000 and 4000 years BP deduced from marine pollen records. *Clim. Past* 5, 615–632. <https://doi.org/10.5194/cp-5-615-2009>.
- Dünkeloh, A., Jacobeit, J., 2003. Circulation dynamics of Mediterranean precipitation variability 1948–98. *Int. J. Climatol.* 23, 1843–1866. <https://doi.org/10.1002/joc.973>.
- D'Ortenzio, F., Ribera d'Alcalá, M., 2009. On the trophic regimes of the Mediterranean Sea: a satellite analysis. *Biogeosciences* 5, 139–148. <https://doi.org/10.5194/bg-6-139-2009>.
- Fabres, J., Calafat, A., Sanchez-Vidal, A., Canals, M., Heussner, S., 2002. Composition and spatio-temporal variability of particle fluxes in the western Alboran Gyre, Mediterranean Sea. *J. Mar. Syst.* 33, 431–456. [https://doi.org/10.1016/S0924-7963\(02\)00070-2](https://doi.org/10.1016/S0924-7963(02)00070-2).
- Filippidi, A., de Lange, G.J., 2019. Eastern mediterranean deep water formation during sapropel S1: a reconstruction using geochemical records along a bathymetric transect in the adriatic outflow region. *Paleoceanogr. Paleoclimatol.* 34, 409–429. <https://doi.org/10.1029/2018PA003459>.
- Fink, H.G., Wienberg, C., De Pol-Holz, R., Hebbeln, D., 2015. Spatio-temporal distribution patterns of Mediterranean cold-water corals (*Lophelia pertusa* and *Madrepora oculata*) during the past 14,000 years. *Deep-Sea Res. I: Oceanogr. Res. Pap.* 103, 37–48. <https://doi.org/10.1016/j.dsr.2015.05.006>.
- Fletcher, W.J., Zielhofer, C., 2013. Fragility of Western Mediterranean landscapes during Holocene rapid climate changes. *Catena* 103, 16–29. <https://doi.org/10.1016/j.catena.2011.05.001>.
- Fletcher, W.J., Sánchez Goñi, M.F., Peyron, O., Dormoy, I., 2010. Abrupt climate changes of the last deglaciation detected in a Western Mediterranean forest record. *Clim. Past* 6, 245–264. <https://doi.org/10.5194/cp-6-245-2010>.
- Fletcher, W.J., Debret, M., Goñi, M.F.S., 2013. Mid-Holocene emergence of a low-frequency millennial oscillation in western Mediterranean climate: implications for past dynamics of the North Atlantic atmospheric westerlies. *Holocene* 23, 153–166. <https://doi.org/10.1177/0959683612460783>.
- Fogel, M.L., Cifuentes, L.A., 1993. *Isotope fractionation during primary production. In: Organic Geochemistry: Principles and Applications*. Springer US, Boston, MA, pp. 73–98.

- Francois, R., Honjo, S., Manganini, S.J., Ravizza, G.E., 1995. Biogenic barium fluxes to the deep sea: implications for paleoproductivity reconstruction. *Global Biogeochem. Cycles* 9, 289–303. <https://doi.org/10.1029/95GB00021>.
- Frigola, J., Moreno, A., Cacho, I., Canals, M., Siero, F.J., Flores, J.A., Grimalt, J.O., Hodell, D.A., Curtis, J.H., 2007. Holocene climate variability in the western Mediterranean region from a deepwater sediment record. *Paleoceanography* 22, PA2209. <https://doi.org/10.1029/2006PA001307>.
- Frigola, J., Moreno, A., Cacho, I., Canals, M., Siero, F.J., Flores, J.A., Grimalt, J.O., 2008. Evidence of abrupt changes in Western Mediterranean Deep Water circulation during the last 50 kyr: a high-resolution marine record from the Balearic Sea. *Quat. Int.* 181, 88–104. <https://doi.org/10.1016/j.quaint.2007.06.016>.
- Fujii, R., Matsuoka, K., 2006. Seasonal change of dinoflagellates cyst flux collected in a sediment trap in Omura Bay, West Japan. *J. Plankton Res.* 28, 131–147. <https://doi.org/10.1093/plankt/fbi106>.
- García-Alix, A., Camuera, J., Ramos-Román, M.J., Toney, J.L., Sachse, D., Schefuß, E., Jiménez-Moreno, G., Jiménez-Espejo, F.J., López-Avilés, A., Anderson, R.S., Yanes, Y., 2021. Paleohydrological dynamics in the Western Mediterranean during the last glacial cycle. *Global Planet. Change* 202, 103527. <https://doi.org/10.1016/j.gloplacha.2021.103527>.
- García-Alix, A., Jiménez-Moreno, G., Gazquez, F., Monedero-Contreras, R., López-Avilés, A., Jiménez-Espejo, F.J., Rodríguez-Rodríguez, M., Camuera, J., Ramos-Román, M.J., Anderson, R.S., 2022. Climatic control on the Holocene hydrology of a playa-lake system in the western Mediterranean. *Catena* 214, 106292. <https://doi.org/10.1016/j.catena.2022.106292>.
- García-Lafuente, J., Naranjo, C., Sammartino, S., Sánchez-Garrido, J.C., Delgado, J., 2017. The Mediterranean outflow in the Strait of Gibraltar and its connection with upstream conditions in the Alborán Sea. *Ocean Sci.* 13, 195–207. <https://doi.org/10.5194/os-13-195-2017>.
- García-Lafuente, J., Sammartino, S., Huertas, I.E., Flecha, S., Sánchez-Leal, R.F., Naranjo, C., Nadal, I., Bellanco, M.J., 2021. Hotter and weaker Mediterranean outflow as a response to basin-wide alterations. *Front. Mar. Sci.* 8, 613444. <https://doi.org/10.3389/fmars.2021.613444>.
- García-Ruiz, J.M., Palacios, D., González-Sampériz, P., De Andrés, N., Moreno, A., Valero-Garcés, B., Gómez-Villar, A., 2016. Mountain glacier evolution in the Iberian Peninsula during the younger Dryas. *Quat. Sci. Rev.* 138, 16–30. <https://doi.org/10.1016/j.quascirev.2016.02.022>.
- García-Jove, M., Mourre, B., Zarokanello, N.D., Lermusiaux, P.F., Rudnick, D.L., Tintoré, J., 2022. Frontal dynamics in the Alboran Sea: 2. Processes for vertical velocities development. *J. Geophys. Res. Oceans* 127, e2021JC017428. <https://doi.org/10.1029/2021JC017405>.
- Gázquez-Sánchez, F., Jiménez-Espejo, F., Rodríguez-Rodríguez, M., Martegani, L., Voigt, C., Ruiz-Lara, D., Moreno, A., Valero-Garcés, B., Morellón, M., Martín-Puertas, C., 2023. Roman water management impacted the hydrological functioning of wetlands during drought periods. *Sci. Rep.* 13, 18815. <https://doi.org/10.1038/s41598-023-46010-5>.
- Gingele, F.X., Zabel, M., Kasten, S., Bonn, W.J., Nürnberg, C.C., 1999. Biogenic barium as a proxy for paleoproductivity: methods and limitations of application. In: Fischer, G., Wefer, G. (Eds.), *Use of Proxies in Paleoceanography*. Springer, Berlin, Heidelberg, pp. 345–364. [https://doi.org/10.1007/978-3-642-58646-0\\_13](https://doi.org/10.1007/978-3-642-58646-0_13).
- Grant, K.M., Grimm, R., Mikolajewicz, U., Marino, G., Ziegler, M., Rohling, E.J., 2016. The timing of Mediterranean sapropel deposition relative to insolation, sea-level and African monsoon changes. *Quat. Sci. Rev.* 140, 125–141. <https://doi.org/10.1016/j.quascirev.2016.03.026>.
- Grema, H.M., Magnall, J.M., Whitehouse, M.J., Gleeson, S.A., Schulz, H.M., 2022. The Formation of highly positive  $\delta^{34}\text{S}$  values in late devonian mudstones: microscale analysis of pyrite ( $\delta^{34}\text{S}$ ) and barite ( $\delta^{34}\text{S}$ ,  $\delta^{18}\text{O}$ ) in the canol formation (selwyn basin, Canada). *Front. Earth Sci.* 9, 784824. <https://doi.org/10.3389/feart.2021.784824>.
- Gruber, N., 2011. Warming up, turning sour, losing breath: ocean biogeochemistry under global change. *Philos. Trans. A Math. Phys. Eng. Sci.* 369, 1980–1996. <https://doi.org/10.1098/rsta.2011.0003>.
- Gruber, N., Boyd, P.W., Frölicher, T.L., Vogt, M., 2021. Biogeochemical extremes and compound events in the ocean. *Nature* 600, 395–407. <https://doi.org/10.1038/s41586-021-03981-7>.
- Hardy, W., Marret, F., Penaud, A., Le Mezo, P., Droz, L., Marsset, T., Kageyama, M., 2018. Quantification of last glacial-Holocene net primary productivity and upwelling activity in the equatorial eastern Atlantic with a revised modern dinocyst database. *Palaeogeogr. Palaeoclimatol. Palaeoecol.* 505, 410–427. <https://doi.org/10.1016/j.palaeo.2018.06.025>.
- Haug, G.H., Hughen, K.A., Sigman, D.M., Peterson, L.C., Rohl, U., 2001. Southward migration of the intertropical convergence zone through the Holocene. *Science* 293, 1304–1308. <https://doi.org/10.1126/science.1059725>.
- Heaton, T.J., Köhler, P., Butzin, M., Bard, E., Reimer, R.W., Austin, W.E., Ramsey, C.B., Grootes, P.W., Hughen, K.A., Kromer, B., Reimer, P.J., Adkins, J., Burke, A., Cook, M.S., Olsen, J., Skinner, L.C., 2020. Marine20—the marine radiocarbon age calibration curve (0–55,000 cal BP). *Radiocarbon* 62, 779–820. <https://doi.org/10.1017/RDC.2020.68>.
- Henkel, S., Mogollón, J.M., Nöthen, K., Franke, C., Bogus, K., Robin, E., Bahr, A., Blumenberg, M., Pape, T., Seifert, R., März, C., de Lange, G., Kasten, S., 2012. Diagenetic barium cycling in Black Sea sediments -A case study for anoxic marine environments. *Geochim. Cosmochim. Acta* 88, 88–105. <https://doi.org/10.1016/j.gca.2012.04.021>.
- Hernández, A., Sáez, A., Santos, R.N., Rodrigues, T., Martín-Puertas, C., Gil-Romera, G., Abbot, M., Carballeira, R., Costa, P., Giral, S., Gomes, S.D., Griffone, M., Ibanez-Insua, J., Leira, M., Moreno, J., Filipa, N., Oliveira, D., Raposo, P.M., Trigo, R.M., Vieira, G., Ramos, A.M., 2023. The timing of the deglaciation in the Atlantic Iberian mountains: Insights from the stratigraphic analysis of a lake sequence in Serra da Estrela (Portugal). *Earth Surf. Process. Landforms* 48, 233–242. <https://doi.org/10.1002/esp.5536>.
- Hurrell, J.W., 1995. Decadal trend in the North Atlantic Oscillation: regional temperatures and precipitations. *Science* 269, 676–679. <https://doi.org/10.1126/science.269.5224.676>.
- Iivonen, L., López-Sáez, J.A., Holmström, L., Alba-Sánchez, F., Pérez-Díaz, S., Carrión, J. S., Ramos-Roman, M.J., Camuera, J., Jiménez-Moreno, G., Ruha, L., Seppä, H., 2022. Spatial and temporal patterns of Holocene precipitation change in the Iberian Peninsula. *Boreas* 51, 776–792. <https://doi.org/10.1111/bor.12586>.
- IPCC, 2023. Climate change 2023: synthesis report. In: Lee, H., Romero, J. (Eds.), *Contribution of Working Groups I, II and III to the Sixth Assessment Report of the Intergovernmental Panel on Climate Change [Core Writing Team. IPCC, Geneva, Switzerland*, pp. 35–115. <https://doi.org/10.59327/IPCC/AR6-9789291691647>.
- Ivy-Ochs, S., Kerschner, H., Maisch, M., Christ, M., Kubik, P.W., Schlüchter, C., 2009. Latest Pleistocene and Holocene glacier variations in the European Alps. *Quat. Sci. Rev.* 28, 2137–2149. <https://doi.org/10.1016/j.quascirev.2009.03.009>.
- Jacobson, D.M., Anderson, D.M., 1986. Thecate heterotrophic dinoflagellates: feeding behavior and mechanisms I. *J. Phycol.* 22, 249–258. <https://doi.org/10.1111/j.1529-8817.1986.tb00021.x>.
- Jalut, G., Amat, A.E., Mora, S.R., Fontugne, M., Mook, R., Bonnet, L., Gauquelin, T., 1997. Holocene climatic changes in the western Mediterranean: installation of the Mediterranean climate. *C. R. Acad. Sci. Ser. II* 325, 327–334. [https://doi.org/10.1016/S1251-8050\(97\)81380-8](https://doi.org/10.1016/S1251-8050(97)81380-8).
- Jalut, G., Amat, A.E., Bonnet, L., Gauquelin, T., Fontugne, M., 2000. Holocene climatic changes in the Western Mediterranean, from south-east France to south-east Spain. *Palaeogeogr. Palaeoclimatol. Palaeoecol.* 160, 255–290. [https://doi.org/10.1016/S0031-0182\(00\)00075-4](https://doi.org/10.1016/S0031-0182(00)00075-4).
- Jiménez-Espejo, F.J., García-Alix, A., Jiménez-Moreno, G., Rodrigo-Gámiz, M., Anderson, R.S., Rodríguez-Tovar, F.J., Martínez-Ruiz, F., Giral, S., Huertas, A.D., Pardo-Igúzquiza, E., 2014. Saharan aeolian input and effective humidity variations over western Europe during the Holocene from a high altitude record. *Chem. Geol.* 374, 1–12. <https://doi.org/10.1016/j.chemgeo.2014.03.001>.
- Jiménez-Espejo, F.J., Martínez-Ruiz, F., Rogerson, M., González-Donoso, J.M., Romero, O.E., Linares, D., Sakamoto, T., Gallego-Torres, D., Rueda-Ruiz, J.L., Ortega-Huertas, M., Perez Claros, J.A., 2008. Detrital input, productivity fluctuations and water mass circulation in the westernmost Mediterranean Sea since the Last Glacial Maximum. *G-cubed* 9, 1525–2027. <https://doi.org/10.1029/2008GC002096>.
- Jiménez-Espejo, F.J., Martínez-Ruiz, F., Sakamoto, T., Iijima, K., Gallego-Torres, D., Harada, N., 2007. Paleoenvironmental changes in the western Mediterranean since the last glacial maximum: high resolution multiproxy record from the Algero-Balearic basin. *Palaeogeogr. Palaeoclimatol. Palaeoecol.* 246, 292–306. <https://doi.org/10.1016/j.palaeo.2006.10.005>.
- Jiménez-Espejo, F.J., Pardo-Gené, M., Martínez-Ruiz, F., García-Alix, A., vande Fliert, T., Toyofuku, T., Bahr, A., Kreissig, K., 2015. Geochemical evidence for intermediate water circulation in the westernmost Mediterranean over the last 20 kyr BP and its impact on the Mediterranean Outflow. *Global Planet. Change* 135, 38–46. <https://doi.org/10.1016/j.gloplacha.2015.10.001>.
- Jiménez-Moreno, G., Anderson, R.S., Ramos-Román, M.J., Camuera, J., Mesa-Fernández, J.M., García-Alix, A., Jiménez-Espejo, F.J., Carrión, J.S., López-Avilés, A., 2020. The Holocene Cedrus pollen record from Sierra Nevada (S Spain), a proxy for climate change in N Africa. *Quat. Sci. Rev.* 242, 106468. <https://doi.org/10.1016/j.quascirev.2020.106468>.
- Jiménez-Moreno, G., García-Alix, A., Anderson, R.S., Ramos-Román, M.J., Camuera, J., Mesa-Fernández, J.M., Toney, J.L., Jiménez-Espejo, F.J., Carrión, J.S., López-Avilés, A., Rodrigo-Gámiz, M., Webster, C.E., 2022. Reconstruction of past environment and climate using wetland sediment records from the Sierra Nevada. In: Zamora, R., Oliva, M. (Eds.), *The Landscape of the Sierra Nevada*. Springer, Cham, pp. 95–114. [https://doi.org/10.1007/978-3-030-94219-9\\_7](https://doi.org/10.1007/978-3-030-94219-9_7).
- Jiménez-Moreno, G., López-Avilés, A., García-Alix, A., Ramos-Román, M.J., Camuera, J., Mesa-Fernández, J.M., Jiménez-Espejo, F.J., López-Blanco, C., Carrión, J.S., Anderson, R.S., 2023. Laguna Seca sediments reveal environmental and climate change during the latest Pleistocene and Holocene in Sierra Nevada, southern Iberian Peninsula. *Palaeogeogr. Palaeoclimatol. Palaeoecol.* 631, 111834. <https://doi.org/10.1016/j.palaeo.2023.111834>.
- Katz, M.E., Pak, D.K., Dickens, G.R., Thomas, E., 1999. The source and fate of massive carbon input during the latest Paleocene thermal maximum. *Science* 286, 1531–1533. <https://doi.org/10.1126/science.286.5444.1531>.
- Kiessling, W., Smith, J.A., Raja, N.B., 2023. Improving the relevance of paleontology to climate change policy. *Proc. Natl. Acad. Sci. USA* 120, e2201926119. <https://doi.org/10.1073/pnas.2201926119>.
- Lambeck, K., Rouby, H., Purcell, A., Sun, Y., Sambridge, M., 2014. Sea level and global ice volumes from the last glacial maximum to the Holocene. *Proc. Natl. Acad. Sci. USA* 111, 15296–15303. <https://doi.org/10.1073/pnas.1411762111>.
- Lane, C.S., Brauer, A., Blockley, S.P., Dulski, P., 2013. Volcanic ash reveals time-transgressive abrupt climate change during the Younger Dryas. *Geology* 41, 1251–1254. <https://doi.org/10.1130/G34867.1>.
- Leblanc, M., Morales, J.A., Borrego, J., Elbaz-Poulichet, F., 2000. 4,500-year-old mining pollution in southwestern Spain: long-term implications for modern mining pollution. *Econ. Geol.* 95, 655–662. <https://doi.org/10.2113/gsecongeo.95.3.655>.
- Light, T., Martínez-Ruiz, F., Norris, R., 2023. Marine barite morphology as an indicator of biogeochemical conditions within organic matter aggregates. *Geochim. Cosmochim. Acta* 358, 38–48. <https://doi.org/10.1016/j.gca.2023.08.012>.
- Lionello, P., Scarascia, L., 2018. The relation between climate change in the Mediterranean region and global warming. *Reg. Environ. Change* 18, 1481–1493. <https://doi.org/10.1007/s10113-018-1290-1>.

- Lionello, P., Malanotte-Rizzoli, P., Boscolo, R., Alpert, P., Artale, V., Li, L., Luterbacher, J., May, W., Trigo, R., Tsimplis, M., Ulbrich, U., Xoplaki, E., 2006. The Mediterranean climate: an overview of the main characteristics and issues. *Developments in Earth and Environmental Sciences* 4, 1–26. [https://doi.org/10.1016/S1571-9197\(06\)80003-0](https://doi.org/10.1016/S1571-9197(06)80003-0).
- Liquete, C., Arnau, P., Canals, M., Colas, S., 2005. Mediterranean river systems of Andalusia, southern Spain, and associated deltas: a source to sink approach. *Mar. Geol.* 222–223, 471–495. <https://doi.org/10.1016/j.margeo.2005.06.033>.
- Little, S.H., Vance, D., Lyons, T.W., McManus, J., 2015. Controls on trace metal authigenic enrichment in reducing sediments: insights from modern oxygen-deficient settings. *Am. J. Sci.* 315, 77–119. <https://doi.org/10.2475/02.2015.01>.
- Lobo, F.J., Fernández-Salas, L.M., Moreno, I., Sanz, J.L., Maldonado, A., 2006. The sea-floor morphology of a Mediterranean shelf fed by small rivers, northern Alboran Sea margin. *Contin. Shelf Res.* 26, 2607–2628. <https://doi.org/10.1016/j.csr.2006.08.006>.
- López-Moreno, J.I., Vicente-Serrano, S.M., Morán-Tejada, E., Lorenzo-Lacruz, J., Kenawy, A., Beniston, M., 2011. Effects of the North Atlantic Oscillation (NAO) on combined temperature and precipitation winter modes in the Mediterranean mountains: observed relationships and projections for the 21st century. *Global Planet. Change* 77, 62–76. <https://doi.org/10.1016/j.gloplacha.2011.03.003>.
- Lozier, M.S., Dave, A.C., Palter, J.B., Gerber, L.M., Barber, R.T., 2011. On the relationship between stratification and primary productivity in the North Atlantic. *Geophys. Res. Lett.* 38, 1–6. <https://doi.org/10.1029/2011GL049414>.
- Ludwig, W., Dumont, E., Meybeck, M., Heussner, S., 2009. River discharges of water and nutrients to the Mediterranean and Black Sea: major drivers for ecosystem changes during past and future decades? *Prog. Oceanogr.* 80 (3–4), 199–217. <https://doi.org/10.1016/j.pocean.2009.02.001>.
- Macias, D.M., Garcia-Gorriz, E., Stips, A., 2015. Productivity changes in the Mediterranean Sea for the twenty-first century in response to changes in the regional atmospheric forcing. *Front. Mar. Sci.* 2, 79. <https://doi.org/10.3389/fmars.2015.00079>.
- Macias, D.M., Garcia-Gorriz, E., Dosio, A., Stips, A., Keuler, K., 2016. Obtaining the correct sea surface temperature: bias correction of region- al climate model data for the Mediterranean Sea. *Clim. Dynam.* 51, 1095–1117. <https://doi.org/10.1007/s00382-016-3049-z>.
- Malanotte-Rizzoli, P., Artale, V., Borzelli-Eusebi, G.L., Brenner, S., Crise, A., Gacic, M., Kress, N., Marullo, S., Ribera d'Alcalá, M., Sofianos, S., Tanhua, T., Theocharis, A., Alvarez, M., Ashkenazy, Y., Bergamasco, A., Cardin, V., Carniel, S., Civitarese, G., D'Ortenzio, F., Font, J., Garcia-Ladona, E., Garcia-Lafuente, J.M., Gogou, A., Gregoire, M., Hainbucher, D., Kontoyannis, H., Kovacevic, V., Kraskapoulou, E., Kroskos, G., Incarbona, A., Mazzocchi, M.G., Orlic, M., Ozsoy, E., Pascual, A., Poulain, P.-M., Roether, W., Rubino, A., Schroeder, K., Siokou-Frangou, J., Souverainzoglou, E., Sprovieri, M., Tintoré, J., Triantafyllou, G., 2014. Physical forcing and physical/biochemical variability of the Mediterranean Sea: a review of unresolved issues and directions for future research. *Ocean Sci.* 10, 281–322. <https://doi.org/10.5194/os-10-281-2014>.
- Mancini, A.M., Bocci, G., Morigi, C., Gennari, R., Lozar, F., Negri, A., 2023a. Past analogues of deoxygenation events in the mediterranean sea: a tool to constrain future impacts. *J. Mar. Sci. Eng.* 11, 562. <https://doi.org/10.3390/jmse11030562>.
- Mancini, A.M., Lozar, F., Gennari, R., Capozzi, R., Morigi, C., Negri, A., 2023b. The past to unravel the future: deoxygenation events in the geological archive and the anthropocene oxygen crisis. *Earth Sci. Rev.* 104664. <https://doi.org/10.1016/j.earscirev.2023.104664>.
- Marret, F., Zonneveld, K.A., 2003. Atlas of modern organic-walled dinoflagellate cyst distribution. *Rev. Palaeobot. Palynol.* 125, 1–200. [https://doi.org/10.1016/S0034-6667\(02\)00229-4](https://doi.org/10.1016/S0034-6667(02)00229-4).
- Martín-Puertas, C., Valero-Garcés, B.L., Brauer, A., Mata, M.P., Delgado-Huertas, A., Dulski, P., 2009. The Iberian-Roman humid period (2600–1600 cal yr BP) in the Zoñar Lake varve record (Andalucía, southern Spain). *Quat. Res.* 71, 108–120. <https://doi.org/10.1016/j.yqres.2008.10.004>.
- Martín-Puertas, C., Jiménez-Espejo, F., Martínez-Ruiz, F., Nieto-Moreno, V., Rodrigo, M., Mata, M.P., Valero-Garcés, B.L., 2010. Late Holocene climate variability in the southwestern Mediterranean region: an integrated marine and terrestrial geochemical approach. *Clim. Past* 6, 807–816. <https://doi.org/10.5194/cp-6-807-2010>.
- Martínez-Ruiz, F., Kastner, M., Paytan, A., Ortega-Huertas, M., Bernasconi, S.M., 2000. Geochemical evidence for enhanced productivity during S1 sapropel deposition in the eastern Mediterranean. *Paleoceanography* 15, 200–209. <https://doi.org/10.1029/1999PA000419>.
- Martínez-Ruiz, F., Kastner, M., Gallego-Torres, D., Rodrigo-Gámiz, M., Nieto-Moreno, V., Ortega-Huertas, M., 2015. Paleoclimate and paleoceanography over the past 20,000yr in the Mediterranean Sea Basins as indicated by sediment elemental proxies. *Quat. Sci. Rev.* 107, 25–46. <https://doi.org/10.1016/j.quascirev.2014.09.018>.
- Masqué, P., Fabres, J., Canals, M., Sanchez-Cabeza, J.A., Sanchez-Vidal, A., Cacho, I., Calafat, A.M., Bruach, J.M., 2003. Accumulation rates of major constituents of hemipelagic sediments in the deep Alboran Sea: a centennial perspective of sedimentary dynamics. *Mar. Geol.* 193, 207–233. [https://doi.org/10.1016/S0025-3227\(02\)00593-5](https://doi.org/10.1016/S0025-3227(02)00593-5).
- McGee, D., Donohoe, A., Marshall, J., Ferreira, D., 2014. Changes in ITCZ location and cross-equatorial heat transport at the last glacial maximum, Heinrich stadial 1, and the mid-holocene. *EPSL* 390, 69–79. <https://doi.org/10.1016/j.epsl.2013.12.043>.
- McManus, J., Berelson, W.M., Klinkhammer, G.P., Johnson, K.S., Coale, K.H., Anderson, R.F., Kumar, N., Burdige, D.J., Hammond, D.E., Brumsack, H.J., McCorkle, D.C., Rushdi, A., 1998. Geochemistry of barium in marine sediments: implications for its use as a paleoproxy. *Geochem. Cosmochim. Acta* 62, 3453–3473. [https://doi.org/10.1016/S0016-7037\(98\)00248-8](https://doi.org/10.1016/S0016-7037(98)00248-8).
- Mena, C., Reglero, P., Hidalgo, M., Sintes, E., Santiago, R., Martín, M., Moya, G., Balbín, R., 2019. Phytoplankton community structure is driven by stratification in the oligotrophic Mediterranean Sea. *Front. Microbiol.* 10, 1698. <https://doi.org/10.3389/fmicb.2019.01698>.
- Mertens, K.N., Price, A.M., Pospelova, V., 2012. Determining the absolute abundance of dinoflagellate cysts in recent marine sediments II: further tests of the Lycopodium marker-grain method. *Rev. Palaeobot. Palynol.* 184, 74–81. <https://doi.org/10.1016/j.revpalbo.2012.06.012>.
- Mesa-Fernández, J.M., Jiménez-Moreno, G., Rodrigo-Gámiz, M., García-Alix, A., Jiménez-Espejo, F.J., Martínez-Ruiz, F., Anderson, R.S., Camuera, J., Ramos-Román, M.J., 2018. Vegetation and geochemical responses to Holocene rapid climate change in the Sierra Nevada (southeastern Iberia): the Laguna Hondera record. *Clim. Past* 14, 1687–1706. <https://doi.org/10.5194/cp-14-1687-2018>.
- Mesa-Fernández, J.M., Martínez-Ruiz, F., Rodrigo-Gámiz, M., Jiménez-Espejo, F.J., García, M., Sierro, F.J., 2022. Paleocirculation and paleoclimate conditions in the western Mediterranean basins over the last deglaciation: new insights from sediment composition variations. *Global Planet. Change* 209, 103732. <https://doi.org/10.1016/j.gloplacha.2021.103732>.
- Meyers, P.A., 1994. Preservation of elemental and isotopic source identification of sedimentary organic matter. *Chem. Geol.* 114, 289–302. [https://doi.org/10.1016/0009-2541\(94\)90059-0](https://doi.org/10.1016/0009-2541(94)90059-0).
- Millot, C., 1999. Circulation in the western Mediterranean Sea. *J. Mar. Syst.* 20, 423–442. [https://doi.org/10.1016/S0924-7963\(98\)00078-5](https://doi.org/10.1016/S0924-7963(98)00078-5).
- Millot, C., 2009. Another description of the Mediterranean Sea outflow. *Prog. Oceanogr.* 82, 101–124. <https://doi.org/10.1016/j.pocean.2009.04.016>.
- Millot, C., Taupier-Letage, I., 2005. Circulation in the Mediterranean Sea. In: Saliot, A. (Ed.), *The Mediterranean Sea*, vol. 5. Springer, Berlin, Heidelberg, pp. 26–66. <https://doi.org/10.1007/b107143>. *Handb. Environ. Chem.*
- Monedero-Contreras, R.D., Martínez-Ruiz, F., Rodríguez-Tovar, F.J., 2023a. Evidence of postdepositional remobilization of redox-sensitive metals across sapropel boundaries: new insights from LA-ICP-MS and EDX mapping analyses. *Chem. Geol.* 636, 121643. <https://doi.org/10.1016/j.chemgeo.2023.121643>.
- Monedero-Contreras, R.D., Martínez-Ruiz, F., Rodríguez-Tovar, F.J., de Lange, G., 2023b. Redox geochemical signatures in Mediterranean sapropels: implications to constrain deoxygenation dynamics in deep-marine settings. *Paleoceanogr. Paleoclimatol. Paleoeoc.* 634, 111953. <https://doi.org/10.1016/j.palaeo.2023.111953>.
- Montresor, M., Zingone, A., Sarno, D., 1998. Dinoflagellate cyst production at a coastal Mediterranean site. *J. Plankton Res.* 20, 2291–2312. <https://doi.org/10.1093/plankt/20.12.4291>.
- Morán, X.A.G., Estrada, M., 2001. Short-term variability of photosynthetic parameters and particulate and dissolved primary production in the Alboran Sea (SW Mediterranean). *Mar. Ecol. Prog. Ser.* 212, 53–67. <https://doi.org/10.3354/meps212053>.
- Morcillo-Montalbá, L., Rodrigo-Gámiz, M., Martínez-Ruiz, F., Ortega-Huertas, M., Schouten, S., Sinnighe Damsté, J.S., 2021. Rapid climate changes in the westernmost mediterranean (Alboran Sea) over the last 35 kyr: new insights from four lipid paleothermometers (UK'37, TEXH86, RI-OH', and LDI). *Paleoceanogr. Paleoclimatol. Paleoeoc.* 36, e2020PA004171. <https://doi.org/10.1029/2020PA004171>.
- Moreno, A., Cacho, I., Canals, M., Grimalt, J.O., Sanchez-Vidal, A., 2004. Millennial-scale variability in the productivity signal from the Alboran Sea record, western Mediterranean Sea. *Paleoceanogr. Paleoclimatol. Paleoeoc.* 211, 205–219. <https://doi.org/10.1016/j.palaeo.2004.05.007>.
- Multiza, S., Heslop, D., Pittauerova, D., Fischer, H.W., Meyer, I., Stuut, J.B., Zabel, M., Mollenhauer, G., Collins, J.A., Kuhnert, H., Schulz, M., 2010. Increase in African dust flux at the onset of commercial agriculture in the Sahel region. *Nature* 466, 226–228. <https://doi.org/10.1038/nature09213>.
- Naidu, P.D., Niituma, N., 2004. Atypical  $\delta^{13}\text{C}$  signature in Globigerina bulloides at the ODP site 723A (Arabian Sea): implications of environmental changes caused by upwelling. *Mar. Micropaleontol.* 53, 1–10. <https://doi.org/10.1016/j.marmicro.2004.01.005>.
- Nieto-Moreno, V., Martínez-Ruiz, F., Giral, S., Jiménez-Espejo, F., Gallego-Torres, D., Rodrigo-Gámiz, M., García-Orellana, J., Huertas-Ortega, M., de Lange, G.J., 2011. Tracking climate variability in the western Mediterranean during the late Holocene: a multiproxy approach. *Clim. Past* 7, 1395–1414. <https://doi.org/10.5194/cp-7-1395-2011>.
- Nieto-Moreno, V., Martínez-Ruiz, F., Willmott, V., García-Orellana, J., Masqué, P., Damsté, J.S., 2013. Climate conditions in the westernmost Mediterranean over the last two millennia: an integrated biomarker approach. *Org. Geochem.* 55, 1–10. <https://doi.org/10.1016/j.orggeochem.2012.11.001>.
- Olías, M., Nieto, J.M., 2015. Background conditions and mining pollution throughout history in the río tinto (SW Spain). *Environments* 2, 295–316. <https://doi.org/10.3390/environments2030295>.
- Olsen, J., Anderson, N.J., Knudsen, M.F., 2012. Variability of the North Atlantic oscillation over the past 5,200years. *Nat. Geosci.* 5, 808–812. <https://doi.org/10.1038/ngeo1589>.
- Oschlies, A., Brandt, P., Stramma, L., Schmidtko, S., 2018. Drivers and mechanisms of ocean deoxygenation. *Nat. Geosci.* 11, 467–473. <https://doi.org/10.1038/s41561-018-0152-2>.
- Palanques, A., El Khatib, M., Puig, P., Masqué, P., Sánchez-Cabeza, J.A., Isla, E., 2005. Downward particle fluxes in the Guadiaro submarine canyon depositional system (north-western Alboran Sea), a river flood dominated system. *Mar. Geol.* 220, 23–40. <https://doi.org/10.1016/j.margeo.2005.07.004>.

- Passier, H.F., Middelburg, J., de Lange, G., Böttcher, M., 1997. Pyrite contents, microtextures, and sulfur isotopes in relation to formation of the youngest eastern Mediterranean sapropel. *Geology* 25, 519–522. [https://doi.org/10.1130/0091-7613\(1997\)025<0519:PCMASI>2.3.CO;2](https://doi.org/10.1130/0091-7613(1997)025<0519:PCMASI>2.3.CO;2).
- Paul, K.M., van Heldmond, N.A.G.M., Slomp, C.P., Jokinen, S.A., Virtasalo, J.J., Filipsson, H.L., Jilbert, T., 2023. Sedimentary molybdenum and uranium: improving proxies for deoxygenation in coastal depositional environments. *Chem. Geol.* 615, 121203. <https://doi.org/10.1016/j.chemgeo.2022.121203>.
- Paytan, A., Griffith, E.M., 2007. Marine barite: recorder of variations in ocean export productivity. *Deep Sea Res. Part Topical Stud. Oceanogr.* 54, 687–705. <https://doi.org/10.1016/j.dsr2.2007.01.007>.
- Penaud, A., Eynaud, F., Turon, J.L., Blamart, D., Rossignol, L., Marret, F., Lopez-Martínez, C., Grimalt, J.O., Malaizé, Charlier, K., 2010. Contrasting paleoceanographic conditions off Morocco during Heinrich events (1 and 2) and the last glacial maximum. *Quat. Sci. Rev.* 29, 1923–1939. <https://doi.org/10.1016/j.quascirev.2010.04.011>.
- Penaud, A., Eynaud, F., Sánchez-Goni, M., Malaizé, B., Turon, J.L., Rossignol, L., 2011. Contrasting sea-surface responses between the western Mediterranean Sea and eastern subtropical latitudes of the North Atlantic during abrupt climatic events of MIS 3. *Mar. Micropaleontol.* 80, 1–17. <https://doi.org/10.1016/j.marmicro.2011.03.002>.
- Penaud, A., Eynaud, F., Voelker, A.H.L., Turon, J.L., 2016. Palaeohydrological changes over the last 50 ky in the central Gulf of Cadiz: complex forcing mechanisms mixing multi-scale processes. *Biogeosciences* 13, 5357–5377. <https://doi.org/10.5194/bg-13-5357-2016>.
- Pérez-Asensio, J.N., Frigola, J., Pena, L.D., Sierro, F.J., Reguera, M.I., Rodríguez-tovar, F. J., Dorador, J., Asioli, A., Kuhlmann, J., Huhn, K., Cacho, I., 2020. Changes in western mediterranean thermohaline circulation in association with a deglacial organic rich layer formation in the Alboran Sea. *Quat. Sci. Rev.* 228, 106075. <https://doi.org/10.1016/j.quascirev.2019.106075>.
- Pérez-Folgado, M., Sierro, F.J., Flores, J.A., Cacho, I., Grimalt, J.O., Zahn, R., Shackleton, N., 2003. Western Mediterranean planktonic foraminifera events and millennial climatic variability during the last 70 kyr. *Mar. Micropaleontol.* 48, 49–70. [https://doi.org/10.1016/S0377-8398\(02\)00160-3](https://doi.org/10.1016/S0377-8398(02)00160-3).
- Polovina, J.J., Howell, E.A., Abecassis, M., 2008. Ocean's least productive waters are expanding. *Geophys. Res. Lett.* 35, L03618, [10.1029/2007GL031745](https://doi.org/10.1029/2007GL031745).
- Pospelova, V., de Vernal, A., Pedersen, T.F., 2008. Distribution of dinoflagellate cysts in surface sediments from the northeastern Pacific Ocean (43–25 N) in relation to sea-surface temperature, salinity, productivity and coastal upwelling. *Mar. Micropaleontol.* 68, 21–48. <https://doi.org/10.1029/2007GL031745>.
- Pospelova, V., Esenkulova, S., Johannessen, S.C., O'Brien, M.C., Macdonald, R.W., 2010. Organic-walled dinoflagellate cyst production, composition and flux from 1996 to 1998 in the central Strait of Georgia (BC, Canada): a sediment trap study. *Mar. Micropaleontol.* 75, 17–37. <https://doi.org/10.1016/j.marmicro.2010.02.003>.
- Powell, A.J., Lewis, J., Dodge, J.D., 1992. The palynological expressions of post-Palaeogene upwelling: a review. *Geol. Soc. Spec. Publ.* 64, 215–226. <https://doi.org/10.1144/GSL.SP.1992.064.01.1>.
- Radi, T., de Vernal, A., 2008. Dinocysts as proxy of primary productivity in mid-high latitudes of the Northern Hemisphere. *Mar. Micropaleontol.* 68, 84–114. <https://doi.org/10.1016/j.marmicro.2008.01.012>.
- Ramos-Román, M.J., Jiménez-Moreno, G., Camuera, J., García-Alix, A., Anderson, R.S., Jiménez-Espejo, F.J., Sachse, D., Toney, J.L., Carrión, J.S., Webster, C., Yanes, Y., 2018a. Millennial-scale cyclical environment and climate variability during the Holocene in the western Mediterranean region deduced from a new multi-proxy analysis from the Padul record (Sierra Nevada, Spain). *Global Planet. Change* 168, 35–53. <https://doi.org/10.1016/j.gloplacha.2018.06.003>.
- Ramos-Román, M.J., Jiménez-Moreno, G., Camuera, J., García-Alix, A., Anderson, R.S., Jiménez-Espejo, F.J., Carrión, J.S., 2018b. Holocene climate aridification trend and human impact interrupted by millennial- and centennial-scale climate fluctuations from a new sedimentary record from Padul (Sierra Nevada, southern Iberian Peninsula). *Clim. Past* 14, 117–137. <https://doi.org/10.5194/cp-14-117-2018>.
- Reitz, A., Thomson, J., de Lange, G.J., Hensen, C., 2006. Source and development of large manganese enrichments above eastern Mediterranean sapropel S1. *Paleoceanography* 21, PA3007. <https://doi.org/10.1029/2005PA001169>.
- Rodó, X., Baert, E., Comin, F.A., 1997. Variations in seasonal rainfall in southern Europe during the present century: relationships with the North Atlantic oscillation and the El Niño-southern oscillation. *Clim. Dynam.* 13, 275–284. <https://doi.org/10.1007/s003820050165>.
- Rodrigo-Gámiz, M., Martínez-Ruiz, F., Jiménez-Espejo, F.J., Gallego-Torres, D., Nieto-Moreno, V., Romero, O., Ariztegui, D., 2011. Impact of climate variability in the western Mediterranean during the last 20,000 years: oceanic and atmospheric responses. *Quat. Sci. Rev.* 30, 2018–2034. <https://doi.org/10.1016/j.quascirev.2011.05.011>.
- Rodrigo-Gámiz, M., Martínez-Ruiz, F., Rampen, S.W., Schouten, S., Sinninghe Damsté, J. S., 2014a. Sea surface temperature variations in the western Mediterranean Sea over the last 20 kyr: a dual-organic proxy UK37 and LDI approach. *Paleoceanography* 29, 87–98. <https://doi.org/10.1002/2013PA002466>.
- Rodrigo-Gámiz, M., Martínez-Ruiz, F., Rodríguez-Tovar, F.J., Jiménez-Espejo, F.J., Pardo-Igúzquiza, E., 2014b. Millennial-to centennial-scale climate periodicities and forcing mechanisms in the westernmost Mediterranean for the past 20,000 yr. *Quat. Res.* 81, 78–93. <https://doi.org/10.1016/j.yqres.2013.10.009>.
- Rodrigo-Gámiz, M., Martínez-Ruiz, F., Chiaradia, M., Jiménez-Espejo, F.J., Ariztegui, D., 2015. Radiogenic isotopes for deciphering terrigenous input provenance in the western Mediterranean. *Chem. Geol.* 410, 237–250. <https://doi.org/10.1016/j.chemgeo.2015.06.004>.
- Rogerson, M., Cacho, I., Jiménez-Espejo, F., Reguera, M.I., Sierro, F.J., Martínez-Ruiz, F., Frigola, J., Canals, M., 2008. A dynamic explanation for the origin of the western Mediterranean organic-rich layers. *G-cubed* 9, Q07U01. <https://doi.org/10.1029/2007GC001936>.
- Rogerson, M., Rohling, E.J., Bigg, G.R., Ramirez, J., 2012. Paleoceanography of the Atlantic-Mediterranean exchange: overview and first quantitative assessment of climatic forcing. *Rev. Geophys.* 50, RG2003. <https://doi.org/10.1029/2011RG000376>.
- Rohling, E.J., Abu-Zied, R., Casford, J.S.L., Hayes, A., Hoogakker, B.A.A., 2009. The marine environment: present and past. *The physical geography of the Mediterranean* 8, 33.
- Romero-Baena, A.J., González, I., Galán, E., 2018. Soil pollution by mining activities in Andalusia (South Spain)—the role of Mineralogy and Geochemistry in three case studies. *J. Soils Sediments* 18, 2231–2247. <https://doi.org/10.1007/s11368-017-1898-7>.
- Rossignol-Strick, M., 1999. The Holocene climatic optimum and pollen records of sapropel 1 in the eastern Mediterranean, 9000–6000 BP. *Quat. Sci. Rev.* 18, 515–530. [https://doi.org/10.1016/S0277-3791\(98\)00093-6](https://doi.org/10.1016/S0277-3791(98)00093-6).
- Ruiz, J., Echevarria, F., Font, J., Ruiz, S., Garcia, E., Blanco, J.M., Jiménez-Gómez, F., Prieto, L., González-Alaminos, A., García, C.M., Cipollini, P., Snaith, H., Bartual, A., Reul, A., Rodríguez, V., 2001. Surface distribution of chlorophyll, particles and gelbstoff in the Atlantic jet of the Alborán Sea: from submesoscale to subinertial scales of variability. *J. Mar. Syst.* 29, 277–292. [https://doi.org/10.1016/S0924-7963\(01\)00020-3](https://doi.org/10.1016/S0924-7963(01)00020-3).
- Sanchez-Vidal, A., Calafat, A., Canals, M., Frigola, J., Fabres, J., 2005. Particle fluxes and organic carbon balance across the eastern Alboran Sea (SW Mediterranean Sea). *Contin. Shelf Res.* 25, 609–628. <https://doi.org/10.1016/j.csr.2004.11.004>.
- Sangiorgi, F., Donders, T.H., 2004. Reconstructing 150 years of eutrophication in the north-western Adriatic Sea (Italy) using dinoflagellate cysts, pollen and spores. *Estuar. Coast Shelf Sci.* 60, 69–79. <https://doi.org/10.1016/j.eccs.2003.12.001>.
- Sangiorgi, F., Dinelli, E., Maffioli, P., Capotondi, L., Giunta, S., Morigi, C., Principato, M. S., Negri, A., Emeis, K.-C., Corselli, C., 2006. Geochemical and micropaleontological characterisation of a Mediterranean sapropel S5: a case study from core BAN89GC09 (south of Crete). *Paleoceanogr. Palaeoclimatol. Palaeoecol.* 235, 192–207. <https://doi.org/10.1016/j.palaeo.2005.09.029>.
- Sangiorgi, F., Quaijaal, W., Donders, T.H., Schouten, S., Louwye, S., 2021. Middle Miocene temperature and productivity evolution at a Northeast Atlantic shelf site (IODP U1318, Porcupine Basin): global and regional changes. *Paleoceanogr. Paleoclimatol.* 36, e2020PA004059. <https://doi.org/10.1029/2020PA004059>.
- Sarhan, T., Lafuente, J.G., Vargas, M., Vargas, J.M., Plaza, F., 2000. Upwelling mechanisms in the northwestern Alboran Sea. *J. Mar. Syst.* 23, 317–331. [https://doi.org/10.1016/S0924-7963\(99\)00068-8](https://doi.org/10.1016/S0924-7963(99)00068-8).
- Schmidt, S., Stramma, L., Visbeck, M., 2017. Decline in global oceanic oxygen content during the past five decades. *Nature* 542, 335–339. <https://doi.org/10.1038/nature21399>.
- Schneider, T., Bischoff, T., Haug, G.H., 2014. Migrations and dynamics of the intertropical convergence zone. *Nature* 513, 45–53. <https://doi.org/10.1038/nature13636>.
- Schouten, S., Hoefs, M.J.L., Damsté, J.S.S., 2000. A molecular and stable carbon isotopic study of lipids in late Quaternary sediments from the Arabian Sea. *Org. Geochem.* 31, 509–521. [https://doi.org/10.1016/S0146-6380\(00\)00031-0](https://doi.org/10.1016/S0146-6380(00)00031-0).
- Scott, C., Lyons, T.W., 2012. Contrasting molybdenum cycling and isotopic properties in euxinic versus non-euxinic sediments and sedimentary rocks: refining the paleoproxies. *Chem. Geol.* 324–325, 19–27. <https://doi.org/10.1016/j.chemgeo.2012.05.012>.
- Sierro, F.J., Hodell, D.A., Curtis, J.H., Flores, J.A., Reguera, I., Colmenero-Hidalgo, E., Bárcena, M.A., Grimalt, J.O., Cacho, I., Frigola, J., Canals, M., 2005. Impact of iceberg melting on Mediterranean thermohaline circulation during Heinrich events. *Paleoceanography* 20, PA2019. <https://doi.org/10.1029/2004PA001051>.
- Siokou-Frangou, I., Christaki, U., Mazzocchi, M.G., Montresor, M., Ribera d'Alcalá, M., Vaqué, D., Zingone, A., 2010. Plankton in the open Mediterranean Sea: a review. *Biogeosciences* 7, 1543–1586. <https://doi.org/10.5194/bg-7-1543-2010>.
- Sluijs, A., Schouten, S., Pagani, M., Woltering, M., Brinkhuis, H., Damsté, J.S.S., Dickens, G.R., Huber, M., Reichert, G.J., Stein, R., Matthiessen, J., Lourens, L.J., Pedentchouk, N., Backman, J., Moran, K., Expedition 302 Scientists, 2006. Subtropical arctic ocean temperatures during the paleoecene/eocene thermal maximum. *Nature* 441, 610–613. <https://doi.org/10.1038/nature04668>.
- Sumner, G., Homar, V., Ramis, C., 2001. Precipitation seasonality in eastern and southern coastal Spain. *Int. J. Climatol.* 21, 219–247. <https://doi.org/10.1002/joc.600>.
- Taylor, F.J.R., 1987. *Dinoflagellate ecology: general and marine ecosystems*. Chapt. 11A. In: Taylor, F.J.R. (Ed.), *The Biology of Dinoflagellates*, vol. 80, pp. 398–502.
- Taylor, F.J.R., Hoppenrath, M., Saldarriaga, J.F., 2008. Dinoflagellate diversity and distribution. *Biodivers. Conserv.* 17, 407–418. <https://doi.org/10.1007/s10531-007-9258-3>.
- Thomson, J., Higgs, N.C., Croudace, I.W., Colley, S., Hydes, D.J., 1993. Redox zonation of elements at anoxic/post-oxic boundary in deep-sea sediments. *Geochim. Cosmochim. Acta* 57, 579–595. [https://doi.org/10.1016/0016-7037\(93\)90369-8](https://doi.org/10.1016/0016-7037(93)90369-8).
- Tierney, J.E., Lewis, S.C., Cook, B.I., LeGrande, A.N., Schmidt, G.A., 2011. Model proxy and isotopic perspectives on the east african humid period. *Earth Planet. Sci. Lett.* 307, 103–112. <https://doi.org/10.1016/j.epsl.2011.04.038>.
- Tintoré, J., La Violette, P.E., Blade, I., Cruzado, A., 1988. A study of an intense density front in the Eastern Alboran Sea: the Almería-Oran front. *J. Phys. Oceanogr.* 18, 1384–1397. [10.1175/1520-0485\(1988\)018<1384:ASOAI>2.0.CO;2](https://doi.org/10.1175/1520-0485(1988)018<1384:ASOAI>2.0.CO;2).
- Toney, J.L., García-Alix, A., Jiménez-Moreno, G., Anderson, R.S., Moossen, H., Seki, O., 2020. New insights into Holocene hydrology and temperature from lipid biomarkers

- in western Mediterranean alpine wetlands. *Quat. Sci. Rev.* 240, 106395. <https://doi.org/10.1016/j.quascirev.2020.106395>.
- Trias-Navarro, S., Pena, L.D., De la Fuente, M., Paredes, E., Garcia-Solsona, E., Frigola, J., Català, A., Caruso, A., Lirer, F., Haghipour, N., Perez-Asensio, J.N., Cacho, I., 2023. Eastern Mediterranean water outflow during the Younger Dryas was twice that of the present day. *Commun. Earth Environ.* 4, 147. <https://doi.org/10.1038/s43247-023-00812-7>.
- Tribouillard, N., 2021. Re-assessing copper and nickel enrichments as paleoproductivity proxies. *Bull. Soc. Geol. Fr.* 192, 54. <https://doi.org/10.1051/bsgf/2021047>.
- Tribouillard, N., Algeo, T.J., Lyons, T., Riboulleau, A., 2006. Trace metals as paleoredox and paleoproductivity proxies: an update. *Chem. Geol.* 232, 12–32. <https://doi.org/10.1016/j.chemgeo.2006.02.012>.
- Tribouillard, N., Algeo, T.J., Baudin, F., Riboulleau, A., 2012. Analysis of marine environmental conditions based on molybdenum-uranium covariation Applications to Mesozoic paleoceanography. *Chem. Geol.* 325, 46–58. <https://doi.org/10.1016/j.chemgeo.2011.09.009>.
- Trigo, R.M., Osborn, T.J., Corte-Real, J.M., 2002. The North Atlantic Oscillation influence on Europe: climate impacts and associated physical mechanisms. *Clim. Res.* 20, 9–17. <https://doi.org/10.3354/cr020009>.
- Trouet, V., Esper, J., Graham, N.E., Baker, A., Scourse, J.D., Frank, D.C., 2009. Persistent positive North Atlantic Oscillation mode dominated the medieval climate anomaly. *Science* 324, 78–80. <https://doi.org/10.1126/science.1166349>.
- Tyson, R.V., 1995. Bulk geochemical characterization and classification of organic matter: stable carbon isotopes ( $\delta^{13}\text{C}$ ). *Sedimentary Organic Matter: Organic Facies and Palynofacies* 395–416.
- Tyson, R., Pearson, T., 1991. Modern and ancient continental shelf anoxia: an overview. *Geol. Soc. Spec. Publ.* 58, 1–24. <https://doi.org/10.1144/GSL.SP.1991.058.01.01>.
- van de Schootbrugge, B., Koutsodendris, A., Taylor, W., Weston, F., Wellman, C., Strother, P.K., 2024. Recognition of an extended record of euglenoid cysts: implications for the end-Triassic mass extinction. *Rev. Palaeobot. Palynol.* 322, 105043. <https://doi.org/10.1016/j.revpalbo.2023.105043>.
- van Helmond, N.A., Hennekam, R., Donders, T.H., Bunnik, F.P., de Lange, G.J., Brinkhuis, H., Sangiorgi, F., 2015. Marine productivity leads organic matter preservation in sapropel S1: palynological evidence from a core east of the Nile River outflow. *Quat. Sci. Rev.* 108, 130–138. <https://doi.org/10.1016/j.quascirev.2014.11.014>.
- Versteegh, G.J.M., 1994. Recognition of cyclic and non-cyclic environmental changes in the Mediterranean Pliocene: a palynological approach. *Mar. Micropaleontol.* 23, 147–183. [https://doi.org/10.1016/0377-8398\(94\)90005-1](https://doi.org/10.1016/0377-8398(94)90005-1).
- Versteegh, G.J., Zonneveld, K.A., 2002. Use of selective degradation to separate preservation from productivity. *Geology* 30, 615–618. [https://doi.org/10.1130/0091-7613\(2002\)030<0615:UOSDTS>2.0.CO;2](https://doi.org/10.1130/0091-7613(2002)030<0615:UOSDTS>2.0.CO;2).
- Voelker, A.H., Lebreiro, S.M., Schönfeld, J., Cacho, I., Erlenkeuser, H., Abrantes, F., 2006. Mediterranean outflow strengthening during northern hemisphere coolings: a salt source for the glacial Atlantic? *Earth Planet Sci. Lett.* 245, 39–55. <https://doi.org/10.1016/j.epsl.2006.03.014>.
- Walker, M.J., Berkelhammer, M., Björck, S., Cwynar, L.C., Fisher, D.A., Long, A.J., Lowe, J.J., Newnham, R.M., Rasmussen, S.O., Weiss, H., 2012. Formal subdivision of the Holocene series/epoch: a discussion paper by a working group of INTIMATE (integration of ice-core, marine and terrestrial records) and the subcommission on quaternary stratigraphy (international commission on stratigraphy). *J. Quat. Sci.* 27, 649–659. <https://doi.org/10.1002/jqs.2565>.
- Wang, H., Lo Iacono, C., Wienberg, C., Titschack, J., Hebbeln, D., 2019. Cold-water coral mounds in the southern Alboran Sea (western Mediterranean Sea): internal waves as an important driver for mound formation since the last deglaciation. *Mar. Geol.* 412, 1–18. <https://doi.org/10.1016/j.margeo.2019.02.007>.
- Wanner, H., Brönnimann, S., Casty, C., Gyalistras, D., Luterbacher, J., Schmutz, C., Stephenson, D.B., Xoplaki, E., 2001. North atlantic oscillation-concepts and studies. *Surv. Geophys.* 22, 321–381. <https://doi.org/10.1023/A:1014217317898>.
- Wanner, H., Beer, J., Bütikofer, J., Crowley, T.J., Cubasch, U., Flückiger, J., Goosse, H., Grosjean, M., Joos, F., Kaplan, J.O., Küttel, M., Müller, S.A., Prentice, I.C., Solomina, O., Stocker, T.F., Tarasov, P., Wagner, M., Widmann, M., 2008. Mid-to Late Holocene climate change: an overview. *Quat. Sci. Rev.* 27, 1791–1828. <https://doi.org/10.1016/j.quascirev.2008.06.013>.
- Warning, B., Brumsack, H.J., 2000. Trace metal signatures of eastern Mediterranean sapropels. *Paleogeogr. Paleoclimatol. Paleoecol.* 158, 293–309. [https://doi.org/10.1016/S0031-0182\(00\)00055-9](https://doi.org/10.1016/S0031-0182(00)00055-9).
- Williams, G.L., Fensome, R.A., MacRae, R.A., 2017. The Lentin and Williams index of fossil dinoflagellates 2017 edition. *Am. Assoc. Stratigr. Palynol. Contrib. Ser. no. 48*.
- Wood, G.D., 1996. Palynological techniques-processing and microscopy. In: Jasonius, J., McGregor, D.C. (Eds.), *Palynology: Principles and Application*, vol. 1. American association of stratigraphic palynologists foundation, pp. 29–50.
- Yang, Y., Wang, W.M., Shu, J.W., Chen, W., Shi, G.L., 2022. Disruption of terrestrial plant ecosystem in Miocene (sub) tropics: a palynological perspective from Fotan Formation, Southeast China. *Rev. Palaeobot. Palynol.* 304, 104715. <https://doi.org/10.1016/j.revpalbo.2022.104715>.
- Yebra, L., Herrera, I., Mercado, J.M., Cortés, D., Gómez-Jakobsen, F., Alonso, A., Sánchez, A., Salles, S., Valcárcel-Pérez, N., 2018. Zooplankton production and carbon export flux in the western Alboran Sea gyre (SW Mediterranean). *Prog. Oceanogr.* 167, 64–77. <https://doi.org/10.1016/j.pocean.2018.07.009>.
- Zirks, E., Krom, M.D., Zhu, D., Schmiel, G., Goodman-Tchernov, B.N., 2019. Evidence for the presence of oxygen-depleted sapropel intermediate water across the Eastern Mediterranean during Sapropel S1. *ACS Earth Space Chem.* 3, 2287–2297. <https://doi.org/10.1021/acsearthspacechem.9b00128>.
- Zonneveld, K.A., Brummer, G.A., 2000. (Palaeo-) ecological significance, transport and preservation of organic-walled dinoflagellate cysts in the Somali Basin, NW Arabian Sea. *Deep Sea Res. Part II Top. Stud. Oceanogr.* 47, 2229–2256. [https://doi.org/10.1016/S0967-0645\(00\)00023-0](https://doi.org/10.1016/S0967-0645(00)00023-0).
- Zonneveld, K.A., Pospelova, V., 2015. A determination key for modern dinoflagellate cysts. *Palynology* 39, 387–409. <https://doi.org/10.3389/fmars.2022.915755>.
- Zonneveld, K.A., Versteegh, G.J., de Lange, G.J., 2001. Palaeoproductivity and post-depositional aerobic organic matter decay reflected by dinoflagellate cyst assemblages of the Eastern Mediterranean S1 sapropel. *Mar. Geol.* 172, 181–195. [https://doi.org/10.1016/S0025-3227\(00\)00134-1](https://doi.org/10.1016/S0025-3227(00)00134-1).
- Zonneveld, K.A., Bockelmann, F., Holzwarth, U., 2007. Selective preservation of organic-walled dinoflagellate cysts as a tool to quantify past net primary production and bottom water oxygen concentrations. *Mar. Geol.* 237, 109–126. <https://doi.org/10.1016/j.margeo.2006.10.023>.
- Zonneveld, K.A., Chen, L., Möbius, J., Mahmoud, M.S., 2009. Environmental significance of dinoflagellate cysts from the proximal part of the Po-river discharge plume (off southern Italy, Eastern Mediterranean). *J. Sea Res.* 62, 189–213. <https://doi.org/10.1016/j.seares.2009.02.003>.
- Zonneveld, K.A., Marret, F., Versteegh, G.J.M., Bogus, K., Bonnet, S., Bouimetarhan, I., Crouch, E., de Vernal, A., Elshaniwanay, R., Edwards, L., Esper, O., Forke, S., Grosfeld, K., Henry, M., Holzwarth, U., Kieft, J.F., Kim, S.Y., Ladouceur, S., Ledu, D., Chen, L., Limoges, A., Londeix, L., Lu, S.H., Mahmoud, M.S., Marino, G., Matsouka, K., Matthiessen, J., Mildenhall, D.C., Mudie, P., Neil, H.L., Pospelova, V., Qi, Y., Radi, T., Richerol, T., Rochon, A., Sangiorgi, F., Solignac, S., Turon, J.L., Verleye, T., Wang, Y., Wang, Z., Young, M., 2013. Atlas of modern dinoflagellate cyst distribution based on 2405 data points. *Rev. Palaeobot. Palynol.* 191, 1–197. <https://doi.org/10.1016/j.revpalbo.2012.08.003>.
- Zúñiga, D., Calafat, A., Heussner, S., Miserocchi, S., Sanchez-Vidal, A., Garcia-Orellana, J., Canals, M., Sánchez-Cabeza, J.A., Carbonne, J., Delsaut, N., Saragoni, G., 2008. Compositional and temporal evolution of particle fluxes in the open Algero-Balearic basin (Western Mediterranean). *J. Mar. Syst.* 70, 196–214. <https://doi.org/10.1016/j.jmarsys.2007.05.007>.
- Zwiep, K.L., Hennekam, R., Donders, T.H., van Helmond, N.A., De Lange, G.J., Sangiorgi, F., 2018. Marine productivity, water column processes and seafloor anoxia in relation to Nile discharge during sapropels S1 and S3. *Quat. Sci. Rev.* 200, 178–190. <https://doi.org/10.1016/j.quascirev.2018.08.026>.